STUDY OF GAS CELL STABILITY DURING BREADMAKING USING X-RAY MICROTOMOGRAPHY AND DOUGH RHEOLOGY

by

MELISSA M. PICKETT

B.S., Kansas State University, 2007

A THESIS

submitted in partial fulfillment of the requirements for the degree

MASTER OF SCIENCE

Department of Grain Science and Industry
College of Agriculture

KANSAS STATE UNIVERSITY
Manhattan, Kansas

2009

Approved by:

Major Professor
Dr. Hulya Dogan

Copyright

Abstract

Viscoelastic wheat flour doughs are renowned for their ability to produce high quality aerated bread products. Dough exhibits extremely complex rheological properties which makes it capable of occluding and retaining gas cells. The ability of these bubbles to resist failure and remain stable throughout the proofing and baking process is critical to final bread structure and volume. Understanding these factors is important when creating the distinct structural and textural characteristics that consumers desire in baked products. In this study, a method was established for using X-ray microtomography (XMT) to study the microstructure of proving dough as well as bread made from three very different wheat flours. Doughs were prepared according to AACC Method 10-10B optimized straight-dough bread-making method. Sections from unproofed (0 min), underproofed (20 min) and optimally proofed (40 min) doughs were carefully cut and frozen at –80°C. Baked loaves were also prepared following standard test bake procedures. Small specimens were cut from two locations of both the proofed and baked loaves prior to microstructural analysis. A total of 96 dough and bread samples were scanned using a high resolution desktop X-ray micro-CT system Skyscan1072 (Skyscan, Belgium) consisting of an X-ray tube, an X-ray detector and a CCD-camera. X-ray images were obtained from 137 rotation views through 180° of rotation. Hundreds of reconstructed cross sectional images were analyzed using CTAn (v.1.7) software. 3-D analysis of the bubbles indicated that average dough void fractions increased dramatically over proof time from 30.9% for the unproofed dough (0 min) to 62.0% and 74.5 % for the underproofed (20 min) and optimally proofed (40 min) doughs respectively. Oven spring caused further expansion in the baked loaves which increased average void fraction to 84.3%. Gas cell size distributions were largely skewed to the right and shifted in that same direction as processing time increased. Differences in gas cell size seen among flour varieties were largely due to variations in the size of the largest cells caused by coalescence.

Table of Contents

List of Figures

List of Tables

Acknowledgements

I would like to express my sincere gratitude to my advisor Dr. Hulya Dogan for her valuable guidance, encouragement, and patience which have enabled me to complete this project. I would also like to thank Dr. Jon Faubion and Dr. Finlay MacRitchie both of whom have taken great interest in my work and provided me with valuable counsel.

I would like to express my gratitude to Dr. Scott Bean at the USDA for the use of the D/R Dough Inflation System and to Dr. Jon Boyer for his help with statistical analysis. Distinct words of appreciation are also due to Dr. Becky Miller, Ms. Margo Caley and Ms. Shuping Yan for their helpful comments on my project. I would also like to thank my lab mates and friends Summer, Hyma, Elisa, Camila and Jhoe for all the fun times and great memories of grad school.

Last but certainly not least I would like to thank my family, my parents, and especially my Husband Michael for loving and supporting me every step of the way!

Dedication

For Michael

And to a life lived fully alive

CHAPTER 1 - **Introduction**

Baked foods rely on their cellular foam structure for value and functionality. Bread is a spongy solid foam formed by a dispersed gas phase (air) occupying a high volume fraction in a continuous solid matrix. Breadmaking is a process in which large extensional deformation of the dough is featured prominently. During the mixing process, small air cells are incorporated into the dough. These bubbles serve as nucleation sites for the diffusion of carbon dioxide and continue to grow during fermentation and proofing. During proofing and baking, expansion of gas cells cause significant extensional strain on the surrounding dough. Dough exhibits extremely complex rheological properties which impact bubble structure and size distribution and overall stability. The ability of the gas cells to resist failure and remain stable throughout the proofing and baking process is critical to final bread texture and volume.

The stability of the cell walls surrounding these cells has a great effect on the final structure of baked products. As cells slowly expand, product volume increases. The failure or coalescence of the gas cells eventually leads to the formation of an open sponge like structure that is commonly seen in bread. Cell wall stability during the proofing and baking stages is important in preventing premature coalescence. Understanding how dough rheology affects dough microstructure during proofing and baking is a fundamental first step in developing high quality baked foods. Figure 1.1 shows both processing and material related factors which can affect end-product microstructure. Process related factors include mixing, proofing and baking. Material related factors are those which are affected by flour quality and can impact the rheological properties of dough.

The ultimate aim of this research is to better understand the effect of temperature, proof time and strain hardening on the microstructure of dough and how this translates into the final baked product quality. Experimental plan and procedures were designed with the following objectives:

- Establish a method for using X-ray microtomography to study the microstructure of proving dough as well as bread
- Compare the stability of three very different wheat flour varieties throughout the proofing and baking process

- Understand the interrelationship between protein quality, biaxial rheological properties and microstructure

Figure 1.1 Flow Diagram displaying factors effecting end-product microstructure

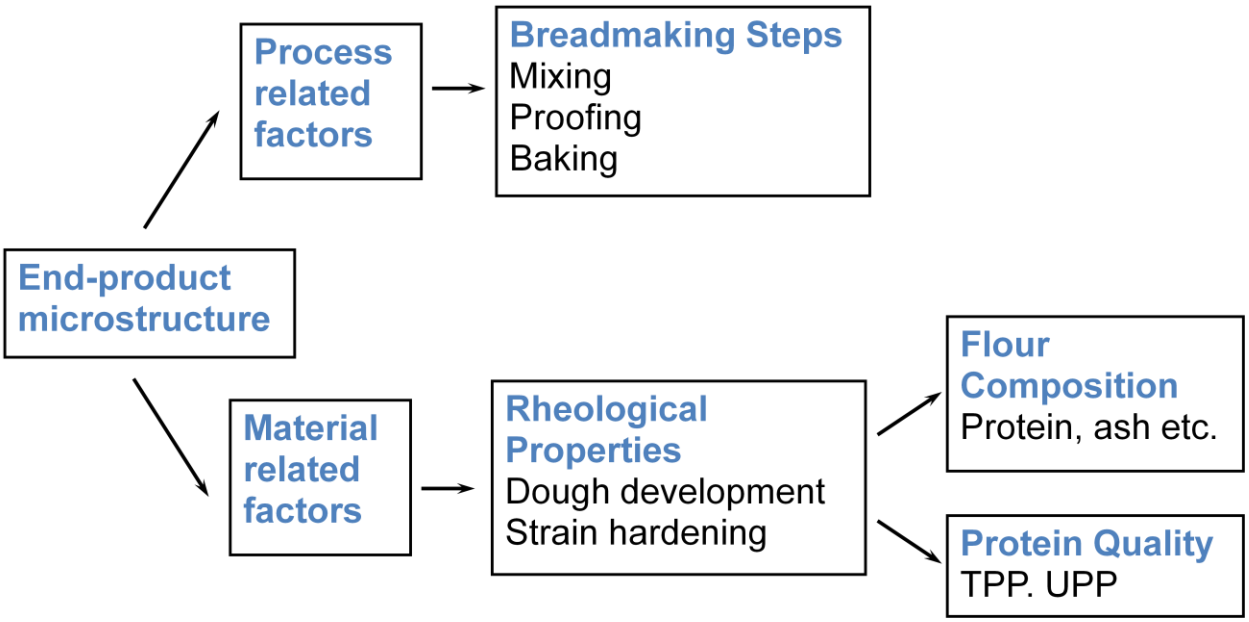

CHAPTER 2 - **Literature Review**

Wheat flour doughs are renowned for their ability to produce high quality aerated bread products. Because of their viscoelastic properties created during mixing, these doughs are able to occlude gas cells (bubbles) and retain them throughout the bread making process. The bread making process is composed of a series of stages including mixing, fermentation, dividing, proving and baking. During mixing, the proper rheological characteristics of dough are developed and tiny air nuclei are incorporated in the dough matrix. As a consequence of fermentation, these nuclei undergo large expansion particularly during the proofing and baking stages of production. It is clear that the rheological properties of the protein matrix constituting expanding gas cells have a significant effect on their stability. The ability of the gas cell walls to resist failure and remain stable throughout the proofing and baking process is, thus, critical to final bread texture and volume. Understanding these factors is important when creating the distinct structural and textural characteristics that consumers desire in baked products.

2.1. Breadmaking: A Process of Incorporating and Retaining Air

2.1.1. Mixing (Occlusion of Gas)

Incorporation of air into dough is a critical part of any breadmaking process. During mixing; flour and water combine to form a viscoelastic dough that is capable of occluding and retaining gas bubbles. Dough development can be described as the formation of a continuous protein network into which starch granules are embedded. During the mixing process, gluten proteins become hydrated and undergo “glass transition at room temperature” causing them to become rubbery (Hoseney et al., 1986). These proteins then form a developed dough matrix which is capable of retaining air (Baker and Mize, 1946).

In their classic article “The origin of the gas cell in bread dough”, Baker and Mize (1941) tested several hypotheses in order to determine the origin of gas cells in bread dough, and concluded that yeast alone is incapable of creating gas cells in dough. Instead, the expansion of

gas cells in dough depends critically on the creation of tiny gas nuclei that are incorporated during the early stages of mixing. These serve as critical nucleation points for the diffusion of CO_2 and consequent expansion of gas cells in the bread making process. Baker and Mize (1946) observed that flours vary widely in the amount of gas they are able to occlude during mixing. They found that strong bread flours typically have more resistance to gas occlusion than do weak flours. The rate at which air is occluded into dough varies throughout the mixing process, being highest at the time when dough provides the greatest resistance to mixing (Baker and Mize, 1946). Junge et al. (1981) confirmed these results. They found that throughout the mixing process, the density of a dough mass can decrease from 1.20 g/cm^3 in a dough that is in the early stages of hydration and mixing to 1.10 g/cm^3 for a dough that is over mixed. The majority of rapid air occlusion however occurs at or even after the dough has been mixed to its optimum.

The gas nuclei incorporated during the mixing process are typically small, ranging in size from 10-100 μm (Bloksma, 1990b). The number of bubbles estimated to be occluded during mixing has varied from 86,700 per cm^{-3} (Carlson and Bohlin, 1978) to 78,500 per cm^{-3} (Campbell et al., 1991). Campbell (2003) suggested that there are four important factors which affect air incorporation during mixing: The gas content of the dough, the rate of turnover of gas during mixing, the distribution of gas in terms of the bubble size distribution, and the gaseous composition of the bubbles. Each of these is affected by process design and parameters such as the mixer type, blade design, and headspace pressure. (Cauvain et al., 1999). Aeration during mixing affects the rheological properties of dough both physically and chemically. The incorporation of oxygen speeds the mixing process by promoting chemical oxidation reactions. Additionally the physical presence of bubbles in dough dilutes the gluten matrix and reduces a dough's resistance to failure under biaxial extension (Chin et al., 2005).

2.1.2. Proving (Gas Cell Expansion)

Soon after mixing, yeast begins fermenting available glucose, producing carbon dioxide. In the early stages of fermentation, the carbon dioxide is dissolved in the liquid phase of the dough. Bloksma (1990a) suggests that gas cells begin to grow only after the liquid phase of dough becomes fully saturated with carbon dioxide at concentrations of 4.3×10^{-2} $kmoles/m^3$. At this point, carbon dioxide will diffuse into gas cells at the same rate that it is produced and gas cells will begin to expand. Under typical bread making conditions (2% compressed yeast 27ºC),

the rate of gas production is $2.5x10^{-5}$ kmoles or $6x10^{-4}$ m^3 gas per m^3 of dough per second (Bloksma, 1990a). Others (Chiotellis and Campbell, 2003) have suggested that carbon dioxide saturation of the liquid dough phase is not required for gas cell growth and that gas cells begin to grow long before the point of saturation.

Expansion of the dough is caused by pressure above atmospheric in the gas cells (Bloksma, 1990a). Bubble growth is affected by four factors including carbon dioxide production, carbon dioxide retention, the rate of CO_2 diffusion from the saturated dough into the nuclei, and the rate of bubble coalescence (Shah et al., 1998). Bread dough is commonly punched and molded during the fermentation and proofing process. These steps serve to subdivide gas cells as well as to increase both their numbers and concentration (Baker and Mize, 1941).

2.1.3. Baking (Oven Spring)

Baking transforms the expanded dough into an aerated loaf of bread. While in the oven, bread reaches interior temperatures of 100°C (Bloksma, 1990a), during which several important physical, chemical and biochemical transformations take place. When bread is first placed in the oven, elevated temperatures cause yeast metabolism to increase and CO_2 production goes up (Campbell, 2003). This begins to taper off as higher temperatures (50°C) kill yeast cells. Heating also causes the thermal expansion of gases trapped within the dough structure. Carbon dioxide, ethanol and other compounds which are dissolved in the liquid phase of dough become less soluble. These components come out of solution and diffuse into the gas cells. Expansion of steam and other gases causes increased pressure within the gas cells (Campbell, 2003). The rheological properties of the cell walls (Dobraszczyk, 1994) and the viscous nature of the protein matrix allows gas cells to respond to increases in pressure by expanding rather than failing in the early stages of baking (Bloksma, 1990a). This phenomenon is known as “oven spring”. When the stress on thin bubble cell walls becomes too great, they rupture. This failure of still viscous cell walls which separate bubbles is called coalescence (Campbell, 2003). Coalescence produces larger round gas cells and is propagated by the pressure caused by crust formation (Hayman et al., 1998). Upon further heating, starch gelatinization occurs, causing the dough matrix to set (Bloksma, 1990a). Cell walls become solid and rupture. The structure becomes an

interconnected porous network of cells which is commonly referred to as bread crumb (Campbell, 2003).

2.2. Molecular Weight Distribution of Gluten Proteins: A Determinant of Physical Dough Properties

2.2.1. Wheat Storage Proteins (Gluten)

It has long been accepted that gluten proteins are largely responsible for the viscoelastic behavior of wheat flour doughs. Wheat gluten is composed of two families of protein polymers known as gliadin and glutenin. Glutenin proteins contribute to the strength and elastic properties of dough, whereas gliadin contributes to the plastic flow properties of dough. Based on molecular size and branching, wheat proteins are also commonly segmented into two groups known as monomeric and polymeric proteins (MacRitchie and Lafiandra, 1997).

2.2.1.1. Monomeric Proteins

Monomeric proteins consist of single chain polypeptides. In wheat, monomeric proteins are classified as either gliadins or albumins/globulins depending on their solubility (MacRitchie and Lafiandra, 1997). Gliadins are low molecular weight storage proteins with molecular weights ranging from 30,000 to 80,000. They can be divided into α-, β-, γ-, ω- gliadins based on molecular weight and electrophoretic mobility on Acid polyacrylamide gel electrophoresis (Acid PAGE) (MacRitchie and Lafiandra, 1997). Gliadins are notably high in glutamic acid but low in basic amino acids such as lysine and arginine (Lasztity, 1995). Albumins/globulins are low molecular weight proteins which are mainly enzymes. Their molecular weights range from 20,000-30,000. Unlike wheat storage proteins, albumins/globulins are high in the essential amino acid lysine.

2.2.1.2. Polymeric Proteins

In wheat, the polymeric protein fraction is mainly comprised of highly polymerized glutenin. These molecules can have molecular weights ranging from the millions to the tens of millions. They are comprised of two families of subunits, termed high and low molecular weight which are held together with disulfide bonds. High molecular weight glutenin subunits (HMW-GS) have molecular weights ranging from 80,000-120,000 (A-subunits) whereas the low

molecular weight glutenin subunits (LMW-GS) fall into two distinct size ranges, 40,000-55,000 (B-subunits) and 30,000-40,000 (C-subunits) (Southan and MacRitchie, 1999). During the post translational process, both HMW-GS and LMW-GS combine to create highly polymeric protein which is largely responsible for dough strength (Gupta et al., 1996).

2.2.2. Molecular Weight Distribution of Gluten Proteins

Determining the molecular weight distribution of wheat proteins has been a difficult task because it is particularly hard to solubilize and quantify the polymeric fractions (Southan and MacRichie, 1999). It is not possible to solubilize these HMW proteins without reducing intermolecular covalent disulfide bonds and as a result, significantly altering the structure (Singh et al., 1990). Singh et al. (1990) developed an extraction method which uses sonication to solubilize unreduced proteins in SDS sodium phosphate buffer. Unlike chemical reduction, the process of sonication selectively degrades only the largest glutenin polymers to make them soluble. If sonication time and intensity are closely controlled, these polymeric but now soluble proteins will still be large enough to distinguish from the other groups (Singh et al., 1990).

This new extraction method was used in combination with SE-HPLC to determine the molecular size distribution of wheat flour proteins and to separate them into three main classes; polymeric protein, gliadins, albumins/globulins (Singh et al., 1990; Gupta et al., 1993). Though this is not a completely ideal method for quantifying molecular size distributions of polymeric protein, it does provide relative size distributions which are based on the inverse relationship between solubility and molecular size (Gupta et al., 1993). Figure 2.1 shows a SE HPLC profile of wheat protein extracted from wheat flour using sonication. Three distinct molecular weight ranges are evident. In order of their elution from the column, they correspond to (1) polymeric proteins (>100,000), (2) gliadins (30,000-80,000) and (3) albumins/globulins (20,000-30,000).

Figure 2.1 SE-HPLC profile of total wheat protein extracted using sonication of a flour suspension in SDS buffer. Three main peaks are seen corresponding to (1) polymeric proteins (>100,000), (2) gliadins (30,000-80,000) and (3) albumins/globulins (20,000-30,000). Adapted from: MacRitchie and Lafiandra (1997)

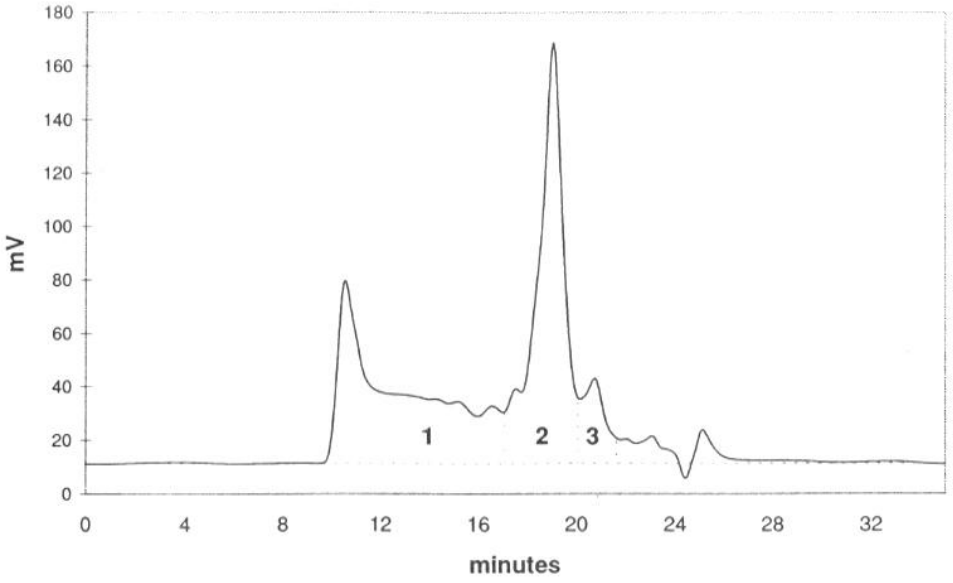

2.2.2.1. Shifts in Molecular Weight Distribution

In recent years, special interest has been given to glutenin proteins and particularly the HMW gluten and other polymeric protein subunits that make them up. These HMW subunits are important because they have the ability to greatly impact the molecular weight distribution of wheat proteins. The MW distribution of protein in wheat flour can be altered in two ways as shown in Figure 2.2; by varying the ratio of monomeric to polymeric proteins or by varying the size distribution of the polymeric proteins. Both of these factors are controlled by genetics and can in turn have a significant effect on dough functionality (MacRitchie and Lafiandra, 1997).

Figure 2.2 Two ways in which the molecular weight distribution of wheat proteins can increase (a) Shift in ratio of monomeric to polymeric protein. (b) Increase in size distribution of polymeric proteins. Adapted from MacRitchie and Lafiandra (1997).

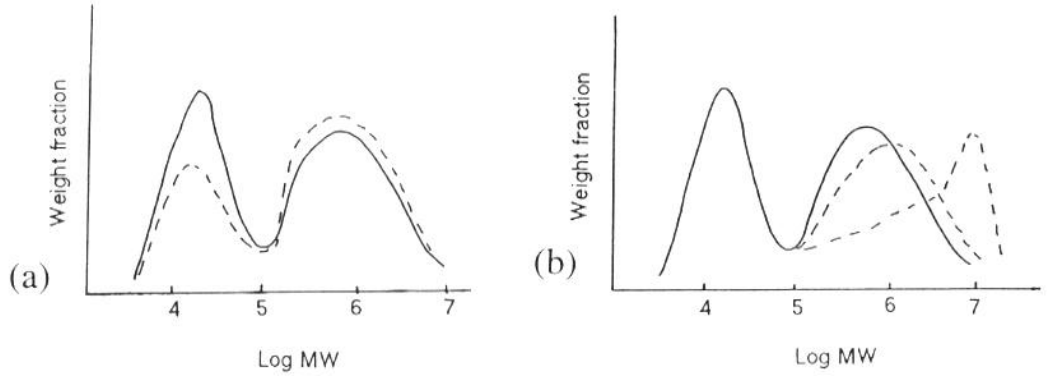

2.2.3. Relationship between Composition and Functionality

The relationship between wheat protein composition and functionality is a topic important to wheat breeders and cereal chemists alike. Gupta et al. (1992) used SE-HPLC to compare the effect of wheat protein content and composition on the functional properties of 15 hexaploid wheat varieties grown at six different nitrogen levels. The results suggest that polymeric glutenin protein has the most significant effect on functionality. Farinograph peak mixing time, and dough extensibility as measured by the extensograph, were dependent on the total glutenin content or the total amount of glutenin present in the flour. Bread loaf volume, dough maximum resistance (R_{max}), and mixograph development, on the other hand, were more dependent on the protein balance or the percentage of glutenin in the protein. These results illustrate that dough is a very complex material and that no single compositional parameter can explain all of it rheological and baking properties (Gupta et al., 1992; MacRitchie and Lafiandra, 1997).

Gupta et al. (1993) separated polymeric wheat storage proteins into two fractions, extractable and unextractable polymeric protein, based on their molecular size. Rheological quality measurements indicated that the relative percentage of each fraction had a significant impact on dough functionality. Figure 2.3 shows the SE-HPLC profiles of wheat proteins solubilized in 0.5% SDS-buffer. The highlighted peak in Figure 2.3a represents the total amount of polymeric protein which can be solubilized with the help sonication. The highlighted peak in Figure 2.3b shows the extractable polymeric protein. This is the proportion of the total polymeric

protein which is soluble in 0.5% SDS-Buffer without the use of sonication. The residue which remains after the extractable polymeric protein is removed (solubilized), is then sonicated in 0.5% SDS-Buffer solution to solubilize the remaining protein. This fraction which represents the percentage of very high molecular glutenins is seen in Figure 2.3. The unextractable polymeric protein fraction contains a significantly greater proportion of large polymers (≥158 K) when compared to the extractable polymeric protein.

Figure 2.3 SE-HPLC profiles of eluted wheat proteins. Highlighted peak (a) represents total polymeric protein which can be separated into peak (b) extractable polymeric protein and peak (c) unextractable polymeric protein. Chromatograms courtesy of Shuping Yan. Graphic modification courtesy of Michael Pickett.

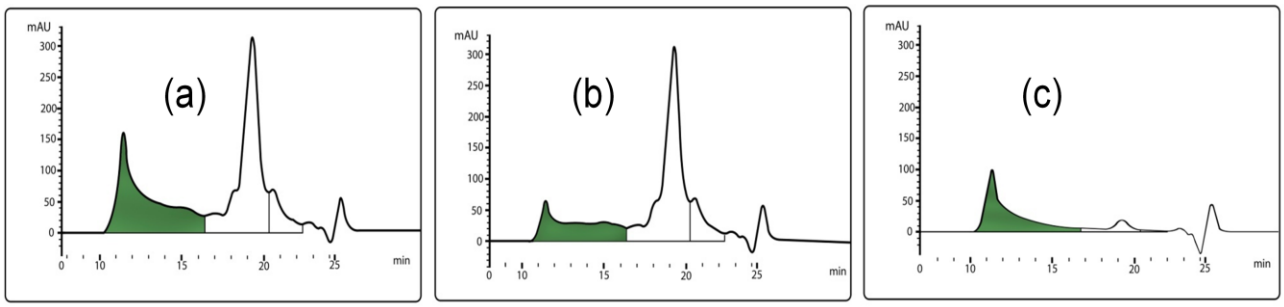

The relative amount of unextractable polymeric protein present in the total polymeric protein is highly correlated with dough strength (Gupta, 1993; MacRitchie and Lafandra, 1997). The top portion of Figure 2.4 shows the molecular weight distribution as well as the (highlighted) total polymeric protein and its correlation with extensograph strength (R_{max}) and mixograph dough development time (MDDT). Neither are well correlated (R^2 of 0.18 and 0.002, respectively) with the total polymeric proteins. The bottom portion of Figure 2.4 demonstrates that the amount of unextractable polymeric protein (highlighted), when separated from the rest of the polymeric protein and measured, is strongly correlated with extensograph strength and reasonably correlated with MDDT (R^2 of 0.86 and 0.58, respectively). This suggests that it is the large sized polymeric proteins (UPP) rather than the total amount of polymeric protein that plays the largest role in dough strength (Gupta, 1993).

Figure 2.4 Top Row: Molecular size distribution showing the total polymeric protein (highlighted) which is correlated with extensograph maximum resistance (R_{max} (BU)) and mixograph dough development time (MDDT). Bottom Row: Molecular size distribution showing only the unextractable polymeric protein (highlighted) which is correlated with extensograph strength and mixograph dough development time. Adapted from MacRitchie and Lafiandra (1997); Gupta, (1993).

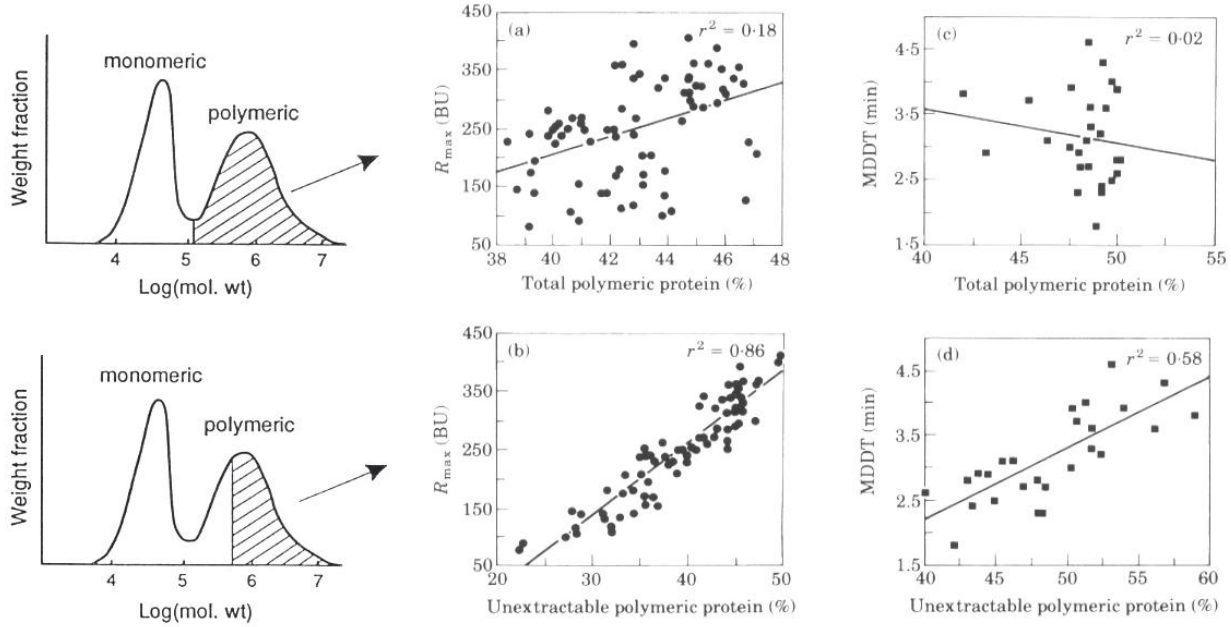

Bangur et al. (1997) presented even more evidence of the importance of HMW glutenins in providing dough strength. In their study 158 flours were analyzed using SE-HPLC and a column for which elution times were calibrated against standard proteins of known molecular weight. The percentage of the protein that eluted up to each time was correlated with extensograph dough maximum resistance (R_{max}) and dough extensibility (E). The highest correlation occurred after 13.2 minutes suggesting that protein polymers at or above the critical molecular weight of 250,000 are most responsible for dough strength. That critical MW was suggested as the point at which high molecular weight protein polymers begin to entangle.

2.3. Protein Entanglements: An Application of Polymer Science

It is clear that HMW glutenin polymers are largely responsible for variations in the important rheological properties of dough (MacRitchie and Lafiandra, 1997). It has been suggested that, at or above a critical molecular weight, entanglements between protein polymers play a significant role in forming the viscoelastic properties of wheat flour doughs (Bangur et al., 1997; Singh and MacRitchie, 2001; Dobraszczyk and Morgenstern, 2003). Termonia and Smith (1987) proposed a model for the tensile deformation of solid flexible polymers which "explicitly takes into account the role of the weak attractive forces between chains as well as chain slippage through entanglements". This theory was illustrated for wheat flour doughs (MacRitchie and Lafiandra, 1997) using a single protein polymer strand as depicted in Figure 2.5. When polymers are stretched, the weak interactive forces (van der Walls) between polymer strands are broken. Further deformation cannot then occur without the slippage of polymer chains through entanglements. Figure 2.5a shows a coiled entangled polymer which has not been elongated. b-d depicts several possible behaviors of those polymers under tensile stress as well as their corresponding draw ratios (extensibility). When the rate of chain slippage is faster than the rate of chain elongation (b), the structure has little strength and both the maximum stress and draw ratio are low. At the opposite extreme, (c) if the rate of elongation is much faster than the rate of chain slippage, than the chains will undergo a high level stress causing them to break suddenly. In the ideal case (d), the rates of both elongation and chain slippage are optimum. This combination leads to the highest draw ratio as well as dough with optimal strength and extensibility.

Figure 2.5 Schematic illustration showing the effects of protein polymer slippage rates on the draw ratio of wheat flour doughs. Adapted from (MacRitchie and Lafiandra, 1997)

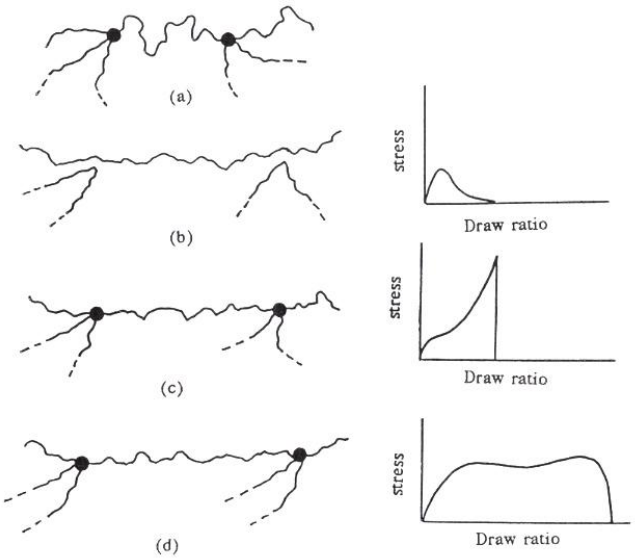

Much of the current understanding about how polymer morphology impacts the rheological properties of a material (polymer melt) has come from the study of petroleum derived polymers. Kraus and Gruver (1965) studied the effect of molecular weight and polymer branching on the rheological properties of multichain polybutadienes. As is seen in Figure 2.6, when a critical molecular weight, M_c, is reached (specific for each polymer), polymer entanglements begin to occur causing a drastic increase in viscosity. The branching of polymers results in an even greater increase in viscosity with strain known as strain hardening (Kraus and Gruver, 1965; Dobraszczyk and Morgenstern, 2003).

MacLeish and Larson (1998) described the rheological properties of HMW polymer melts by comparing them to a "pom pom" model. This model describes polymers with a single flexible backbone and branch points at their ends. As stress is placed on the polymer network, the flexible backbone between polymer entanglements stretches, causing strain hardening (MacLeish and Larson, 1998).

Figure 2.6 Effect of molecular weight and branching on the zero-shear viscosity for polymer melts. (M_c) represents the critical molecular weight for entanglements. (o) rapid increase in zero-shear viscosity for the linear polymer. (□) 3-armed branched polymer. (Δ) 4-armed branched polymer. Adapted from Kraus and Gruver (1965)

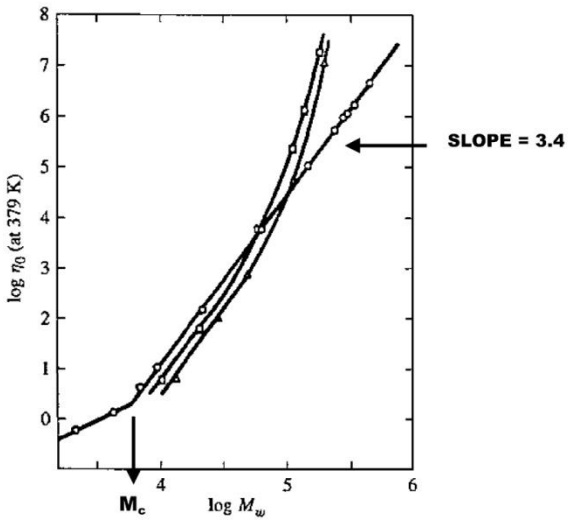

2.4. Rheological Properties of Expanding Gas Cells

During proofing and baking, gas cells undergo large biaxial extension at estimated strain rates of 10^{-3} sec^{-1} to 10^{-4} sec^{-1} (proofing) and 10^{-2} sec^{-1} to 10^{-3} sec^{-1} (baking) (Dobraszczyk, 1997). As they expand, cell walls must become thinner (Figure 2.7a). Plastic (unrecoverable) strain remains largely uniform until a maximum force is reached. After this point, expansion is no longer uniform, and inhomogeneities or areas of localized thinning begin to form on the gas cell surface (Dobraszczyk, 1999). These thin spots experience increased localized stress compared to the surrounding material. This can lead to "catastrophic failure" (Dobraszczyk, 1997) and coalescence of cell walls (vanVliet et al., 1992). Dough however, exhibits strain hardening ability. Strain hardening is defined as the phenomenon whereby stress increases more than proportionally with strain (van Vliet et al., 1992). As gas cells expand at high strain rates, entanglements between branched HMW gluten polymers create constrictions which resist the continued weakening of thin spots (Figure 2.7b) (Dobraszczyk and Morgenstern, 2003; Dobraszczyk 2004). Strain hardening, thus, causes the thin inhomogeneities in gas cells to expand at a rate slower than that of the surrounding area and thus "the initial damage is repaired"

(van Vliet, 1992). Doughs with a high amount of strain hardening ability inflate to higher volumes, have thinner cell walls and more even bread crumb than do those with less ability to strain harden (Dobraszczyk, 1997). Figure 2.8 shows the strong linear relationship (R=0.971) between strain hardening index of doughs made from various flours and the baked loaf volume of those doughs.

Figure 2.7 Schematic illustration showing (a) biaxial expansion and thinning of gas cell walls. Adapted from Dobraszczyk (1999) (b) A high molecular weight entangled protein polymer network where entanglements produce strain hardening. Adapted from Dobraszczyk and Morgenstern (2003)

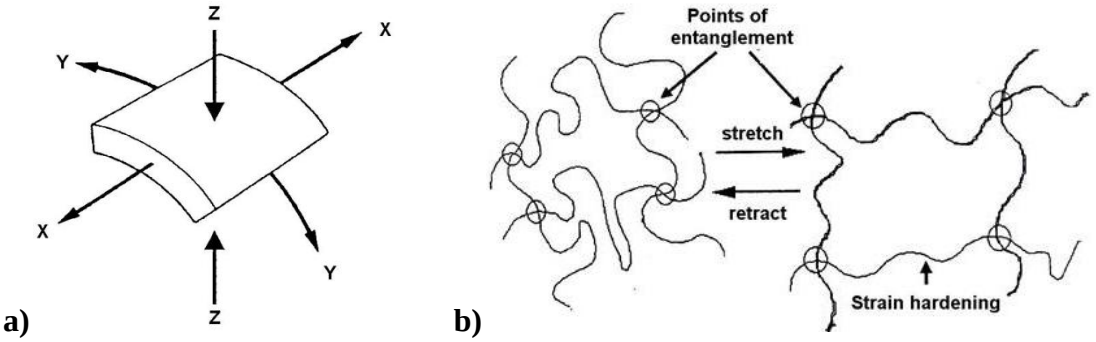

Figure 2.8 Relationship between baking volume and mean bubble cell wall strain hardening values measured at 50°C (R=0.971). Adapted from Dobraszczyk et al. (2003)

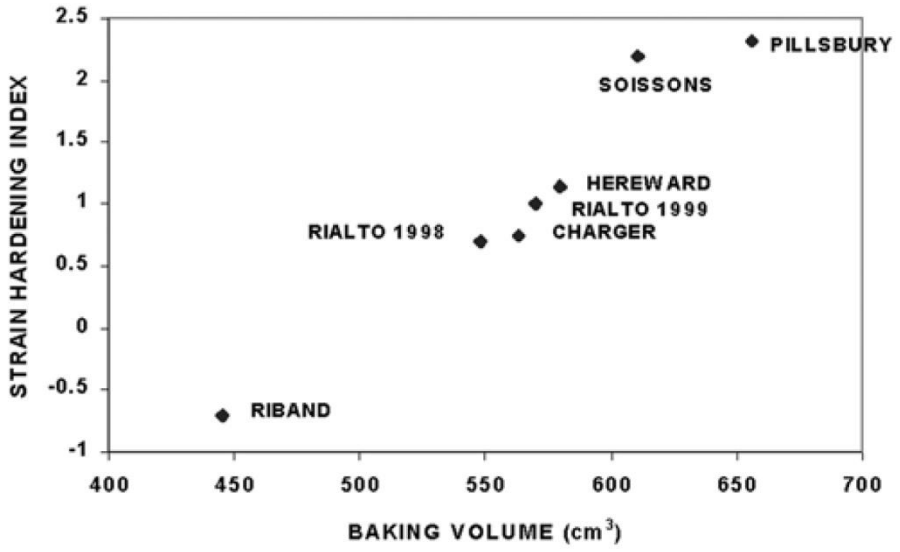

2.4.1. Measuring Strain Hardening (Dough Inflation System)

The strain hardening ability of dough is a key factor in gas cell stability, gas retention capacity, and over all bread quality (van Vliet et al., 1992; Dobraszczyk and Roberts, 1994; Dobraszczyk, 1997; Dobraszczyk and Morgenstern, 2003). During the breadmaking process, the majority of dough deformation (proofing and baking) is extensional in nature. Traditional empirical and fundamental dough testing methods however, measure dough rheology under shear deformation at strain rates that are quite different from those experienced by dough during breadmaking. The Dobraszczyk/Roberts dough inflation system is a device which measures extensional "dough rheology under conditions of strain similar to those of baking expansion" (Dobraszczyk, 1997). The inflation system uses "volume displacement of air" to inflate a sheet of dough into a bubble. When used in conjunction with a TA.XT2 plus texture analyzer, the system is capable of varying inflation speed so that the extensional rheology of the bubble walls can be measured at a constant strain rate of 0.1/sec. Bubbles are inflated until the point of rupture. Each inflation test generates a curve which is plotted as stress versus Hencky strain (Figure 2.9) The strain hardening index can then be calculated as the exponent of the stress-Hencky strain curve (Dobraszczyk et al., 2003).

Figure 2.9 Typical stress/Hencky strain curve for dough inflated at a constant strain rate of ($0.1s^{-1}$). Stress-strain data fitted to exponential model to calculate the strain hardening index (HI= 2.522). Courtesy of Bogdan Dobraszczyk

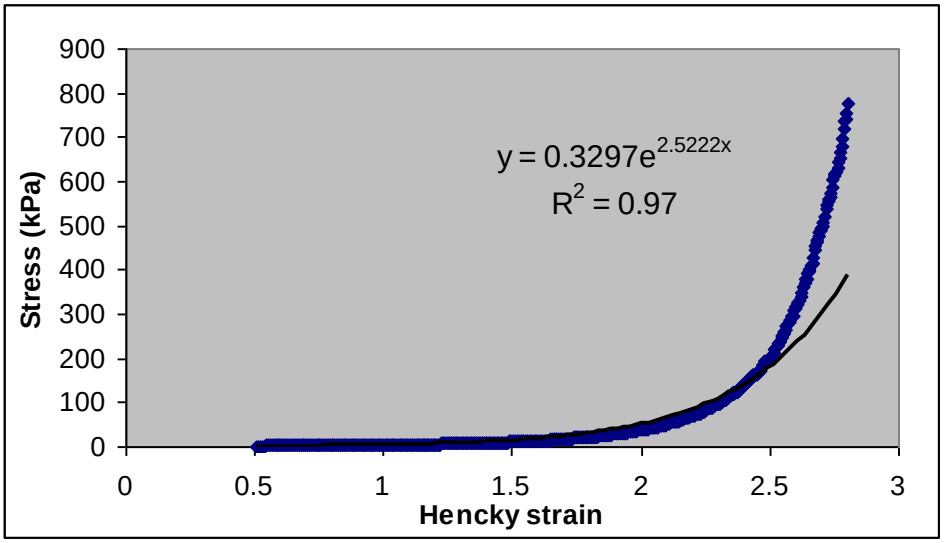

2.4.2. Strain Hardening at Elevated Temperatures

During baking, expanding gas cells undergo large extensional strains, at low strain rates and elevated temperatures (Dobraszczyk, 2004). Therefore, the ability of gas cells to undergo large deformation at high temperatures and remain stable, dictates the final crumb structure (Dobraszczyk and Morgenstern, 2003). Doughs that have high strain hardening ability form cell walls that are more able to resist rupture during the early stages of baking (van Vliet et al., 1992). Strain hardening ability varies among flour varieties and is also largely temperature dependent (Dobraszczyk et al., 2003)

Dobraszczyk et al. (2003) used the dough inflation system to study the effect of heat on the strain hardening properties of doughs made from both weak and strong wheat flours. When tested at 20°C, weak doughs displayed some strain hardening ability. These same doughs when tested at 40°C were virtually unstable and had lost their strain hardening ability. The strong doughs on the other hand retained all of their strain hardening ability even when tested at temperatures of 50°C. This comparison makes it possible to place flours into two distinct groups: Weak doughs, whose gas cells become unstable when heated and strong doughs whose gas cells remain stable even at temperatures nearing the gelatinization temperature of starch.

2.4.3. Disabling Mechanisms

There has been a great deal of work done to develop better understanding of gas stability in breadmaking (van Vliet et al., 1992; Dobraszczyk, 1997; Dobraszczyk, 2004). As gas cells expand during the proofing and baking process, there are several disabling mechanisms that can have a negative effect on their stability.

2.4.3.1. Coalescence

Coalescence is a gas cell disabling mechanism that occurs when the films separating gas cells fail. During gas cell growth, dough films undergo biaxial extension. The ability of these films to withstand biaxial extension will determine their ability to resist coalescence. During the early stages of proofing, gas cells are spherical in shape (Figure 2.11a) and do not physically contact each other. By the end of the proofing stage however, expanded gas cells begin to touch causing them to take on a polyhedral shape as seen in Figure 2.11b. When in close contact, the formation and propagation of localized weak spots in dough films may ultimately lead to gas cell

Figure 2.10 Stress/Hencky strain curves for doughs made from wheat flour varieties inflated at 20, 40, 50 and 60°C. (a) Strong dough (Hereward) displays high strain hardening ability even when tested at 50°C (b) Weak dough (Riband) displays very little stability at increased temperatures. Adapted from Dobraszczyk et al. (2003)

(a)

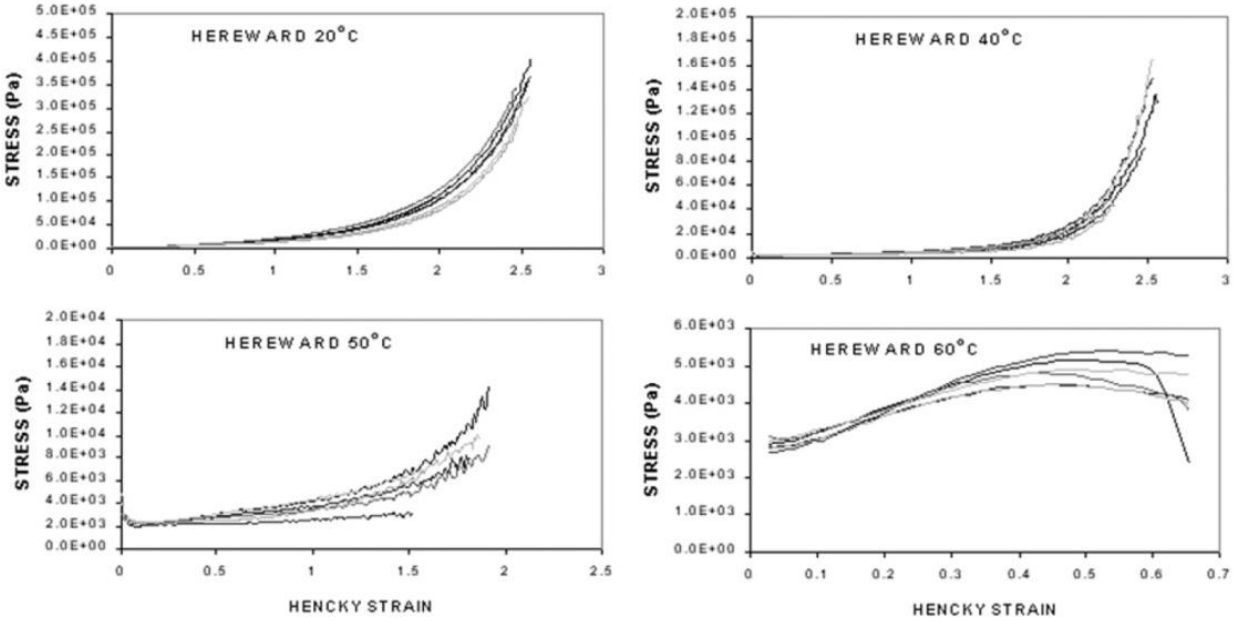

(b)

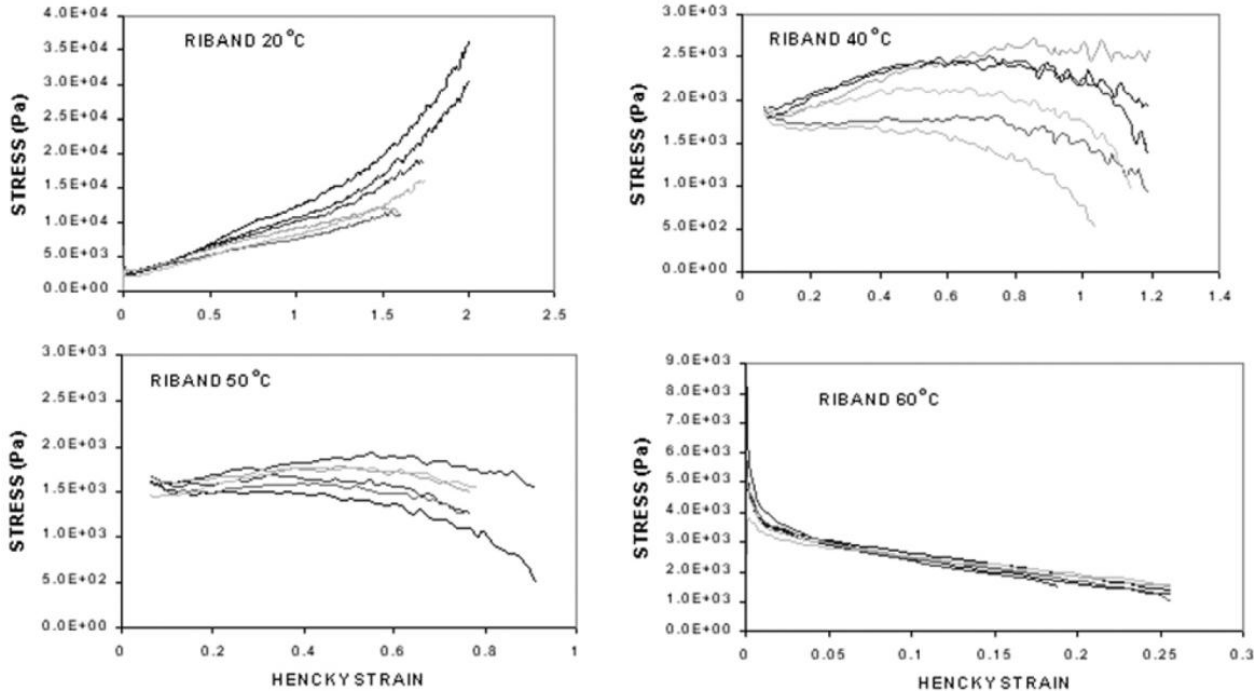

rupture or coalescence (van Vleit et al., 1992). This mechanism causes both a decrease in bubble numbers as well as the coarsening of bubble structure (Campbell, 2003).

2.4.3.2. Disproportionation

Disproportionation, also known as Ostwalt ripening, is a failure theory that has been proposed for bread dough. It is defined as the growth of large gas cells at the expense of small ones which is caused by differences in Laplace pressure between gas cells. This pressure difference is caused by the curvature of the liquid gas interface and is given by the equation:

$$\Delta P = 2\gamma / R$$

where R = radius of the gas cell and γ = interfacial tension. Small gas cells have higher ΔP values than do larger gas cells causing the walls of small gas cells to have higher equilibrium gas concentrations than larger cells. This difference in concentration can result in the transport of gas through the liquid phase of small gas cells and into larger ones causing an increase in the number of large gas cells contained in a dough (van Vliet et al., 1992).

Figure 2.11 Schematic illustration of proving dough. (a) Spherical shape of gas cells in the initial stages of proving (b) polyhedral shape of expanded gas cells in the later stages of proving. Adapted from van Vleit et al. (1992)

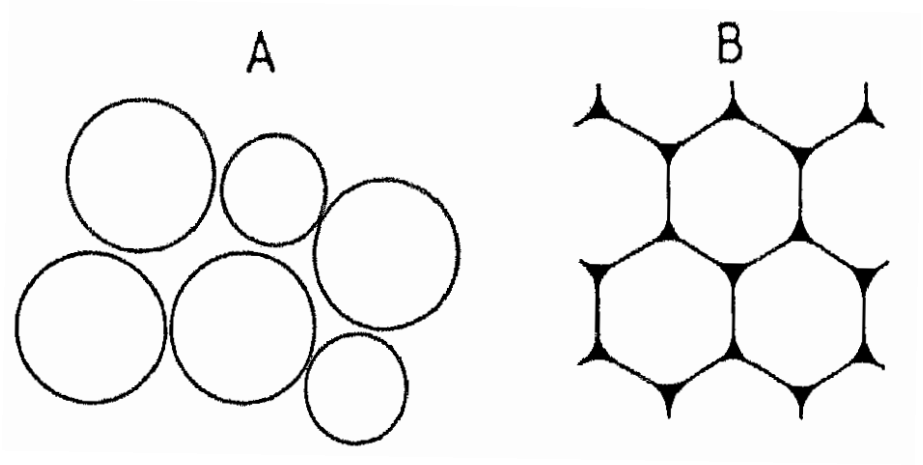

2.5. Characterization of Dough Microstructure

The microstructure of food products determines to a large extent the physical, textural and sensory properties of these products. Developing a proper understanding of the microstructure, particularly the spatial distribution and interaction of food components is a key tool in developing products with desired mechanical and organoleptic properties.

There has been an increased interest in food microstructures due to the fact that consumers' preferences have shifted to foods with more aesthetic appeal, superior taste, and convenient products. Most elements that determine these food qualities exist at micro-level and have focused the attention of food manufacturers (Aguilera, 2005; Lim and Barigou, 2004). Several techniques have been used to study food microstructures and these include microscopy (Ferrando and Spiess, 2000), magnetic resonance imaging (Maas and Line, 1995), computer vision technique (cameras) (Hullberg, and Ballerini, 2003; Du and Sun, 2006), porosimetry (Rahman et al., 2002; Kassama and Ngadi, 2005) and most recently X-ray computed tomography (Falcone et al., 2004; Trater et al., 2005; Leonard et al., 2008).

Quantification of occluded air in dough and gas cell distributions is challenging due to the very nature of dough matrix. The density measurement is a simple procedure to determine the extent to which dough can incorporate and retain air in the form of gas cells as a bulk. Previous studies have shown that strong flours occlude less air than weak flours during mixing (Baker and Mize, 1946; Chiotellis and Campbell, 2003). However density measurement technique does not provide information on the distribution of air cells within the dough matrix.

Several researchers used digital imaging techniques to obtain more detailed information on gas cell distribution (Zghal et al., 1999; Rouille et al., 2005; Whitworth et al., 2005). Digital imaging techniques use simple photographic procedures to determine gas cell distribution by evaluating differences in the intensity of reflected light. Conventional 2D digital imaging techniques, e.g. light microscopy, scanning electron microscopy and digital video imaging, are destructive in nature because sample preparation involves cutting to expose the cross-section to be viewed, which can alter structural features. Additionally, results from 2D images do not provide accurate information on cell size distribution, as cells are generally sliced-off center and the diameters measured from the image depend on the depth of the cut (Campbell and Mougeot, 1999; Scanlon and Zghal, 2001; Lim and Barigou, 2004). Another problem in conventional imaging techniques is obtaining adequate contrast between air and solid phases, for which

lighting and angle of illumination play an important role. Image post processing techniques and mathematical treatments such as Fourier transformation techniques to enhance distinction between the phases are often complex and time consuming (Smolarz et al., 1989; Gao et al., 1999; Barret and Peleg, 1992). Despite the technological and scientific importance of acquiring quantitative data on the cell size distribution in dough, dough's opacity and fragility make it difficult to acquire such data.

The advent of powerful non-invasive techniques such as X-ray microtomography (XMT) enable better characterization of internal structures of food products. Microtomographical techniques work in the same way as the x-ray tomography systems (CAT-scans) used in medicine but with much finer resolution. They involve targeting the specimen with a polychromatic X-ray beam with high spatial coherence. The x-rays not absorbed by the specimen fall on specifically designed x-ray scintillators that produce visible light, which is then recorded by a charge-coupled device (CCD) camera (Trater et al., 2005). A tomographic scan is accomplished by rotating the specimen between a fixed x-ray source and detector, around the axis perpendicular to the x-ray beam while collecting radiographs of the specimen at small angular increments in the range 0-360°. The radiographs are reconstructed into a series of 2-D slices. The series of 2-D slices are then reconstructed into a 3-D image. The resulting XMT data can be visualized by 3-D rendering of 2-D slices derived from a virtual model using dedicated software that allows reconstruction of cross-sections at various depth increments and along any desired orientation of the plane of cut.

High resolution XMT has been used to interrogate the microstructure of a number of materials in a wide variety of applications in science and engineering where accurate 3-D imaging of internal structure of objects is crucial, such as bone analysis, microelectronics, and materials, biological and geological sciences (Trater et al., 2005; Dogan 2007). Lim and Barigou (2004) studied 3-D cellular microstructures of a number of solid and semi-solid food products (aerated chocolate, mousse, marshmallow, muffin) using XMT. They developed a 3-D model of foam microstructures by combining image analysis with a stereological technique to obtain quantitative information on spatial cell size distribution, cell wall thickness distribution, connectivity, and voidage.

Bellido et al. (2006) measured gas cell size distributions in non-yeasted wheat flour doughs using x-ray tomography. That analysis showed gas cells typically range from between

10 and 300 μm in diameter. The number of gas cells was also measured and found to be 30,000 and 56,000 per cm^3 for stiff and slack doughs, respectively (Bellido et al., 2006).

Babin et al. (2006) used fast X-ray microtomography to study bubble growth during breadmaking. Their experimental findings confirm that the cellular structure is largely acquired during proofing, the gas cells and cell wall distributions are not significantly changed when compared with their evolution during proofing. The radii of thousands of bubbles were tracked throughout the process. Analysis showed that the dough void fractions increased from 0.1 to 0.7 during proving. The first stage of bubble growth was dominated by smooth size increases due to free bubble growth. In the second stage of proving, cell structure becomes more heterogeneous with the formation of many larger gas cells. Finally, gas cell coalescence prevailed, creating voids or gas cavities in the structure. Both of these studies demonstrate the usefulness of X-ray tomography for studying bread aeration and gas cell stability (Babin et al., 2006).

2.6. References

Aguilera, J.M. 2005. Why food microstructure? Journal of Food Engineering 67(1-2), 3-11.

Babin, P., Della Valle, G., Chiron, H., Cloetens, P., Hoszowska, J., Pernot, P., Reguerre, A.L., Salvo, L. and Dendievel, R. 2006. Fast X-ray tomography analysis of bubble growth and foam setting during breadmaking. Journal of Cereal Science. 43, 393-397.

Baker, J.C. and Mize, M.D. 1941. The origin of the gas cell in bread dough. Cereal Chemistry 18, 19-34.

Baker, J.C. and Mize, M.D. 1946. Gas occlusion during dough mixing. Cereal Chemistry 23, 38-51.

Bangur, R., Batey, I.L., McKenzie, E. and MacRitchie, F. 1997. Dependence of extensograph parameters on wheat protein composition measured by SE-HPLC. Journal of Cereal Science. 25, 237-241.

Barilan, J. and Peleg, D. 1992. Distributed resource-allocation algorithms. Lecture Notes in Computer Science 647, 227-291.

Bellido, G.G., Scanlon, M.G., Page, J.H. and Hallgrimsson, B. 2006. The bubble size distribution in wheat flour dough. Food Research International 39, 1058-1066.

Bloksma, A.H. 1990a. Rheology of the breadmaking process. Cereal Foods World 35(2), 228-235.

Bloksma, A.H. 1990b. Dough structure, dough rheology and baking quality. Cereal Foods World 35(2), 237-243.

Campbell, G.M., Rielly, C.D., Fryer, P.J. and Sadd, P.A. 1991. "The measurement of bubble size distributions in an opaque food fluid." Trans. IChemE, Part C: Food and Bioproducts Processing, 69, 67-76.

Campbell, G.M. and Mougeot, E. 1999. Creation and characterization of aerated food products. Trends in food science and Technology 10(9), 283-296.

Campbell, G.M, 2003. Bread aeration, in *Breadmaking: Improving Quality,* S. Cauvain (Ed.), pp. 352-374, Woodhead Publishing Ltd.,Cambridge, UK

Carlson, T. and Bohlin, L. 1978. Free surface energy in the elasticity of wheat flour dough. Cereal Chemistry 55, 539-544.

Cauvain, S.P., Whitworth, M.B. and Alava, J.M. 1999. The evolution of bubble structure in bread doughs and its effect on bread structure, in *Bubbles in Food*, Campbell, G.M., Webb, C., Pandiella, S. and Niranjan, K. (Ed.), pp 85-88, American Association of Cereal Chemists, St. Paul, Minnesota.

Chin, N.L., Martin, P.J. and Campbell, G.M. 2005. Dough aeration and rheology: Part 3. Effect of the presence of gas bubbles in bread dough on measured bulk rheology and work input rate. Journal of the Science of Food and Agriculture 85, 2203-2212.

Chiotellis, E. and Campbell, G.M. 2003. Proving of bread dough II measurement of gas production and retention. Trans IChemE 81(C), 207-216.

Dobraszczyk, B.J. and Roberts, C.A. 1994. Strain hardening and dough gas cell-wall failure in biaxial extension. Journal of Cereal Science 20, 265-274.

Dobraszczyk, B.J. 1997. Development of a new dough inflation system to evaluate doughs. Cereal Foods World 42(7), 516-519.

Dobraszczyk, B.J. 1999. Measurement of biaxial extensional rheological properties using bubble inflation and the stability of bubble expansion in bread doughs, in *Bubbles in Food,* Campbell, G.M., Webb, C., Pandiella, S. and Niranjan, K. (Ed.) pp 173-182, American Association of Cereal Chemists, St. Paul, Minnesota.

Dobraszczyk, B.J. and Morgenstern, M.P. 2003. Rheology and the bread making process. Journal of Cereal Science 38, 229-245.

Dobraszczyk, B.J., Smewing, J., Albertini, M., Maesmans, G. and Schofield, J.D. 2003. Extensional rheology and stability of gas cell walls in bread doughs at elevated temperatures in relation to breadmaking performance. Cereal Chemistry 80(2), 218-224.

Dobraszczyk, B.J. 2004. The physics of baking: rheological and polymer molecular structure function relationships in breadmaking. Journal of Non-Newtonian Fluid Mechanics 124, 61-69.

Du, C.J. and Sun, D.W. 2006. Learning techniques used in computer vision for food quality evaluation: a review. Journal of Food Engineering 72 (1), 39-55.

Falcone, P.M., Baiano, A., Zanini, F., Mancini, L., Tromba, L. and Dreossi, D. 2004. A novel approach to the study of bread porous structure: Phase-contrast X-ray microtomography. Journal of Food Science 69 (1), 38-43.

Ferrando, M. and Spiess, W.E.L. 2000. Review: Confocal scanning laser microscopy. A powerful tool in food science. Food Science and Technology International 6, 267-284.

Gao, Q.H., Yin, F.F. and Nie, K.W. 1999. Treatment field shape verification using elliptic Fourier transform. Medical Physics 26(11), 2415-2421.

Gupta, R.B., Batey, I.L. and MacRitchie, F. 1992. Relationships between protein composition and functional properties of wheat flours. Cereal Chemistry 69(2), 125-131.

Gupta, R.B., Khan, K. and MacRitchie, F. 1993. Biochemical basis of flour properties in bread wheats I. Effects of variation in the quantity and size distribution of polymeric protein. Journal of Cereal Science 18, 23-41.

Gupta, R.B., Masci, S., Lafiandra, D., Bariana, H.S. and MacRitchie, F. 1996. Accumulation of protein subunits and their polymers in developing grains of hexaploid wheats. Journal of Experimental Botany 47(302), 1377-1385.

Hayman, D., Hoseney, R.C. and Faubion, J.M. 1998. Effect of pressure (crust formation) on bread crumb grain development. Cereal Chemistry 75(5), 585-589.

Hoseney, R.C., Zeleznak, K. and Lai, C.S. 1986. Wheat gluten: A glassy polymer. Cereal Chemistry 63(3), 285-286.

Hullberg, A. and Ballerini, L. 2003. Pore formation in cured-smoked pork determined with image analysis - effects of tumbling and RN- gene. Meat Science 65(4), 1231-1236.

Junge, R.C., Hoseney, R.C. and Varriano-Marston, E. 1981. Effect of surfactants on air incorporation in dough and the crumb grain of bread. Cereal Chemistry 58(4), 338-342.

Kassama, L.S. and Ngadi, M.O. 2005. Pore structure characterization of deep-fat-fried chicken meat. Journal of Food Engineering 66 (3), 369-375.

Kraus, G. and Gruver, J.T. 1965. Rheological properties of multichain polybutadienes. Journal of Polymer Science: Part A 3, 105-122.

Lasztity, R. 1995. Wheat Proteins, in *Chemistry of Cereal Proteins*, pp. 19-138, CRC Press, New York.

Leonard, A., Wullens, H., Blacher, S., Marchot, P., Toye, D., Crine, M. and Lodewyckx, P. 2008. In situ observation of wall effects in activated carbon filters by X-ray microtomography. Separation and Purification Technology 64(1), 127-130.

Lim, K.S. Barigou, M. 2004. X-ray micro-computed tomography of cellular food products, Food Research International, 37(10), 1001-1012.

Maas, J.L. and Line, M.J. 1995. Nuclear-magnetic-resonance microimaging of strawberry flower buds and fruit. Horticulture Science 30(5), 1090-1096.

MacLeish, T.C.B. and Larson, R.G. 1998. Molecular constitutive equations for a class of branched polymers. Journal of Rheology 42, 81-110.

MacRitchie, F. and Lafiandra, D. 1997. Structure-function relationships of wheat proteins in: *Food Proteins and Their Applications*. S. Damodaran and A. Paraf (Eds), pp. 293-323, Marcel Dekker: New York.

Rahman, M.S., Al-Amri, O.S. and Al-Bulushi, I.M. 2002. Pores and physico-chemical characteristics of dried tuna produced by different methods of drying. Journal of Food Engineering. 53 (4), 301-313.

Rouille, J., Della Valle, G., Devaux, M.F., Marion, D. and Dubreil, L. 2005. French bread loaf volume variations and digital image analysis of crumb grain changes induced by the minor components of wheat flour. Cereal Chemistry 82(1), 22-27.

Scanlon, M.G. and Zghal, M.C. 2001. Bread properties and crumb structure. Food Research International 34(10), 841-864.

Shah, P., Campbell, G.M., Mckee, S.L. and Rielly, C.D. 1998. Proving of bread dough: modeling the growth of individual bubbles. Trans IChemE 76, 73-79.

Singh, N.K., Donovan, G.R., Batey, I.L. and MacRitchie, F. 1990. Use of sonication and size-exclusion high-performance liquid chromatography in the study of wheat flour proteins. I. Dissolution of total proteins in the absence of reducing agents. Cereal Chemistry 67(2), 150-161.

Singh, H. and MacRitchie, F. 2001. Application of polymer science to properties of gluten. Journal of Cereal Science. 33, 231-243.

Smolarz, A., Vanhecke, E. and Bouvier, J.M. 1989. Computerized image-analysis and texture of extruded biscuits. Journal of Texture Studies 20(2), 223-234.

Southan, M. and MacRichie, F. 1999. Molecular weight distribution of wheat proteins. Cereal Chemistry 76(6), 827-836.

Termonia, Y. and Smith, P. 1987. Kinetic model for tensile deformation of polymers. 1. Effect of molecular weight. Macromolecules 20(4), 835-838.

Trater, A.M., Alavi, S. and Rizvi, S.S.H. 2005. Use of non-invasive X-ray microtomography for characterizing microstructure of extruded biopolymer foams. Food Research International 38 (6), 709-719.

van Vleit, T. 1999. Physical factors determining gas cell stability in a dough during bread making. in *Bubbles in Food*, Campbell, G.M., Webb, C., Pandiella, S. and Niranjan, K. (Ed.) pp 121-128, American Association of Cereal Chemists, St. Paul, Minnesota.

Whitworth, M. B. and Alava, J. M. 2005. Non-destructive imaging of bread and cake structure during baking. Source: Using cereal science and technology for the benefit of consumers. Proceedings of the 12th International ICC and Bread Congress, 456-460.

Zghal, M.C., Scanlon, M.G. and Sapirstein, H.D. 1999. Prediction of bread crumb density by digital image analysis. Cereal Chemistry 76(5), 734-742.

CHAPTER 3 - **Materials and Methods**

3.1. Materials

Three untreated and unbleached flours of distinctly different strength, Karl92, BZ20 and Alpowa, were selected for use in this study. Karl 92, a hard red winter variety commonly grown in Kansas (2006 growing season), was obtained from KSU Foundation Seed, Kansas State University. BZ 20 is a hard white spring wheat commonly known to have strong baking properties. Alpowa is a soft white spring wheat which is known to contain the 5+10 HMW glutenin banding pattern. Both BZ 20 and Alpowa flours were obtained from the USDA Western Wheat Quality Lab (2007 growing season), Pullman Washington. Karl92 was milled on the Buhler mill in the Department of Grain Science and Industry, while BZ20 and Alpowa were milled on the Miag Multomat mill prior to shipping to Kansas State.

In order to compare protein quality of flour varieties at equal protein content, part of the Karl 92 sample was mixed with native wheat starch (Midsol 50, MGP ingredients, Atchison, KS) to adjust its protein content to that of BZ 20. The resulting flour was used as the fourth type of flour and for the purpose of this study will be called Karl Adjusted. All flours were packed in airtight plastic bags and stored at -20ºC until the time of use. For the sake of brevity Karl 92, Karl Adjusted, and BZ 20 flours will simply be referred to as Karl, KA and BZ.

3.2. Physico-chemical Analysis of Wheat Flours

3.2.1. Proximate Analysis

Flour protein content was determined by the nitrogen combustion method using the LECO Fp-2000 Nitrogen/protein analyzer using a factor of 5.7 to convert N to protein (AACC 46-30). Moisture content was measured by the oven-air method (AACC 44-15A). Flour ash content was measured using the muffle furnace overnight method (AACC 08-02).

3.2.2. Protein Quality

Size exclusion high performance liquid chromatography (SE-HPLC) (Hewlett-Packard 1100 Agilent HPLC) was performed on each flour to characterize the relative proportions and size of gluten proteins. Proteins were fractionated on a Biosep SEC-4000 column with a Phenomenex, Torrance, CA system using Phosphate/SDS buffer (pH 6.9) as the mobile phase

injected at a flow rate of 0.5 ml/min and a the total injection volume of 20 µl/sample. Proteins were detected by absorption at 214 nm in SE-HPLC. Separate samples were prepared to analyze total, extractable and unextractable polymeric protein. SEC-HPLC data was analyzed using software program ChemStation (Agilent Technologies, USA).

3.2.2.1. Total Protein Analysis

For the total protein analysis, 10 mg of flour sample was weighed into a 1.7 mL microfuge tube along with 1mL of phosphate/SDS buffer. Samples were placed in a vortex for 5 minutes to disperse flour into solution. That was followed by sonication at 6 watts for 15 seconds (60 Sonic Dismembrater, Fisher Scientific) at room temperature. The solutions were then centrifuged at 12,000 rpm for 20 minutes. The supernatant was filtered (0.45µm pore) before loading into an HPLC vial.

3.2.2.2. Extractable and Unextractable Protein Analysis

For the extractable protein analysis, 10 mg of flour sample was weighed into a 1.7mL microfuge tube along with 1mL of phosphate/SDS buffer. Samples were placed in a vortex for 5 minutes to disperse flour into solution. The solutions were then centrifuged a 12,000 rpm for 20 minutes. The supernatant was filtered (0.45µm) for SE HPLC analysis. The pellet was retained for unextractable protein analysis. Phosphate/SDS buffer (1 mL) was added to the pellet and then vortexed for 10 minutes. After vortexing, the solutions were sonicated for 25 seconds at 6 watts to systematically reduce the size of the high molecular weight proteins. Protein samples were then centrifuged at 12,000 rpm for 20 minutes. The filtered supernatant was used for SE-HPLC analysis.

3.3. Dough Mixing Properties

Dough mixing properties were evaluated using a 10g mixograph (National Manufacturing Co., Lincoln, NE) using AACC method no 55-40. Flour weights were adjusted to a 14% moisture basis. Peak development time was used as a basis to determine optimum mix times for test baking.

3.4. Biaxial Extensional Rheology

Doughs were tested using the Dobrazyzyk-Roberts dough inflation system (D/R DIS) (Stable Micro Systems, Godalming, Surrey, UK) mounted on a TAXT2Plus texture analyzer (Texture Technologies, Scarsdale, NY). Water absorptions for dough inflation testing were optimized using a 10 g mixograph (National Manufacturing Co., Lincoln, NE). Doughs for rheological testing were mixed in a 100 g pin mixer (National Manufacturing Co., Lincoln, NE). After mixing, doughs were gently pressed by hand and placed onto an oiled plastic mat. A thin layer of paraffin oil was brushed over the dough to prevent drying. After 5 minutes of resting, doughs were hand rolled out to a thickness of 8 mm. After each pass, of the dough roller was rotated 90º and then given a few seconds to relax. This was done to prevent anisotropic effects during the dough inflation. Total sheeting time was two minutes. After sheeting, doughs were given 10 minutes to relax and then were cut into circular discs using a 55mm cookie cutter. Dough disks were placed in well oiled dough inflation pots and then compressed to a thickness of 2.67 mm for 30 seconds. The pots were stored covered at 30°C in the temperature controlled chamber for 30 minutes prior to inflation. Doughs were inflated at room temperature at a constant strain rate of 0.1/sec until the point of bubble rupture. The inflation curve generated for each test plotted as stress versus Hencky strain as discussed by Dobraszczyk (1997). The strain hardening index was then calculated as the exponent of the stress-Hencky strain curve. Three replicates (separate dough batches) were performed for each flour type. The data for each replicate was taken as an average of three inflated dough disks taken from independently mixed doughs.

3.5. Test Baking

Baked loaves were prepared using the 100g (flour weight) straight-dough procedure (AACC 10-10B). Doughs were mixed in a 100g National pin mixer. Water absorptions and mix times were optimized for each of the flours according to the method. Doughs were punched twice throughout the process and then molded using a Tompson pup loaf molder. All doughs were proved at 30°C and 95% relative humidity for 40 minutes, then baked at 210°C in a reel oven (National Manufacturing, Lincoln, NE) for 24 minutes. Loaf volume was measured using a calibrated rape seed displacement meter (400 cm^3) immediately after the loaves were removed from the oven.

Crumb structure of baked loaves was characterized using C-Cell image analysis software and equipment (Calibre Control International Ltd., UK). Loaves were sliced into 1.5 cm thick slices using a rotary disc food slicer (Chefs Choice International). Only the central (middle) slice was used for analysis. Image analysis parameters collected include: number of cells, average cell wall thickness, and cell diameter.

3.6. Dough and Bread Microstructure

Both bread and frozen dough samples were scanned using a high resolution desktop X-ray microtomograph (XMT) (Skyscan1072, Belgium) (Figure 3.1a). consisting of an X-ray tube, an X-ray detector and a CCD-camera (Figure 3.1b). The scanning process was controlled by a software package which also allowed for microtomographical reconstruction using a filtered back-projection algorithm. Angular projections were used to generate hundreds of 2-D cross-sectional images for each sample scanned. 3-D objects were then reconstructed from multiple 2-D shadow images (radiographs) and virtually sliced to create 2-D cross-sectional images for quantitative analysis. The gas bubbles were identified by their low grey value (low absorption coefficient) within the dough and bread matrix.

Figure 3.1 (a) High resolution desktop X-ray microtomograph (Skyscan1072, Belgium) (b) Schematic diagram of X-ray microtomography (Lim and Barigou, 2004)

(a) (b)

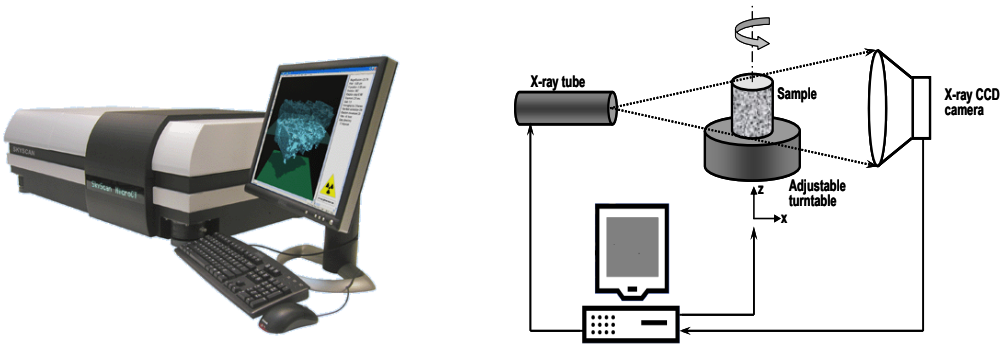

3.6.1. Frozen Dough Sample Preparation

Frozen doughs samples were needed in order to study gas cell structure and stability throughout the proofing process. Being a dynamic biological system, dough microstructure

changes continuously during scanning (typically 20-30 min) which causes blurry shadow images (radiographs). In order to stabilize specimen microstructure the dough samples were frozen to inactivate yeast and thus to terminate fermentation prior to scanning.

Doughs were prepared by the same procedure used for baking (AACC straight-dough Method 10-10B). After molding, doughs were placed on a flat plastic sheet and frozen after 0 min, 20 min, and 40 min of proving. Before freezing, a bread knife was used to gently remove approximately the ends of each of the proofed loaves to speed up the freezing process. The remaining loaf center sections which were approximately 1.5 inches long were then frozen (Legaci Refrigeration Systems, Asheville, NY) at -80°C to prepare for XMT scanning.

Frozen sections were cut in half in parallel to the cut ends. A thin blade saw was used to cut a slice (7-8 mm) of frozen dough from the middle of each of the sections. Frozen dough slices were kept on dry ice in styrofoam boxes to prevent melting during the cutting process. Two dough specimens approximately 12mm x 8mm each were carefully cut from the top and middle (Figure 3.2a) of each dough slice using a thin blade saw and X-acto knife™. Any freezing artifacts (holes) were avoided by moving slightly to the left or right of center to cut the sample. After cutting, the bottom of each frozen specimen was marked using a permanent marker so that top/bottom sample orientation could be maintained. Samples were stored frozen in small air tight containers until XMT scanning.

Frozen dough specimens were removed from the freezer and cryomounted on 12 mm sticky Styrofoam discs to adhere the sample firmly in place. Samples on the discs were then secured to the bottom of a 15 mm diameter insulated plastic container with a lid (Figure 3.2 c). A small cylinder shaped piece of dry ice was placed at the top of the tube to keep the sample frozen during the scanning process. Finally the insulated plastic container was secured on the sample stage (turntable).

Figure 3.2 (a) Top and middle sampling locations of frozen dough slice, (b) Pieces of cut frozen dough sample, (c) Sample holder used for XMT scanning of frozen dough

(a) 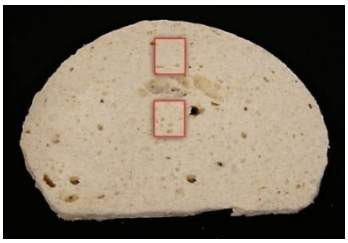 (b)  (c) 

3.6.2. Bread Sample Preparation

24 hours after baking, a center slice (8 mm thick) was cut from each of the baked loaves using an electric food slicer (Chefs Choice International). Rectangular specimens approximately 12mm x 8mm were then carefully cut from the top and middle (Figure 3.3) of each slice using a bread knife and a pair of sharp scissors. A clear plastic craft tube (15 mm diameter) was used as a sample holder to prevent drying of the bread sample during the scanning process. The bread samples were adhered bottom down to a foam circle (13 mm diameter, 3 mm thickness) with two sided adhesive and gently stuck to the sample holder for XMT scanning. The sample holder was then attached to the flat XMT sample base using parafilm.

Figure 3.3 (a) Top and middle sampling locations of bread slice. (b) Sample holder used for XMT scanning.

(a)  **(b)** 

3.6.3. X-ray Microtomography and Image Reconstruction

The bread and frozen dough samples were scanned using the desktop X-ray microtomography (XMT) imaging system (Model 1072, Skyscan, Aartselaar, Belgium). The X-ray tube was operated at a voltage/current of 40 kV/248 µA and 75 kV/131 µA for the bread and frozen dough samples respectively, to obtain optimum contrast of void (air cells) and matter (cell walls). Shadow images were captured using a 12-bit, cooled CCD camera (1024×1024 pixels). Samples were scanned at a magnification of 24 resulting in a pixel size of 11.12 µm. Samples were rotated a total of 180° during the scanning process. The exposure times were 1.3 seconds for the bread samples and 1.1 seconds for the dough samples. X-ray images were obtained every 1.33° of rotation for a total of 137 shadow images (radiographs) per sample. The total scanning

time was 13-15 minutes. After scanning, shadow images (scan file sets of 137 images) for each of the bread and frozen dough samples were loaded into NRecon reconstruction software (V1.5.1.). This software combines the images graphically into a 3D object from which 2D cross sectional images can be taken. Before the reconstruction process, the CS rotation feature was used to rotate the (sample) cross sections making them parallel to the view window. Beam hardening was set a 40% to reduce beam hardening artifacts. The sample specimens were larger than the field of view. Reconstructions of the grey scale histograms were set at a dynamic range of 0.015-0.06 for bread samples and 0.005-0.05 for the dough samples. No smoothing of the sample was done. The reconstruction process produced nearly 1000 cross sectional images per sample which were .0011mm thick.

Figure 3.4 shows shadow image of a frozen dough sample during the scanning process along with two representative axial images obtained through reconstruction.

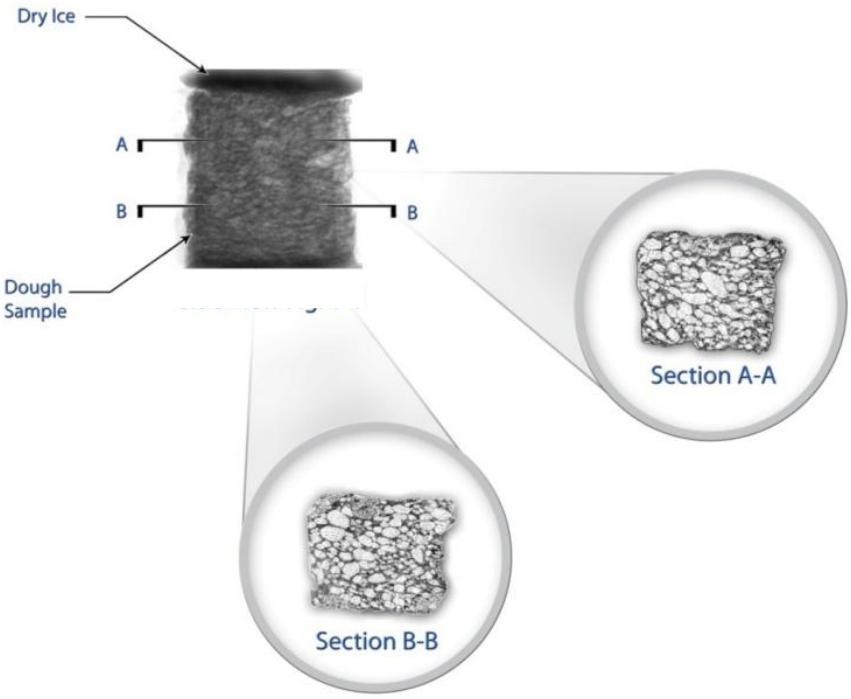

3.6.4. Image Analysis

Quantitative analysis of XMT images involves several steps: Image reconstruction (3-D virtual model generation), creation of axial images (cross-sectional slices), defining the region of interest (ROI) and the volume of interest (VOI), thresholding (creating binary images), despeckling and finally calculation of structural properties.

Analysis of 3D frozen dough and bread structure was done using CTAn processing and analysis software (v.1.7). The 700-1000 reconstructed images comprising each 7-10 mm tall sample were in turn fed into the software. In order to eliminate potential artifacts at the top (caused by dry ice) and bottom (caused by frozen water and sample holder) the selection level tool was used to select approximately 400-500 images which correspond to 4-5mm from the middle of the sample. These slices were highlighted as a part of the volume of interest (VOI), the part of the sample which is to be analyzed. The rectangular region of interest (ROI) tool was then used to draw a 5mm x 6mm rectangle (Figure 3.5a) in the center of the bottom slice in the level selection. This rectangular selection was then interpolated by the software across all of the selected image layers, cropping them to create a 3D VOI. These selected regions of interest were then saved as independent data sets. Cropping the original sample cross sectional images into selected ROIs reduces the file size of sample images and greatly lowers the burden of sample processing on the computer system.

Figure 3.5 (a) Image showing rectangular selection made for quantitative analysis, (b) Cropped cross sectional image of dough. A stack of 400-500 such images make up the volume of interest (VIO).

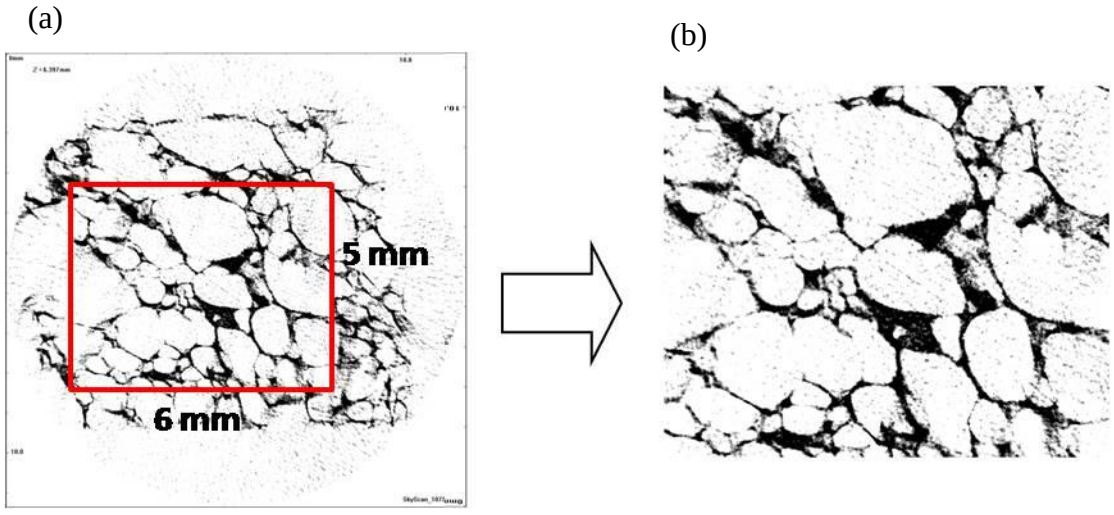

Original (raw) cross sectional images (Figure 3.6a), which have pixel grey scale values ranging from 1-255, were converted into pure white and black images for subsequent analysis (to calculate a set of structural properties). Image pixels in the grey scale ranges of 65-255 and 75-255 were converted to white pixels, which represent the cell walls (structure) of the bread and

frozen dough respectively. Image pixels in the grey scale ranges of 0-64 and 0-74 were converted to black pixels representing the gas cells or bubbles of the bread and frozen dough respectively. Figure 3.6b shows a sample binary image converted to pure black and white pixels based on the image selection (grey scale) ranges listed above. These images are referred to as binary images. The CTAn (v.1.7) despeckling feature was used to eliminate noise from the images. White speckles made up of less than 20 pixels and black speckles made up of less than 5 pixels were removed from the 2-D space by the software system. Final despeckled and processed images (Figure 3.6c) were now ready for quantitative analysis (to calculate a set of structural properties).

Figure 3.6 (a) Raw cross sectional image with pixel grey scale values ranging from 1-255, (b) binary image which has been converted to pure black and white pixels, (c) Processed despeckled image used for quantitative analysis.

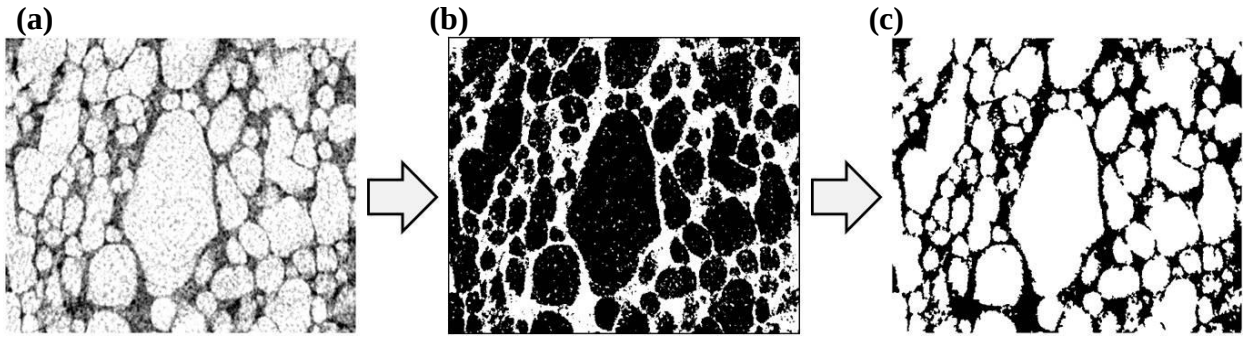

3.6.5. Micro-structural Parameters

The spatial boundary between air cell and the cell walls was established due to the difference in densities from the X-ray CT images. After despeckling, algorithms developed by CT-Analyser (version 1.4, Skyscan, Belgium) were used to extract microstructural features of dough/bread matrices. Various morphometric parameters such as void volume, structure separation (average cell size), cell size distribution, structure thickness (average cell wall thickness) and cell wall thickness distribution, fragmentation index, and structure model index, were calculated in 3D from the hexahedral marching cubes volume model and marching cubes 3D surface construction algorithms. The information about these methods can be found elsewhere (Feldcamp et al., 1984; Lorensen and Cline, 1987). A list of parameters used to

characterize microstructure of dough and baked samples are described in Table 3.1. The terms "structure" and "object" refer to the bread or dough cell walls.

Table 3.1 Structural parameters measured by the Skyscan™ CT-Analyser software

Analysis Parameter	Description
Void Fraction (VF)	Void volume/total volume of the region of interest (ROI); measure of % volume occupied by air cells
Structure Surface Density (SSD) (Object Surface/Total Volume)	SSD is calculated as the ratio of total surface area of the cell walls to the total volume of the object (dough of bread sample). This ratio allows for direct comparisons of cell wall surface area on a per unit volume basis, thus making them independent of individual sample (VOI) size.
Specific Surface (SS) (Object Surface/Volume ratio)	The specific surface (SS) is measured as the ratio of total cell wall surface area to the total volume of cell walls measured within 3D within the volume of interest (VOI). This ratio is independent of sample size and is helpful in characterizing thickness and complexity of structures.
Fragmentation Index (FI)	Index of connectivity of air cells; measures relative convexity or concavity of the total surface which is calculated on the principle that concavity indicates connectivity (and the presence of nodes) and, convexity indicates isolated disconnected structures (struts). FI is calculated in 3D, by comparing area and perimeter (or volume and surface, respectively) of binarized solid before and after an image dilation: $FI = \frac{P_1 - P_2}{A_1 - A_2}$ where P and A are solid area and perimeter, and the subscript numbers 1 and 2 indicate before and after image dilation. Lower fragmentation index or negative values signify better connected lattices while the higher value of Fr.I indicates more disconnected void (air cell) structures.
Structure Thickness (St.Th)	Average structure thickness; measure of average cell walls thickness
Structure Separation (St.Sep)	Average structure separation; measure of average cell size

Degree of Anisotropy (DA)	Isotropy is a measure of 3D symmetry or the presence or absence of preferential alignment of structures along a particular directional axis. If a sample is isotropic then a line passing through the sample at any 3D orientation will make a similar number of intercepts. Samples having structures which are equally spaced and of consistent size are considered to be isotropic and can have DA values that are close to zero. Samples which contain structures which are unequally spaced or vary in shape or size are considered anisotropic can have values greater than 1.
Fractional Dimension (FD)	Indicator of surface complexity of an object, which quantifies how that object's surface fills space. FD is a non-integer dimension, i.e. a plane trying to fill a 3D space, ranging between 2 and 3.

3.6.6. Cell Size and Cell Wall Thickness Distributions

Gas cell size and cell wall thickness distributions (histograms) were obtained through the 3-D analysis and are plotted as normalized frequency vs. size curves. Normalization was done by taking the ratio of volume to the total volume. In order to obtain single parameters rather than set of distribution data for statistical analysis, the histograms were converted into cumulative distribution curves. Four points at percentile limits of 25%, 50%, 75%, 95% were then defined for each curve. At each percentile limit the corresponding size value in millimeters was recorded for analysis. The percentile limits corresponding to cell size value in millimeters was recorded and labeled as 25%, 50%, 75% or 95 %. Figure 3.7 shows a cumulative cell wall thickness distribution curve and indicates both the 50% limit, and its corresponding thickness value of .132 mm. This process was performed for both the structure separation (gas cell size) and structure thickness (cell wall thickness) distributions.

Figure 3.7 Size distribution histogram and cumulative distribution curve showing 50 percentile limit.

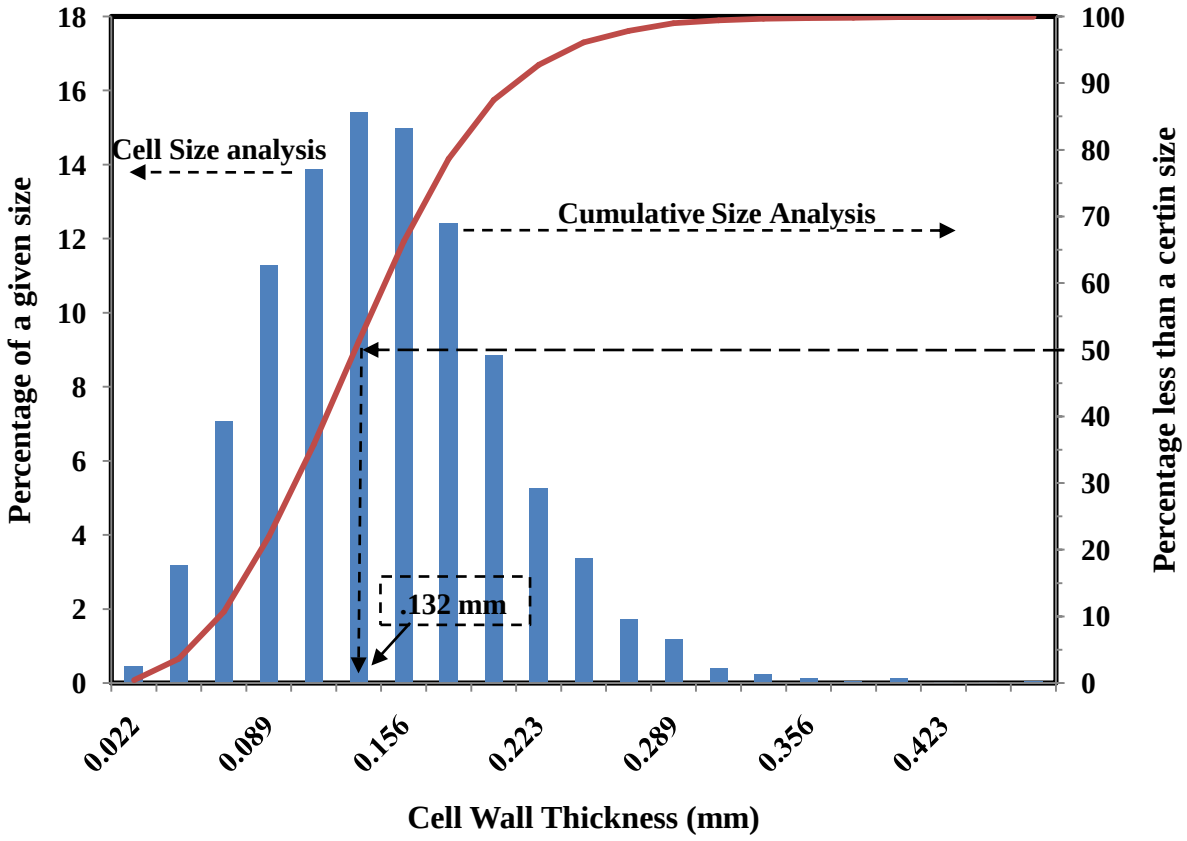

3.6.7. Statistical Analysis

For this study, a randomized block design including four factors (4 flour varieties, 4 processing stages, 2 sample locations, 3 replicates) for a total of 96 bread and dough specimens was used. Results for both top (48 specimens) and middle (48 specimens) samples were analyzed separately using a 3 factor general linear model analysis of variance (ANOVA) to determine significant differences between treatments. Means were compared using L S means procedure at an alpha level of 0.05. Statistical analyses were performed using SAS (Statistical Analysis Software version 9.1).

3.7. References

AACC. 2001. Approved Methods of the AACC, tenth edition. American Association of Cereal Chemists, St. Paul, Minnesota, USA.

Dobraszczyk, B.J. 1997. Development of a new dough inflation system to evaluate doughs. Cereal Foods World 42(7), 516-519.

Feldkamp, L.A., Davis, L.C. and Kress, J.W. 1984. Practical cone-beam algorithm. Journal of the Optical Society of America 1, 612–619.

Lorensen, W.E. and Cline, H.E. 1987. Marching cubes: A high resolution 3D surface construction algorithm. Computer Graphics 21, 163-169.

CHAPTER 4 - **Results and Discussion**

4.1.1. Physio-chemical Analysis of Wheat Flours

Moisture, protein and ash values for flour varieties used for this study are found in Table 4.1. Both Karl and BZ are considered to be strong bread making varieties. At 13.56%, Karl was more than 1% higher in protein than was BZ (12.43% protein). The KA flour had its protein content adjusted to 12.43% to match BZ. As expected, Alpowa which is a soft variety had a considerably lower protein content (9.44%).

Table 4.1 Chemical analysis of wheat flours.

Flour Variety	Moisture%	Protein %**	Ash %**
Karl	14.31	13.56	0.438
KA	14.14*	12.43*	0.419*
BZ	10.45	12.43	0.485
Alpowa	11.69	9.44	0.435

** Calculated values **14% moisture basis*

4.1.1.1. Relative Protein Composition

The relative composition of flour proteins was obtained using SE-HPLC. The total polymeric protein (TPP) and the unextractable polymeric protein (UPP) contents of the flours were calculated as a percentage area under the chromatogram curve. The percentage of TPP (Table 4.2) was significantly higher ($P < 0.05$) for the BZ and Alpowa flours than it was for Karl. Significant differences ($P < 0.05$) in UPP were also seen between flours. The Karl flour gave the highest percentage of UPP followed by BZ and Alpowa. This fraction (UPP) contains a high proportion of very large polymers (≥ 158K) and has been shown to be largely responsible for dough strength (Gupta, 1993). Thus flours with high UPP typically produce stronger doughs.

Table 4.2 Relative composition of flour proteins obtained through SE-HPLC

Flour Variety	Area % under chromatogram curve	
	% Total Polymeric Protein	% Unextractable Polymeric Protein
Karl	$40.63^{a} \pm 0.08$	$52.68^{a} \pm 0.48$
KA*	$40.63^{a} \pm 0.08$	$52.68^{a} \pm 0.48$
BZ	$42.55^{b} \pm 0.74$	$50.31^{b} \pm 1.14$
Alpowa	$42.35^{b} \pm 0.14$	$45.80^{c} \pm 0.32$

**KA is same as Karl*

Values represent mean ± standard deviation for duplicate determinations

Means with the same letter within columns are not significantly different ($p < 0.05$)

4.1.2. Dough Mixing Properties

Overall, the Karl flour had the highest absorption (64%) and mixing time (6:20 min.). The relatively strong behavior of this flour is visible in its mixogram (Figure 4.1) where the wide mixing curve remains stable long after the mixing peak is reached. As expected, the KA flour produced a very similar curve but with a shorter peak mixing time of 5:40 min. The BZ flour was of intermediate strength. Its representative mixogram develops more rapidly, is wide at the peak and break down more rapidly than the curves for the stronger flours. Alpowa exhibited the weakest mixing properties of the four flours with a mixing peak of only 4:00 min. The mixogram of Alpowa flour was a relatively weak curve that breaks down very quickly after reaching a peak.

Table 4.3 Dough mixing parameters

Flour Variety	Mixograph Absorption (%)	Midline Peak Mixing Time (min)
Karl	64	6:20
KA	63	5:40
BZ	61	5:00
Alpowa	54	4:00

Figure 4.1 Mixograms for wheat flours.

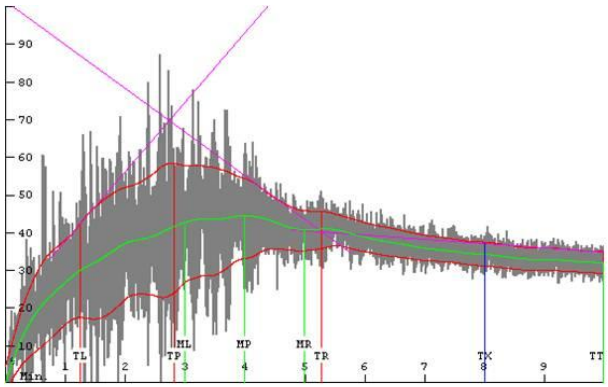

Alpowa (SWS)

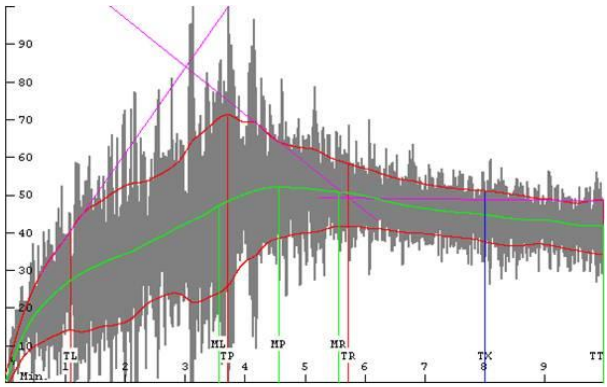

BZ 20 (HWS)

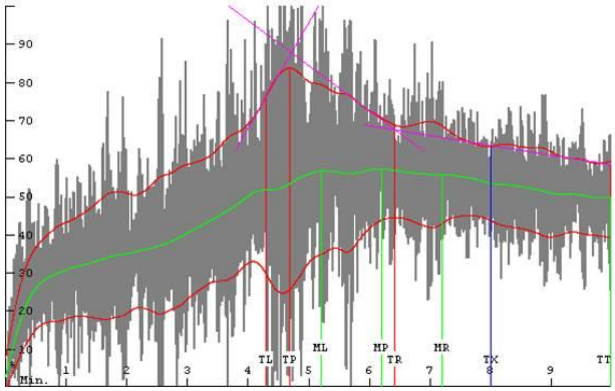

Karl 92 (HRW)

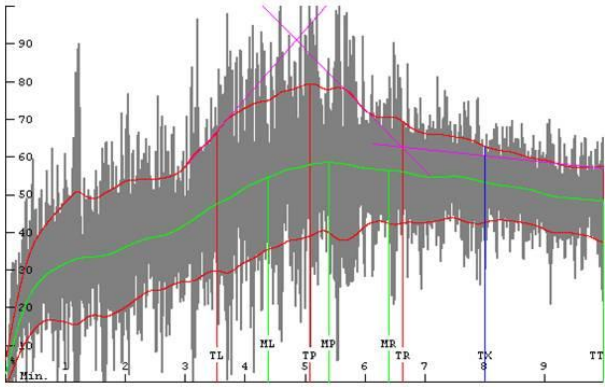

Karl Adjusted (HRW)

4.1.3. Biaxial Extensional Rheology

Biaxial extensional rheological tests were performed on doughs made from Karl, BZ, and Alpowa flours. Rheological parameters for each of the flours are seen in Table 4.4. The high strain hardening values seen for BZ (2.03) and Karl (2.01) indicate a high degree of gas cell stability. Doughs with a high amount of strain hardening ability inflate to higher volumes, have thinner cell walls and more even bread crumb than do those with less ability to strain harden. (Dobraszczyk, 1997). The Alpowa flour had a much lower strain hardening value (1.29).

Figure 4.2 Stress vs. Hencky strain curves for Karl, BZ and Alpowa wheat flour doughs.

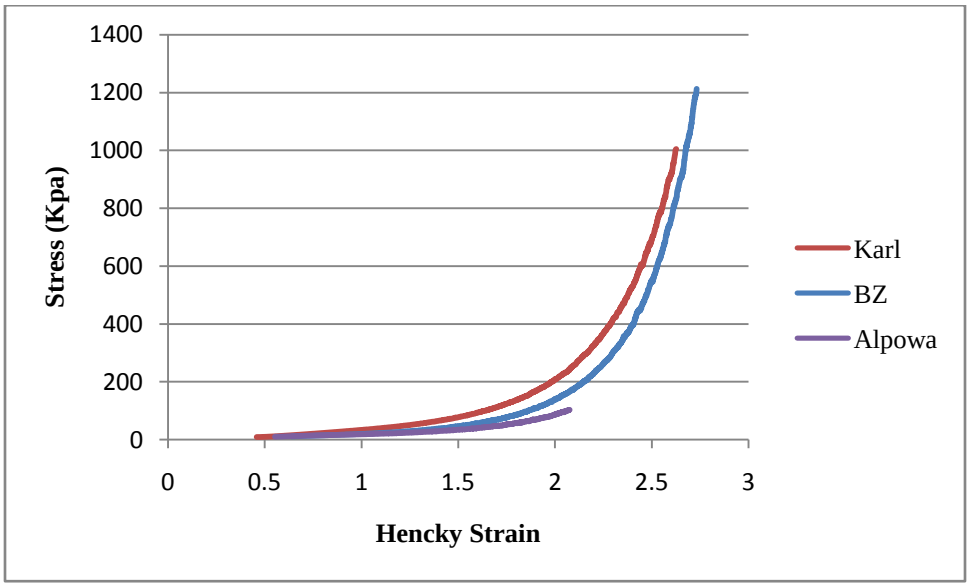

Table 4.4 Dough inflation system (biaxial rheology) responses

	Strain Hardening Index	Failure Strain
Karl	2.01 ± .084	2.61 ± .156
BZ	2.03± .087	2.70 ± .102
Alpowa	1.29± .114	1.97 ± .126

Values represent mean ± standard deviation triplicate determinations

4.1.4. Baking and Crumb Texture

The baking data followed a trend similar to the mixing behavior with the strongest flours (Karl and KA) giving the highest loaf volumes. BZ had a significantly ($P<0.02$) lower loaf volume of 855 cm^3. Alpowa had the lowest loaf volume of 733 cm^3. C-cell macro-structural parameters, which were obtained through whole slice images are found in Table 4.5. The reader should be warned that these data represent gross parameter averages across a whole slice of bread, and are not necessarily comparable to the individual location based samples used for micro-structural analysis (XMT). As expected, the number of cells increased significantly ($P<0.05$) as loaf volume increased. Significant differences in cell wall thickness were also seen with Alpowa having the largest average cell walls (0.413 mm) and BZ having the thinnest (0.398 mm). No significant differences in overall cell diameter were observed in the C-cell data.

Table 4.5 Macro-structural properties (whole slice) bread crumbs obtained by C-cell

Flour Variety	Loaf Volume (cm^3)	Number of Gas Cells	Cell Wall Thickness (mm)	Cell Diameter (mm)
Karl	985 ± 31^{a}	4913 ± 139^{a}	0.405 ± 0.001^{b}	1.68 ± 0.04^{a}
KA	932 ± 46^{ab}	4838 ± 95^{ab}	0.405 ± 0.002^{b}	1.69 ± 0.03^{a}
BZ	855 ± 9^{c}	4620 ± 56^{bc}	0.398 ± 0.004^{c}	1.64 ± 0.03^{a}
Alpowa	733 ± 30^{d}	3638 ± 151^{d}	0.413 ± 0.004^{a}	1.67 ± 0.04^{a}

Values represent mean ± standard deviation for triplicate determinations

Means with the same letter within columns are not significantly different ($p < 0.05$)

4.2. Dough and Bread Microstructure: Effect of Processing Stage

After collecting and analyzing XMT image data, it is clear that the largest amount of variation in the data parameters was due to processing stage. In this section, these data will be discussed for each parameter with respect to processing stage.

4.2.1. Gas Cells

4.2.1.1 Gas Cell Size Distribution

Gas cell size distributions were obtained for each of the bread and dough samples and are discussed here with regard to processing stage (0, 20 and 40 min of proof times, and baking). As discussed in section 2.6.1, two specimens cut from the top and middle of the middle slice of the proofed dough and baked loaves were used for microstructural characterization. The resulting distribution data were plotted with respect to processing stage and flour types both for top and middle samples individually and reported in Appendix A and B. As can be seen from Figures A.1, A.2, B.1, and B.2, generally speaking, little difference was observed between the microstructure of top and middle samples.

Shifts in gas cell size distribution across processing stages were similar for each of the flour varieties (Figure A.1), which will be discussed in detail in the next section (4.2.2). Gas cell size distributions for the unproofed doughs (0 min, green) presents tall sharp peaks. This indicates presence of large number of very small gas cells occluded during mixing. As the proofing process progresses, gas cells become larger and distributions shift to the right towards to larger gas cell range as shown for 20 min (blue) and 40 min (red) samples. Gas cells

continued to expand further during the baking process, as expected. Distributions for the baked bread seen in purple are shifted to the right and largely skewed in that same direction. The short columns at the very far right represent a small number of very large gas cells (Figure A.2).

Changes in gas cell size distribution for Karl are seen in (Figure 4.3) The distribution for unproofed dough (0 minutes) samples is as a tall sharp peak (seen in green) on the left side of the cell size axis indicating a large number of very small gas cells. At this point, the average cell size for Karl dough is 0.24 mm with a median size of 0.16 mm. This indicates that 50% of the total volume is made up of cells that are less than 0.16 mm. As proof time increased, the resulting distributions shifted to the right, increasing the average cell size to 0.35mm (20 min) and 0.45mm (40 min). This technique was also capable of measuring (recording) the dramatic increases in gas cell size during the baking process. The columns on the far right of the skewed distributions represent a small percentage of the total volume which is made up of very large gas cells measuring in the 1.50 to 2.40 mm range. Distributions for KA, BZ and Alpowa flours shifted in a similar way across processing time.

Figure 4.3 Gas cell size distribution for Karl samples showing comparison across processing stage. Average of 6 (3 top, 3 middle) replicate measurements

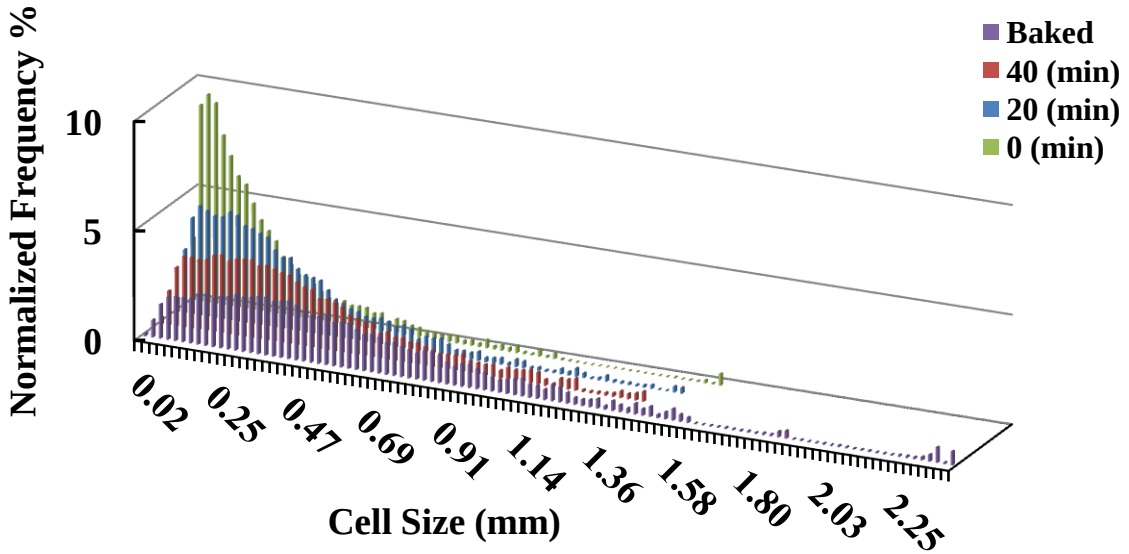

4.2.1.2. Cumulative Gas Cell Size Distributions

In addition to the histograms provided in section 4.2.1.1., cumulative distribution curves shown in were used to underline the changes in gas cell size observed at each of the four processing stages. Values were then determined for the curves at four percentile limits (25%, 50%, 75%, 95%). Figure 4.4 shows cumulative gas cell size distribution curves for Karl flour. Clear differences in gas cell size distribution are observed across processing time. At the 50th percentile, cell size values increase from 0.16 mm (0 min proof) to 0.53 mm (baked) during the bread making process (Figure 4.4).

Figure 4.4 Cumulative gas cell size distribution curves for Karl flour across processing stage. (Curves represent means of three independent replicates)

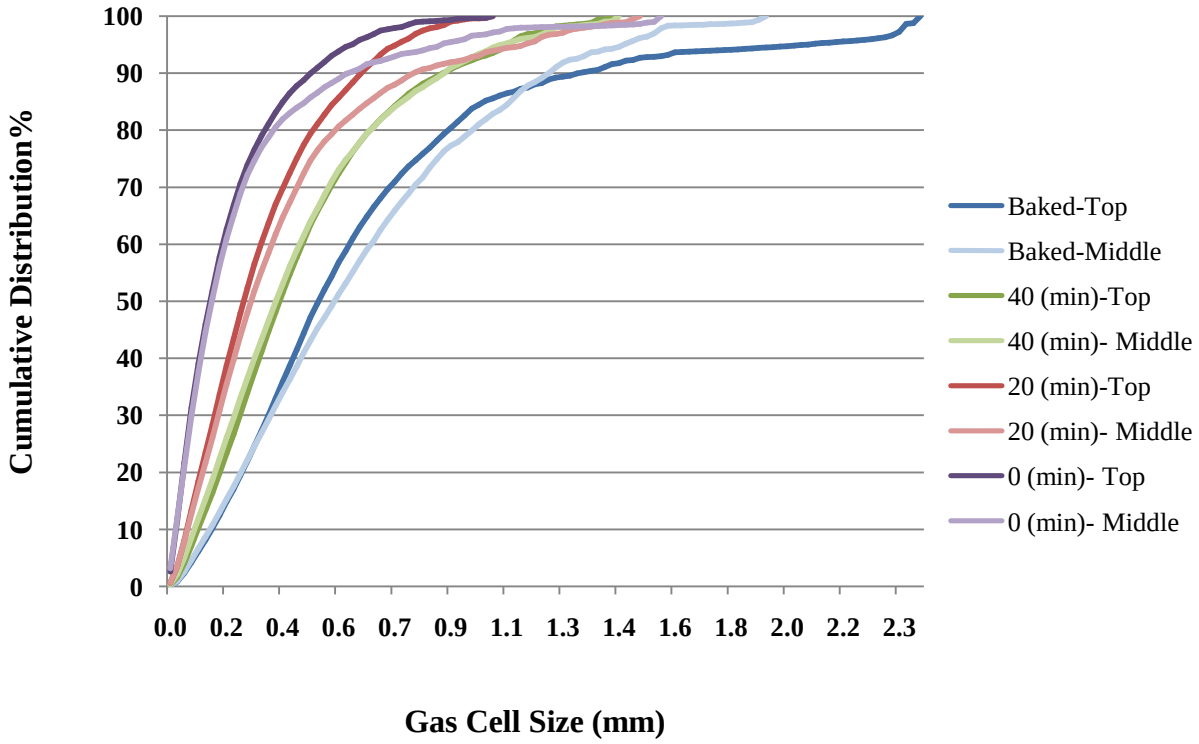

These cumulative distribution points were used in order to quantitatively compare the effects of processing stage on gas cell size. Much like medians, these cumulative distribution points give information about how the distributions are skewed and provide a means for

comparison between treatments. A cumulative distribution point at the 25th percentile of 0.20 mm would indicate that 25% of the total gas cell volume was made up of cells with sizes less than 0.20 mm. The higher this value at certain percentage (25%, 50%, 75%, 95%) of the total volume, the larger the gas cells and the more the distribution is shifted to the right (larger cell size).

Table 4.6 presents comparisons of cumulative distribution points at each processing time. Values represent means for all flour types at each processing stage. The results show a general trend toward increasing cell size as processing (0 min, 20 min, 40 min, baked) time increases. During the early stages of proofing (0-20 min), cumulative distribution point values for the 25th and 50th percentiles nearly doubled were as distribution points in the 95th percentile did not significantly ($P< 0.05$) increase. This suggests that shifts in gas cell size distribution during this time period (0-20 min) were most largely due to the expansion of small gas cells below the 50th percentile.

During the later stages of proofing a similar shifting pattern was observed. Gas cell size distribution values at the 25th percentile increased significantly ($P< 0.05$) between 20 and 40 min of proof time. Values at the 50th, 75th and 95th percentiles however, did not increase as rapidly (Table 4.6). This indicates that shifts in gas cell size distribution (20 and 40 min), due to the growth and expansion of gas cells, are most largely dominated by the growth of small gas cells which are below the 25th percentile.

Increases in gas cell size during the early stages of baking also caused gas cell size distributions to shift to the right. Largely significant increases ($P< 0.001$) in values between the fully proofed dough (40 min) and the final baked product are seen at each of the percentiles (25th, 50th, 75th and 95th) (Table 4.6). This indicates that the baked samples have a greater percentage of volume that is made up of large cells and would be expected given the large increase in overall volume early in baking. During the baking process, values increased from 0.1935 mm to 0.3573 mm for the 25th percentile and from 0.3424 mm to 0.6499 mm for the 50th percentile (top samples). This indicates that small gas cells in the lower one fourth and one half of the distribution are expanding during the early stages of baking (oven spring). Significant increases in values for the 75th and 95th percentiles during baking indicate expansion of the larger gas cells

in the upper half of the distribution. This growth might also be caused by coalescence which leads to a small number of very large gas cells, as appear at the far right of the distribution.

Gas cell size distributions also varied, based on sample location. Cumulative distribution point values were typically higher for the top samples than for the middle samples (Table 4.6). This is likely due to the fact that top samples had more space for expansion upward and outward whereas middle samples were more confined. The larger gas cell size of the top baked samples are likely the result of coalescence. Hayman et al. (1998) reported that excess pressure caused by crust formation leads to gas cell coalescence and a more open crumb structure. Such pressure is more likely to affect top samples due to their close proximity to the crust.

Table 4.6 Gas cell size cumulative distribution means for top and middle samples with respect to processing stage

	Processing Stage	Gas cell size (mm) at cumulative distribution points				Average gas cell size (mm)
		25%	50%	75%	95%	
Top	0 (min)	0.08^{d}	0.17^{c}	0.34^{b}	0.67^{b}	0.25^{d}
	20 (min)	0.14^{c}	0.25^{bc}	0.42^{b}	0.73^{b}	0.31^{cd}
	40 (min)	0.19^{b}	0.34^{b}	0.54^{b}	0.89^{b}	0.40^{bc}
	Baked	0.36^{a}	0.65^{a}	1.20^{a}	2.03^{a}	0.84^{a}
	Processing Stage	Gas cell size (mm) at cumulative distribution points				Average gas cell size (mm)
		25%	50%	75%	95%	
Middle	0 (min)	0.07^{c}	0.15^{c}	0.31^{c}	0.71^{c}	0.23^{c}
	20 (min)	0.15^{b}	0.29^{b}	0.50^{b}	0.94^{bc}	0.37^{b}
	40 (min)	NA	NA	NA	NA	NA
	Baked	0.30^{a}	0.56^{a}	0.94^{a}	1.60^{a}	0.68^{a}

Values reported are the average of 3 replicate measurements for each of the four flour types (total of 12)

Means with the same letter within columns are not significantly different ($p < 0.05$)

4.2.1.3. Average Gas Cell Size

Average gas cell size was also calculated for each of the samples from the distributions (Table 4.6). Values shown in Table 4.6 represent means for all flour types at each processing time. All across the flour types, average gas cell size increased as a function of processing stage with largely significant differences ($P<0.0001$) between values at 0 min proof time and 40 min

proof time. Although the differences between 20 and 40 min (top sample) of proof time were not significant ($P<0.05$), during the baking process average gas cell size for the top samples more than doubled. This is expected to be largely a result of oven spring as well as coalescence of gas cells in the early stages of baking.

Comparisons of the average gas cell size for each individual flour type are shown for each processing stage (0 min, 20 min, 40 min, Baked) in Figure 4.5. Each bar represents the mean calculated from three independent replicates. Clear increases in average gas cell size are seen as proofing time increases. Non-proofed samples had average gas cell sizes in the 0.194 mm to 0.339 mm range. Average cell size increased with proof time to ranges of 0.300 mm to 0.411 mm (20 min) and 0.374 mm to 0.469 mm (40 min). Due to the large amount of expansion caused by oven spring, baked samples had dramatically larger average cell sizes ranging from 0.619 mm to 1.136 mm in size.

Average gas cell sizes were also observed to be dependent on sample location with top samples tending to have larger gas cells than middle samples. These differences in gas cell size are most prevalent in the baked product which has undergone the most expansion. During baking, gas cells at the top of loaf are able to expand both upward and outward. Middle samples however are much more confined by the walls of the baking pan and the dough mass on top.

Figure 4.5 Means of average cell size (structure separation) for flour varieties plotted according to processing stage. (a) Top samples, (b) Middle samples

(a)

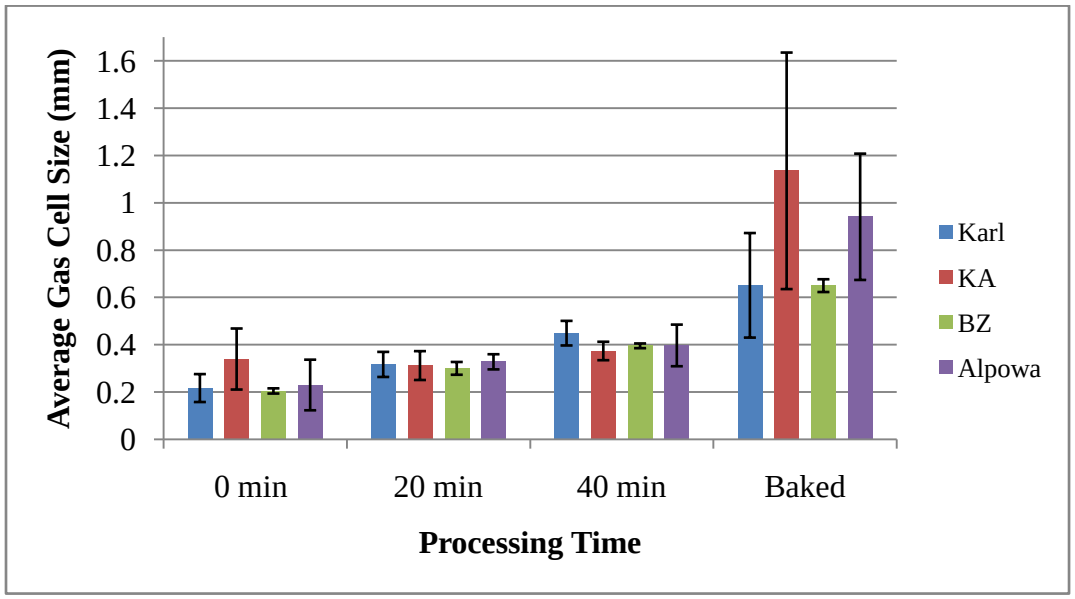

(b)

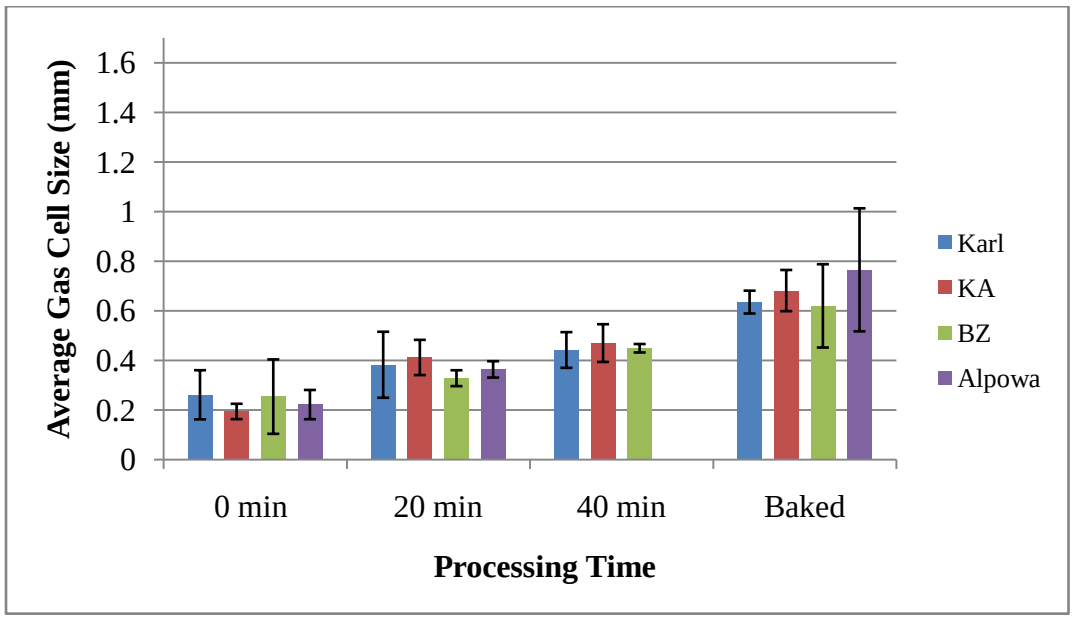

4.2.2. Cell Wall Thickness

4.2.2.1. Cell Wall Thickness Distributions

Cell wall thickness distributions were obtained from the 3D analysis of bread and dough samples. These distributions, which provide detailed information regarding the dough and bread structure, are discussed in this section with regard to processing time. Shifts in cell wall thickness distribution across processing stages (0 min, 20 min, 40 min, baked) were similar for each of the flour varieties (Figure 4.6). Figure 4.6 shows the change in cell wall thickness distributions for Karl with respect to bread making processing stages as an example. Distributions for the unproofed samples (green) have the broadest range with a mean value of 0.14 mm. Cell walls become thinner and the distributions shift to the left as gas cells expand during proofing (20 min, blue; 40 min, red). During baking, as cell walls continue to undergo biaxial deformation causing the thin films to stretch and rupture, the cell wall thickness distribution for the baked crumb (purple) is shifted far to the left resulting in a narrow distribution. This indicates that a large proportion (25%) of the total cell volume is made up of very thin cell walls (< 0.052 mm).

Figure 4.6 Cell wall thickness distributions for Karl samples; comparison across processing stage [average of 6 (3 top, 3 middle) replicates]

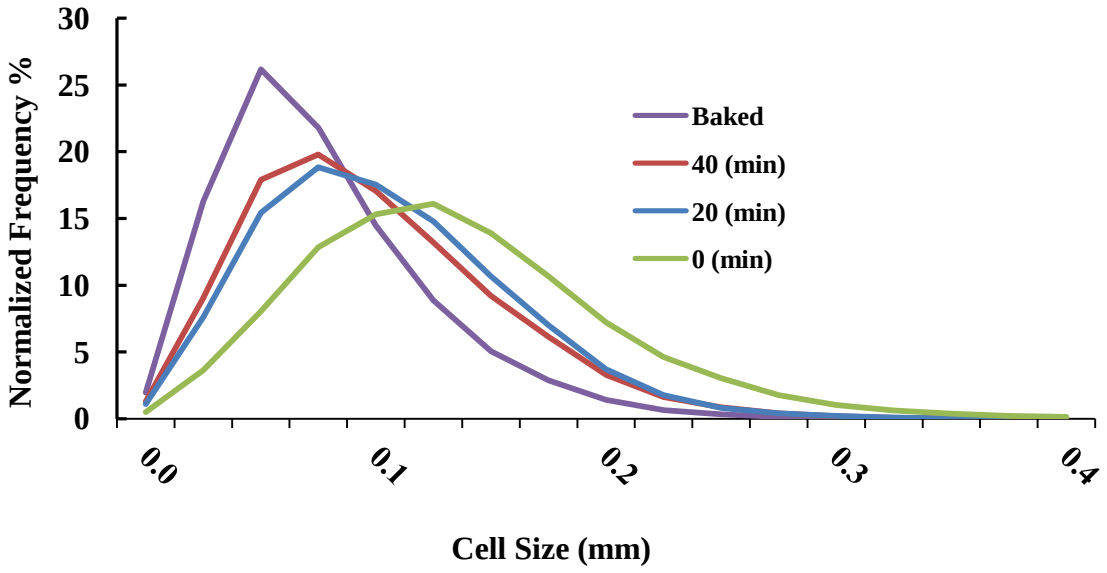

4.2.2.2 Cumulative Cell Wall Thickness Distributions

The effects of processing time on cell wall thickness distribution were measured quantitatively using cell size point values at various cumulative percentages (25%, 50%, 75%, 95%). Comparisons of these values for both top and middle samples across processing time are presented in Table 4.7. The table illustrates the general trend of decreasing cell wall thickness as processing time increases. Values shown are means which include all flour varieties at a given processing stage.

During the early stages of proofing (0-20 min.), the free growth of gas cells caused cell wall thicknesses to decrease. Cumulative distribution values decreased significantly ($P< 0.05$) during this time (0-20 min.) for each of the four percentiles (25^{th}, 50^{th}, 75^{th}, 95^{th}) measured (Table 4.7). This indicates that large decreases in gas cell wall thickness taking place in the earliest stage of proofing occur throughout the entire distribution.

During the later stages of proofing (20-40 min), cell wall thickness distribution values continued to decrease but at a slower rate (Table 4.7). When distributions are compared at the 50^{th} and 95^{th} percentiles, no significant differences ($P< 0.05$) between the 20 and 40 minutes distribution values were detected. This indicates that decreases in cell wall thickness are beginning to slow down and reach a plateau. These results are consistent with Babin et al. (2006) who found that in the early stages of proofing, decreases in cell wall thickness, were consistent with free bubble growth. Later on however, (25-45 min at 3% yeast or 65-105 min at 1.5% yeast), coalescence begins to prevail. Cell wall thicknesses reach a plateau and actually start to increase due to rupture and consequent loss of thinner cell walls (Babin et al., 2006). In the current study, doughs (2% yeast) were baked after an optimal amount of proof time (40 min). Had they been allowed to continue proofing, excessive coalescence would have likely caused cell wall thickness distribution values to increase.

Expansion of gas cell walls during baking caused cell wall thickness distribution values to decrease from 0.0581 mm to 0.0490 mm for the 25^{th} percentile (top samples). This indicates a significant increase in the number of very thin gas cell walls which occurs during the early stages of baking.

Table 4.7 Cell wall thickness means for top and middle samples listed by processing stage

	Processing Stage	Cell wall thickness values (mm) at cumulative distribution points				Average cell wall thickness
		25%	50%	75%	95%	
Top	0 (min)	0.089^{a}	0.124^{a}	0.162^{a}	0.227^{a}	0.140^{a}
	20 (min)	0.065^{b}	0.093^{b}	0.125^{b}	0.171^{b}	0.107^{bc}
	40 (min)	0.058^{c}	0.084^{bc}	0.114^{c}	0.163^{bc}	0.099^{c}
	Baked	0.049^{d}	0.070^{c}	0.097^{d}	0.146^{c}	0.087^{d}
	Processing Stage	Cell wall thickness values (mm) at cumulative distribution points				Average cell wall thickness
		25%	50%	75%	95%	
Middle	0 (min)	0.092^{a}	0.117^{a}	0.161^{a}	0.221^{a}	0.140^{a}
	20 (min)	0.071^{b}	0.103^{b}	0.123^{b}	0.195^{b}	0.119^{b}
	40 (min)	NA	NA	NA	NA	NA
	Baked	0.056^{c}	0.082^{c}	0.114^{b}	0.169^{c}	0.099^{c}

Values reported are the average of 3 replicate measurements for each of the four flour types (total of 12)
Means with the same letter within columns are not significantly different ($p < 0.05$)

4.2.2.3. Average Cell Wall Thickness

Average cell wall thicknesses (Table 4.7) decreased as a function of processing stage with largely significant differences ($P< 0.0001$) between values at 0 min proof time and 20 min proof time. Decreases in average cell wall thickness at the later stages of proofing (20 to 40 min) were not significant ($P< 0.05$). This is similar to the decreases that were seen in the distribution point values at the 50^{th} % (Table 4.7). Baked samples had the lowest average cell wall thickness with values reaching 0.087 mm (top) and 0.099 mm (middle).

Average gas cell wall thickness comparisons for each individual flour type are shown for all processing stages (0 min, 20 min, 40 min, baked) in Figure 4.7. Each bar represents the mean calculated from three independent replicates. Average cell wall thickness decreased as a function of processing stage. Non-proofed samples gave the largest values for thickness, ranging from 0.126 mm to 0.148mm. Average wall thickness decreased as a function of proof time to ranges of 0.104 mm to 0.143 mm (20 min.) and 0.092 mm to 0.128 mm (40 min.). As expected, the baked samples had the lowest average cell wall thickness ranging from just 0.083 mm to 0.110 mm.

Average cell wall thickness values were also somewhat dependent on sample location. Comparisons of the plotted values (Figure 4.7a and Figure 4.7b) show a general trend with top

samples having thinner gas cell wall than middle samples. Top samples are free to expand both upward and outward (reducing cell wall thickness) whereas middle samples remain much more confined. This is particularly true for the processing stages where at least some gas cell wall expansion has occurred (20 min, 40 min, and baked).

Figure 4.7 Means of average cell wall thickness for flour varieties plotted according to processing stage (a) Top samples (b) Middle samples

(a)

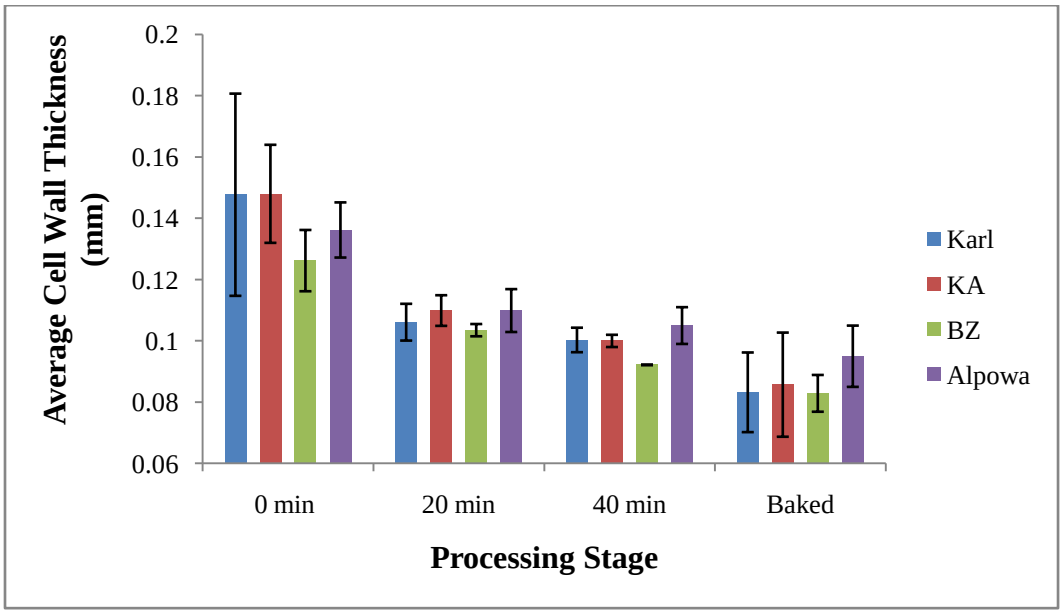

(b)

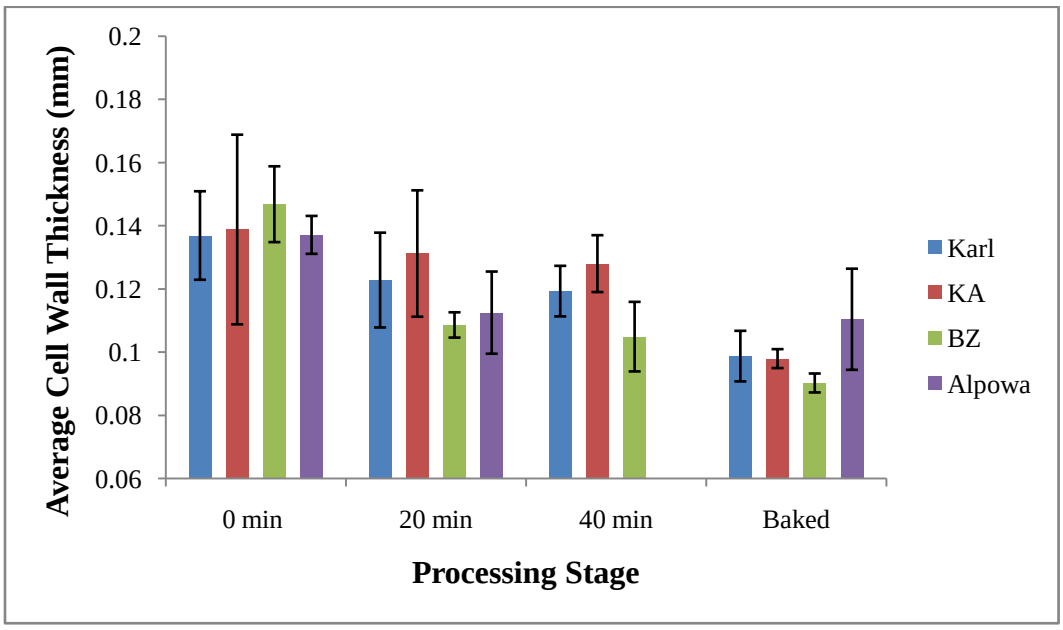

4.2.3. Other Structural Parameters

In addition to gas cell size and cell wall thickness distributions, various morphometric parameters such as void fraction (VF), fragmentation index (FI), structure surface density (SSD), specific surface (SS), degree of anisotropy (DA) and fractal dimensions (FD) were calculated in 3D using the techniques mentioned in section 3.6.5. Results are summarized in Table 4.8.

Table 4.8 Parameter means for top and middle samples listed by processing stage

	Processing Stage	VF (%)	FI	SSD (1/mm)	SS (1/mm)	DA	FD
Top	0 (min)	33.20^{d}	-54.97^{d}	13.72^{a}	20.74^{d}	1.48^{a}	2.47^{a}
	20 (min)	63.72^{c}	-18.01^{c}	12.65^{b}	34.97^{c}	1.43^{b}	2.41^{b}
	40 (min)	74.50^{b}	-9.17^{b}	10.15^{c}	39.83^{b}	1.52^{a}	2.35^{c}
	Baked	86.98^{a}	-0.37^{a}	6.07^{d}	47.01^{a}	1.64^{a}	2.26^{d}
	Processing Stage	VF (%)	FI	SSD (1/mm)	SS (1/mm)	DA	FD
Middle	0 (min)	28.78^{c}	-59.98^{c}	13.45^{a}	19.24^{c}	1.56^{a}	2.47^{a}
	20 (min)	62.62^{b}	-19.90^{b}	11.67^{b}	31.67^{b}	1.65^{a}	2.39^{b}
	40 (min)	NA	NA	NA	NA	NA	NA
	Baked	81.86^{a}	-4.99^{a}	7.23^{c}	40.06^{a}	1.51^{a}	2.31^{c}

Values reported are the average of 3 replicate measurements for each of the four flour types (total of 12)

Means with the same letter within columns are not significantly different ($p < 0.05$)

4.2.3.1. Void Fraction

Void fraction (VF) is defined as the ratio of the volume taken up by air spaces (gas cells) to the total volume of the dough sample being measured. Thus it reflects expansion of the gas cells in the sample. The change in the mean VF values for each of the breadmaking processing stages can be seen in Table 4.8. Overall, expansion of gas cells during the proofing process caused VF of samples to increase from 33.2 to 74.5%. Similar increases in VF (after mixing), 10% to 70 % (end of 180 min proof), have been reported by Babin et al. (2006) who used fast x-ray tomography to measure gas cell size. However, these studies are difficult to compare due to differences in yeast contents and proofing times.

Oven spring, in the early baking process, leads to additional expansion of the still viscous dough as well as rapid increases in loaf volume. Void fractions increased to 86.98% and 81.86%

for the top and middle samples, respectively. As expected, top samples, which had greater space to expand upward and outward had higher void fractions. All differences in VF with regard to processing stage were highly significant ($P < 0.0001$).

4.2.3.2. Fragmentation Index

Fragmentation index (FI) is a measure of the relative connectivity of the cell wall structure. The higher the FI, the more disconnected a structure is considered to be.

FI values increase as a function of processing stage (Table 4.8). The low mean fragmentation indices of the non-proofed doughs (-54.97 top sample, and -59.98 middle sample) indicate a highly connected cell wall structure. At this stage gas cells are small and are surrounded by thick connected cell walls. Doughs which have undergone more proofing and expansion have higher fragmentation indices of -18.01 (20 min) and -9.17 (40 min) (top samples). In the later stages of proofing, cells in the dough matrix become larger and consequently cell walls become thinner which increases the possibility for cell wall failure. During the baking process cell walls become solid and rupture under pressure, creating an interconnected porous network of cells. This results in an increase in FI. The baked samples had the highest FI with values of -0.37 (top) and -4.99 (middle). All differences in FI with regard to processing stage were highly significant ($P < 0.0001$).

4.2.3.3. Structure Surface Density

Structure surface density (SSD) is calculated as the ratio of total surface area of the cell walls to the total volume of the object (dough or bread sample). This ratio allows for direct comparisons of cell wall surface area on a per unit volume basis, thus making them independent of individual sample (VOI) size. Overall, the SSD decreased from the no proof through baked bread with the unproofed samples having the highest amount of surface area (mm^2) per unit volume (mm^3) and the baked samples having the lowest (Table 4.8).

Decreases in SSD were significant ($P<0.02$) during the early stages of proofing, going from 13.72 mm^{-1} (top samples) and 13.45 mm^{-1} (middle samples) at 0 min, to 12.65 mm^{-1} (top samples) and 11.67 mm^{-1} (middle samples) at 20 min. Values decreased to an even greater degree in the later stages of proofing (20-40 min). At a time when gas cells are growing, these decreases in surface area suggests that small gas cells are being exchanged for larger ones. Coalescence and disproportionation are two possible mechanisms by which this decrease in

surface area could occur. Coalescence is the rupture of thin films which separate gas cells causing them to combine (Campbell, 2003).

van Vleit (2008) suggested that disproportionation occurs during the early stages of proofing when high Laplace pressure inside small gas cells causes gas to be transported through the liquid phase gas and into large gas cells. Thus large gas cells grow at the expense of smaller ones.

Changes in SSD during baking were also highly significant ($P< 0.001$) with values decreasing from 10.05 mm^{-1} (40 min) to 6.07 mm^{-1} (baked) (top samples). Campbell (2003) credited the large decreases in gas cells observed during proofing and baking to extensive and rapid coalescence.

4.2.3.4. Specific Surface

The specific surface is measured as the ratio of total cell wall surface area to the total volume of cells within the volume of interest (VOI). This ratio is independent of sample size and is useful in characterizing thickness and complexity of structures. Though total surface area per unit dough sample volume (SS) increased as a function of processing stage, the total surface area per unit cell wall volume showed the opposite trend (Table 4.8). Increases in SS were highly significant ($P<0.0001$) between proofing times, going from 20.74 mm^{-1} (top samples) at 0 min to 39.83 mm^{-1} (top samples) at 40 min. These differences are largely driven by total cell volume which deceases during proofing and baking. Baked samples had the highest SS ratios reaching 47.01 and 40.06 for the top and middle samples respectively.

4.2.3.5. Degree of Anisotropy

Degree of anisotropy (DA) values are calculated from 2D cross sectional images. A sample is isotropic if a line passing through the volume at any 3D orientation makes a similar number of structural intercepts. Isotropic samples have structures that are equally spaced and have a consistent thickness. Anisotropic structures by contrast are quite irregular. The number and length of line intercepts are largely dependent on the 3D orientation of the crossing line. Anisotropic samples have structures that are unequally spaced and may vary somewhat in shape and thickness.

DA values for the bread and dough samples were largely anisotropic ranging from 1.43 to 1.64. These high values indicate a large degree of variation in gas cell wall thickness and gas

cell size at varying 3D orientation. These values also suggest that gas cells in all stages of bread making have an irregular shape that is not spherical.

4.3. Dough and Bread Microstructure: Effect of Flour Type

A smaller amount of the variation in the overall image analysis data was due to flour type as compared to variations with respect to processing stages discussed in section 4.2. Those differences within parameters are discussed below with regard to flour type.

4.3.1. Gas Cells

4.3.1.1. Gas Cell Size Distributions

Gas cell size distributions provide very useful information about the structure of proofing dough and baked bread making it possible to compare quantitatively the effect of different flour types on the size and structure of gas cells. The cumulative distribution points used in these comparisons can be seen in Table 4.9. Overall, KA had the largest gas cells and BZ had the smallest. Differences in gas cell size seen among flour varieties were largely due to variations in the size of the largest cells seen at the 95^{th} percentile in the top samples. Very few differences were seen between varieties with regard to smaller gas cells found in the three lower percentiles (25^{th}, 50^{th}, 75^{th}).

At the 95^{th} percentile KA and Alpowa had values that were higher than those of the other two flours (Table 4.9). This indicates that differences in distributions with respect to flour type occur largely at the higher percentiles and are mainly due to a small percentage of very large gas cells. A clear example of this is seen in the gas cell size distributions for the baked bread samples which are shown for each flour type in Figure 4.8. The columns on the far right of the distributions represent gas cells in the 2.0 mm to 3.3 mm range for KA and the 2.0 mm to 3.0 mm range for Alpowa. These larger gas cells are likely the result of coalescence caused by the instability of bubble walls. The KA dough has an increased proportion of starch granules compared to Karl that gluten must stretch around, making cell walls more susceptible to bubble failure. This is consistent with the results of Hayman et al. (1998) who found that increasing the proportion of starch granules in dough causes coalescence and a more open crumb grain. It is interesting to note that although KA had the largest gas cells it had only the second highest loaf

volume (932 cm^3). This confirms what was suggested by Campbell (2003) that coalescence causes "the loss of bubble numbers" and the "coarsening of bubble structure" but does not affect the amount of gas retained by the cell structure. The fact that KA does not have the highest loaf volume confirms that the very large gas cells found in the sample are in fact due to coalescence and cannot be explained by gas cell expansion.

Alpowa also had an increased proportion of very large gas cells (95^{th} percentile) when compared to the Karl and BZ flours. Due to its relatively low percentage of unextractable polymeric protein (UPP) (45.80%) and low overall protein content (9.44%), the cell walls tend to easily rupture under the deformation of proofing and baking. Alpowa also had a relatively low strain hardening index (1.29) when compared to the other flours. Doughs with low strain hardening ability are not able to resist premature gas cell failure (Dobraszczyk and Morgenstern, 2003).

Table 4.9 Gas cell size means for top and middle samples listed by flour variety

	Flour Variety	Gas cell size (mm) at cumulative distribution points				Average gas cell size (mm)
		25%	50%	75%	95%	
Top	Karl	0.18^{ab}	0.32^{ab}	0.55^{a}	0.97^{b}	0.41^{ab}
	KA	0.22^{a}	0.41^{a}	0.78^{a}	1.29^{a}	0.54^{a}
	BZ	0.17^{b}	0.31^{b}	0.53^{a}	0.91^{b}	0.39^{b}
	Alpowa	0.19^{ab}	0.37^{ab}	0.65^{a}	1.15^{ab}	0.47^{ab}

	Flour Variety	Gas cell size (mm) at cumulative distribution points				Average gas cell size (mm)
		25%	50%	75%	95%	
Middle	Karl	0.18^{a}	0.34^{a}	0.58^{a}	1.07^{a}	0.43^{a}
	KA	0.19^{a}	0.35^{a}	0.59^{a}	1.08^{a}	0.44^{a}
	BZ	0.17^{a}	0.32^{a}	0.57^{a}	1.02^{a}	0.41^{a}
	Alpowa*	NA	NA	NA	NA	NA

Values reported are the average of 3 replicate measurements for each of the four processing stages (total of 12)

Means with the same letter within columns are not significantly different ($p < 0.05$)

** Sampling not possible due to structural artifacts.*

Figure 4.8 Gas cell size distributions of baked samples for each flour variety

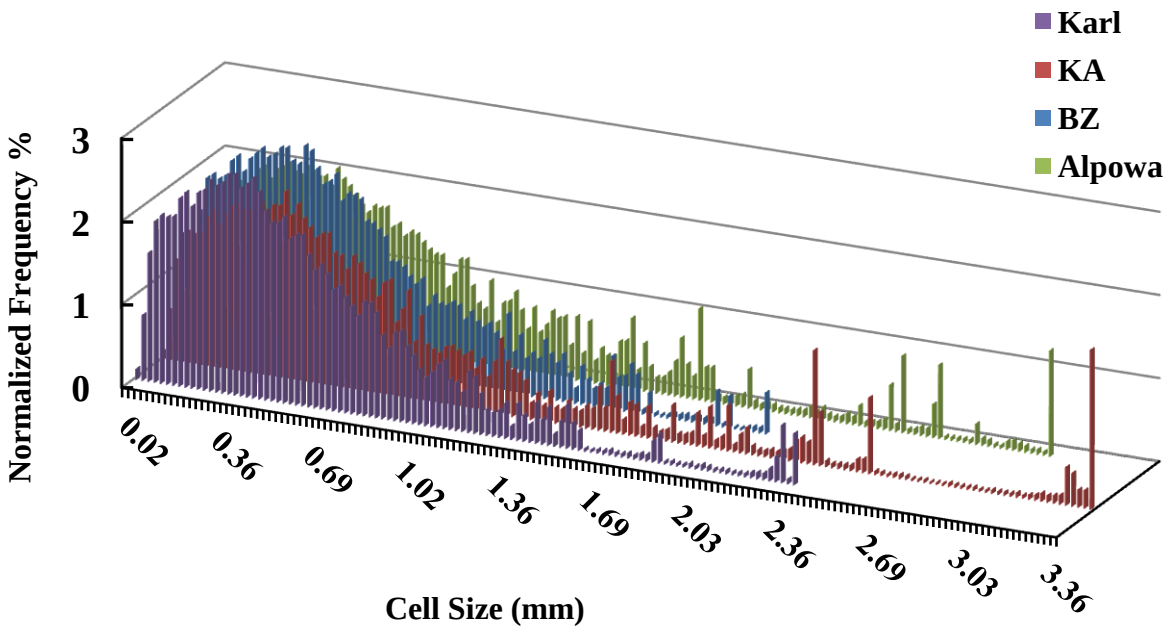

4.3.1.2. Average Gas Cell Size

Average gas cell size values were also calculated across flour variety and are shown in Table 4.9. KA had the highest average gas cell size values at 0.54 mm (top samples) and 0.44 mm (middle samples) followed closely by Alpowa. BZ had the smallest average gas cell size with values reaching 0.39 mm (top samples) and 0.41 mm (middle samples). This indicates that the gas cell walls for BZ had greater overall stability during proofing and baking.

4.3.2 Cell Wall Thickness

4.3.2.1. Cell Wall Thickness Distributions

Cell wall thickness distributions were also compared across flour variety using cumulative distribution points (Table 4.10). Points for Alpowa, KA, Karl, and BZ were not significantly different ($P < 0.05$) at the 25th percentile. This indicates that the 25th percentile (total volume) fell in the same place for all four flours. At the 75th and 95th percentiles however the values for Alpowa, KA and Karl were significantly higher than those for BZ. This implies that BZ had thinner cell walls at the higher percentiles. This trend was most apparent in the 40

min proofed samples distributions which are graphed for each flour type in Figure 4.9. BZ (Figure 4.9 green) is a strong breadmaking variety which contains a high percentage of unextractable polymeric protein (UPP) (50.31%). The UPP is made up of only the highest MW polymers (glutenins). Strong evidence has been provided suggesting that this fraction (MW > 250,000) is important for dough strength (Bangur et al., 1997) and gas cell stability (Sroan et al., 2008) which allows gas cell walls to expand during proofing and makes them less prone to premature failure or coalescence. BZ also had a high strain hardening index (2.03) which explains the thin cell walls. Doughs which have a high strain hardening index have gas cell walls that are able to "resist failure by locally increasing resistance to extension", allowing cell wall expand to smaller thicknesses (Dobraszczyk and Morgenstern, 2003).

When looking at the distributions for the baked product, Alpowa (Figure 4.10 purple) has the thickest cell walls. Though not significant in the overall data, the high cell wall thickness seen for Alpowa in the baked bread is a clear indication of cell wall weakness. Alpowa has low levels of UPP which cause cell walls to be unstable. Due to their lack of strength and strain hardening ability these cell walls easily rupture when exposed to the heat of baking.

Table 4.10 Cell wall thickness means for top and middle samples listed by flour variety

	Flour Variety	Cell wall thickness values (mm) at cumulative distribution points				Average wall thickness (mm)
		25%	50%	75%	95%	
Top	Karl	0.067^{a}	0.094^{a}	0.126^{ab}	0.177^{ab}	0.109^{a}
	KA	0.066^{a}	0.095^{a}	0.128^{a}	0.184^{a}	0.111^{a}
	BZ	0.062^{a}	0.086^{a}	0.115^{b}	0.162^{b}	0.101^{a}
	Alpowa	0.067^{a}	0.095^{a}	0.129^{a}	0.184^{a}	0.112^{a}
	Flour Variety	Cell wall thickness values (mm) at cumulative distribution points				Average wall thickness (mm)
		25%	50%	75%	95%	
Middle	Karl	0.072^{a}	0.103^{ab}	0.140^{a}	0.197^{ab}	0.119^{ab}
	KA	0.074^{a}	0.107^{a}	0.137^{ab}	0.207^{a}	0.124^{a}
	BZ	0.069^{a}	0.089^{b}	0.120^{b}	0.182^{b}	0.113^{b}
	Alpowa	NA	NA	NA	NA	NA

Values reported are the average of 3 replicate measurements for each of the four processing stages (total of 12)

Means with the same letter within columns are not significantly different ($p < 0.05$)

Figure 4.9 Cell wall thickness distributions of 40-min proofed samples for each flour variety (Values reported are the average of 6 (3 top, 3 middle) replicate measurements)

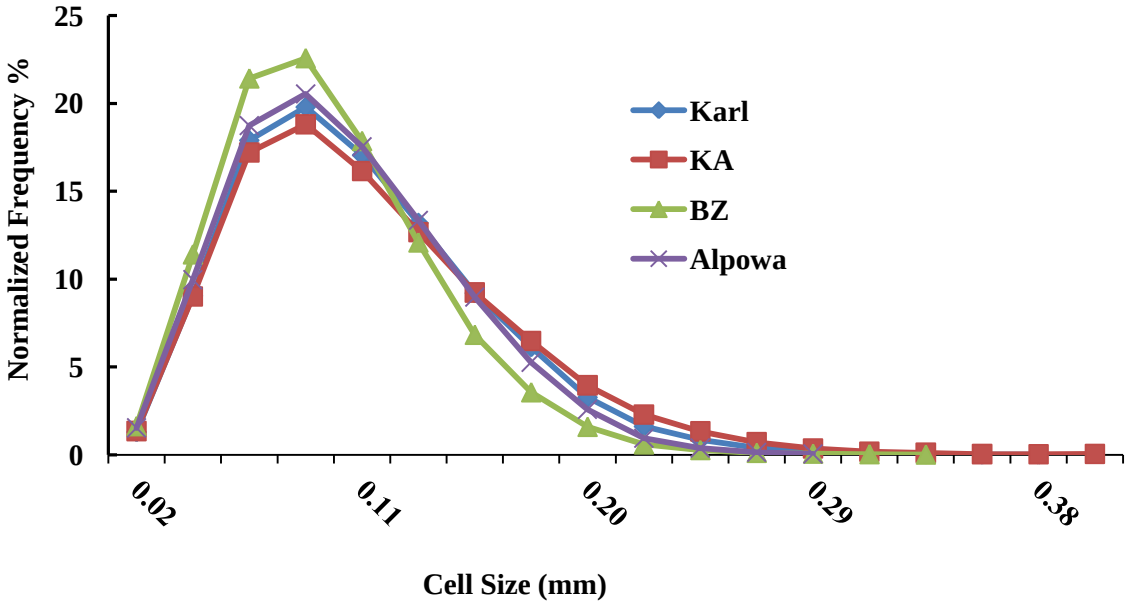

Figure 4.10 Cell wall thickness distributions of baked samples for each flour variety
Values reported are the average of 6 (3 top, 3 middle) replicate measurements

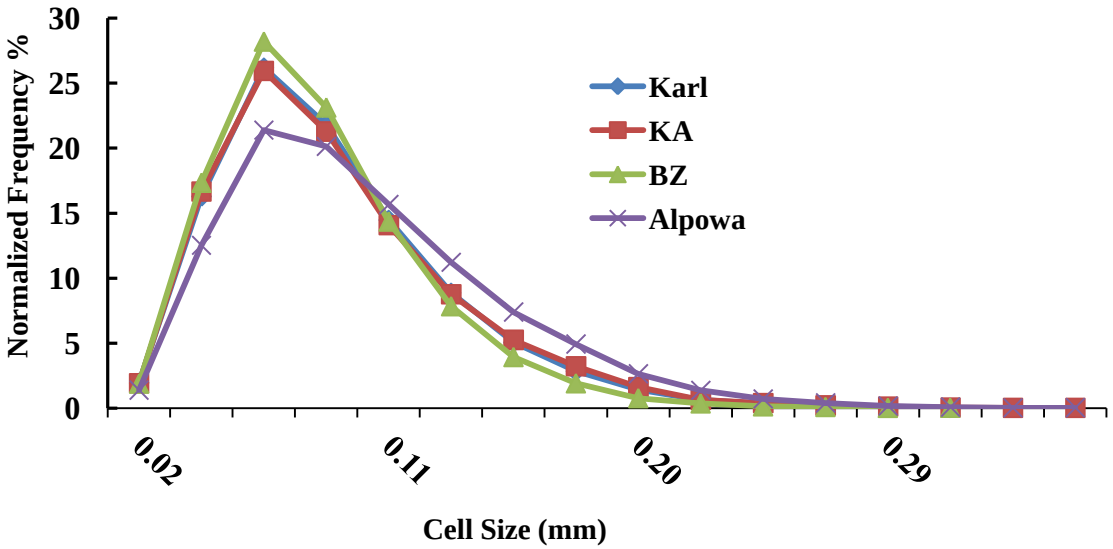

4.3.2.2. Average Cell Wall Thickness

Similar to the distribution values, average gas cell wall thicknesses reflected the ability of dough to resist expansion. Though not significantly different (P<.05) from the others, Alpowa flour had the highest mean average cell wall thickness value (0.1115 mm). KA and Karl had values with intermediate thickness values. BZ had the thinnest cell walls with mean average cell wall thickness values of only 0.1012 mm and 0.1127 mm for the top and middle sample locations respectively. When comparing the middle samples, values for BZ were significantly lower than those for KA. The cell walls of BZ have greater stability than those of KA. This allows them to stretch to smaller thicknesses before experiencing failure under the strains of proofing and baking.

4.3.3. Other Structural Parameters

In addition to gas cell size and cell wall thickness distributions, various morphometric parameters such as void fraction (VF), fragmentation index (FI), structure surface density (SSD), specific surface (SS), degree of anisotropy (DA) and fractal dimensions (FD) were compared with respect to different flour types. Results summarized in Table 4.11are the average of 3 replicate measurements for each of the four processing stages (total of 12).

Table 4.11 Parameter means for top and middle samples listed by flour variety

		VF (%)	FI	SSD (1/mm)	SS (1/mm)	DA	FD
Top	Karl	64.85^{a}	18.64^{a}	10.48^{b}	35.82^{ab}	1.53^{a}	2.36^{b}
	KA	65.65^{a}	-19.81^{a}	10.10^{b}	35.36^{ab}	1.53^{a}	2.36^{b}
	BZ	64.67^{a}	-20.40^{ab}	11.41^{a}	37.70^{a}	1.51^{a}	2.39^{a}
	Alpowa	63.24^{a}	-23.67^{b}	10.60^{ab}	33.67^{b}	1.50^{a}	2.38^{ab}
		VF (%)	FI	SSD (1/mm)	SS (1/mm)	DA	FD
Middle	Karl	61.48^{a}	-23.31^{a}	10.44^{a}	30.78^{ab}	1.62^{a}	2.37^{a}
	KA	59.85^{a}	-27.30^{a}	10.12^{a}	29.60^{b}	1.57^{a}	2.37^{a}
	BZ	61.13^{a}	-24.64^{a}	10.81^{a}	33.27^{a}	1.62^{a}	2.39^{a}
	Alpowa	NA	NA	NA	NA	NA	NA

Values reported are the average of 3 replicate measurements for each of the four processing stages (total of 12)

Means with the same letter within columns are not significantly different ($p < 0.05$)

4.3.3.1. Void Fraction

Void fractions did not differ significantly (P< 0.05) between flour types. Mean values for void fraction did however follow at trend with stronger flours (Karl and KA) tending to have higher void fractions than weaker ones (BZ and Alpowa). This trend is similar to that seen for loaf volume. Flours which produced a loaf of high volume also had a crumb of high void fraction.

4.3.3.2. Fragmentation Index

Differences in FI were also related to flour strength. Overall, Alpowa (top samples) had a significantly lower (P< 0.05) FI than Karl or KA indicating that it has more connected cell wall structure (Table 4.11). Individual means for fragmentation index are graphed in Figure 4.11. The low values for Alpowa are most evident at the beginning of proofing and indicate a well connected gas cell wall structure.

Figure 4.11 Fragmentation index top samples

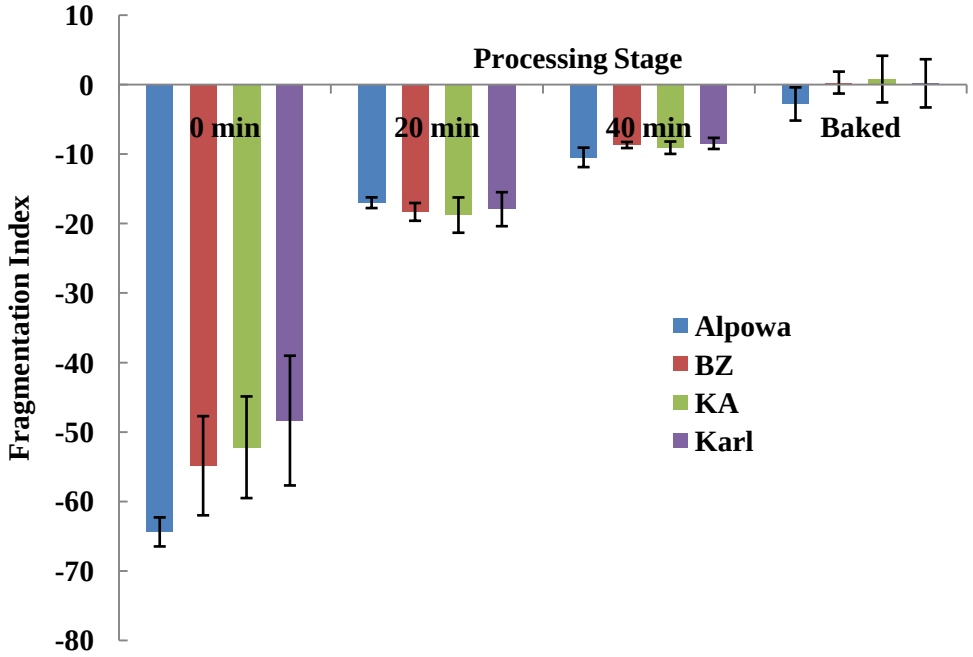

4.3.3.3. Structure Surface Density

Structure surface density is a measure of the surface area per unit volume. Overall the BZ flour had the highest SSD with values (11.41 1/mm top sample) being significantly larger than those for the other flours (Table 4.11). These high SSD values indicate that BZ forms a tight stable crumb structure with a high surface area. This is supported by previous discussions (section 4.3.2.1) suggesting that BZ forms a strong dough matrix which remains relatively stable throughout processing.

4.3.3.4. Specific Surface

Specific surface (SS) is measured as the ratio of total cell wall surface area to cell wall volume. BZ had the highest SS values (37.7 1/mm, top) but was followed closely by Karl (35.8 1/mm, top) and KA (35.4 1/mm, top) (Table 4.11). These high surface area to cell wall volume ratios indicate a complex cell structure with thin gas cell walls. As previously discussed in section 4.3.2.1, both the BZ and Karl are strong flours with cell walls capable of expanding to small thicknesses. Alpowa had the lowest mean SS value (33.7 1/mm, top) which was significantly ($P < 0.02$) lower than the value for BZ.

4.4. References

Babin, P., Della Valle, G., Chiron, H., Cloetens, P., Hoszowska, J., Pernot, P., Reguerre, A.L., Salvo, L. and Dendievel, R. 2006. Fast X-ray tomography analysis of bubble growth and foam setting during breadmaking. Journal of Cereal Science. 43, 393-397.

Baker, J.C. and Mize, M.D. 1946. Gas occlusion during dough mixing. Cereal Chemistry 23, 38-51.

Bangur, R., Batey, I.L., McKenzie, E. and MacRitchie, F. 1997. Dependence of extensograph parameters on wheat protein composition measured by SE-HPLC. Journal of Cereal Science 25, 237-241.

Campbell, G.M, 2003. Bread aeration, in *Breadmaking: Improving Quality*, S. Cauvain (Ed.), pp. 352-374, Woodhead Publishing Ltd.,Cambridge, UK

Chiotellis, E. and Campbell, G.M. 2003. Proving of bread dough II measurement of gas production and retention. Trans IChemE 81(C), 207-216.

Dobraszczyk, B.J. 1997. Development of a new dough inflation system to evaluate doughs. Cereal Foods World 42(7), 516-519.

Dobraszczyk, B.J. and Morgenstern, M.P. 2003. Rheology and the bread making process. Journal of Cereal Science 38, 229-245.

Gupta, R.B., Khan, K. and MacRitchie, F. 1993. Biochemical basis of flour properties in bread wheats I. Effects of variation in the quantity and size distribution of polymeric protein. Journal of Cereal Science 18, 23-41.

Hayman, D., Hoseney, R.C. and Faubion, J.M. 1998. Effect of pressure (crust formation) on bread crumb grain development. Cereal Chemistry 75(5), 585-589.

Sroan, B.S., Bean, S.R. and MacRitchie, F. 2008. Mechanism of gas cell stabilization in bread making. I. The primary gluten-starch matrix. Journal of Cereal Science. 49, 32-40.

van Vliet, Tom. 2008. Strain hardening as an indication of bread-making performance: A review with discussion. Journal of Cereal Science 48, 1-9.

CHAPTER 5 - **Conclusions**

In this study a method was established for using X-ray microtomography (XMT) to study the microstructure of proving dough as well as bread. Both dough freezing and sampling protocols were developed so that microstructure could be determined using XMT. This technique made possible the most complete and accurate characterization of bread and dough microstructure to date. Previous imaging techniques including digital image analysis (Zghal et al., 1999) and light microscopy (Whitworth and Alava, 1999) required sectioning of sample specimens in order to obtain scanned images. X-ray microtomography is a non-invasive technique which provides the user with thousands of detailed sample images that make up a complete three dimensional view of the sample. This XMT data along with the use of an advanced software package (CT-Analyser) made it possible to obtain gas cell size distributions, cell wall thickness distributions, void fractions and a variety of other parameters which were used to objectively and completely characterize the structure of both bread and dough samples.

This study provides, for the first time, a complete characterization of proofing dough and bread microstructure with sufficient replication so that the effects of both processing stage and flour variety could be quantified. Overall, the largest amount of variability seen in the samples structures was due to the processing stage. 3-D analysis of the bubbles indicated that average dough void fractions increased dramatically over proof time from 30.9% for the unproofed dough (0 min) to 62.0% and 74.5 % for the underproofed (20 min) and optimally proofed (40 min) doughs respectively. Oven spring caused further expansion in the baked loaves which increased average void fraction to 84.3%. Gas cell size distributions shifted to larger values (to the right) as proofing time increased. These shifts in gas cell size distribution during proofing were largely the result of a decreased number of very small gas cells in the dough matrix. During the baking process, average gas cell size values effectively doubled, increasing from 0.40 mm for the fully proofed dough to 0.84 mm for the baked bread. These increases in average cell size were driven by the rapid expansion of gas cells (oven spring) as well as a small number of very large gas cells which are the result of coalescence. Proofing and baking also caused remarkable decreases in cell wall thickness which are reflected both in the distribution and average values. The largest decrease in cell wall thickness occurred in the early stages of proofing (0-20 min) where gas cells experience free growth.

The microstructures of bread and dough made from three very different wheat varieties were compared in this study. Differences in gas cell size seen among flour varieties were largely due to variations in the size of the largest cells seen at the 95th percentile in the (top samples). Overall, KA had the highest average gas cell size but only the second highest loaf volume. This is a clear indication that the high gas cell size is due to coalescence and not only gas cell expansion. Alpowa also had an increased proportion of very large gas cells but a low loaf volume. This is evidence that weaker doughs from flours such as Alpowa are not able to withstand the strains of proofing and baking. The premature rupture of thin films as well as overall dough weakness contributed to large gas cell size and low loaf volume.

Karl and BZ, which are strong bread making varieties, displayed the highest amount of gas cell stability. BZ in particular maintained a tight crumb with a high SSD (surface area/volume) value through out the proofing and baking process. Both BZ and Karl are strong bread making varieties with high UPP values and high strain hardening ability. During proofing and baking, their cell walls were able to resist premature rupture and expand to very small thicknesses.

The results of this study were also affected by sampling location. The top part of the loaf clearly has more space for expansion and growth than the middle part of the loaf which is much more confined. Specimens which were sampled from the top part of the loaf generally had higher void fractions, larger gas cells and thinner gas cell walls than there middle counterparts. The high amount of expansion at the top of the loaf, made top samples ideal for distinguishing differences in microstructure between treatments.

CHAPTER 6 - **Future Studies**

1. XMT is clearly the most advanced tool for characterizing the structure of cereal products. The potential for its future use in characterizing the cell structure of bread products is nearly limitless. With the rising interest in whole grain and high fiber foods is becomes necessary to explore the effect of cereal fibers and pentosans on the stability of gas cells. XMT is a technique that is well suited for this purpose and will likely provide insight as to how these healthy ingredients can be more functional in bread products.

2. This study compared the microstructural properties of bread and dough made from three distinctly different wheat varieties. Future studies should also explore the microstructural properties of bread made from a large a variety of genetically diverse wheat cultivars. This will ultimately help breeders to a better understand of the genetic factors which effect functionality.

3. Future studies should focus on the link between the biaxial rheological properties of dough and gas cell stability during proofing and baking. Important rheological parameters such as strain hardening should be measured at low and high temperatures in order to gain a better understanding of gas cell stability both before and during baking.

Appendix A - Gas Cell Size Distribution Data

Figure A.1 Gas cell size distributions with respect processing stage (a) Karl, top sample, (b) Karl, middle sample, (c) KA, top sample, (d) KA, middle sample, (e) BZ, top sample, (f) BZ, middle sample, (g) Alpowa, top sample, (h) Alpowa sample. (Data presented is the average of 3 replicate measurements)

(a)

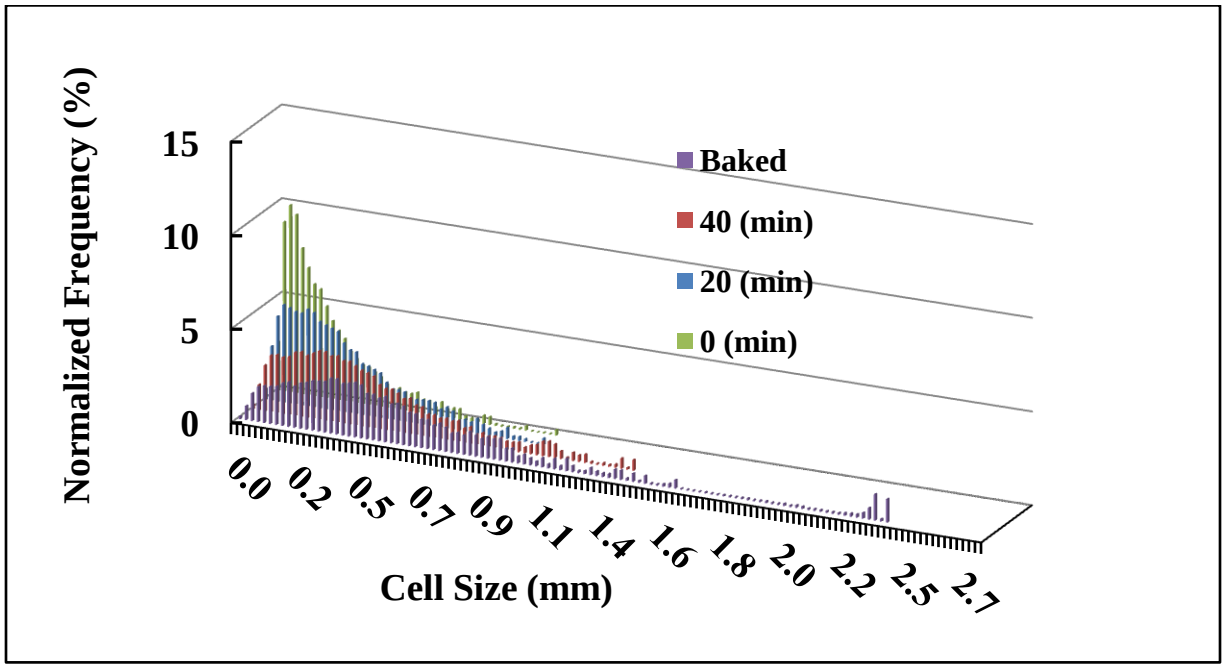

(b)

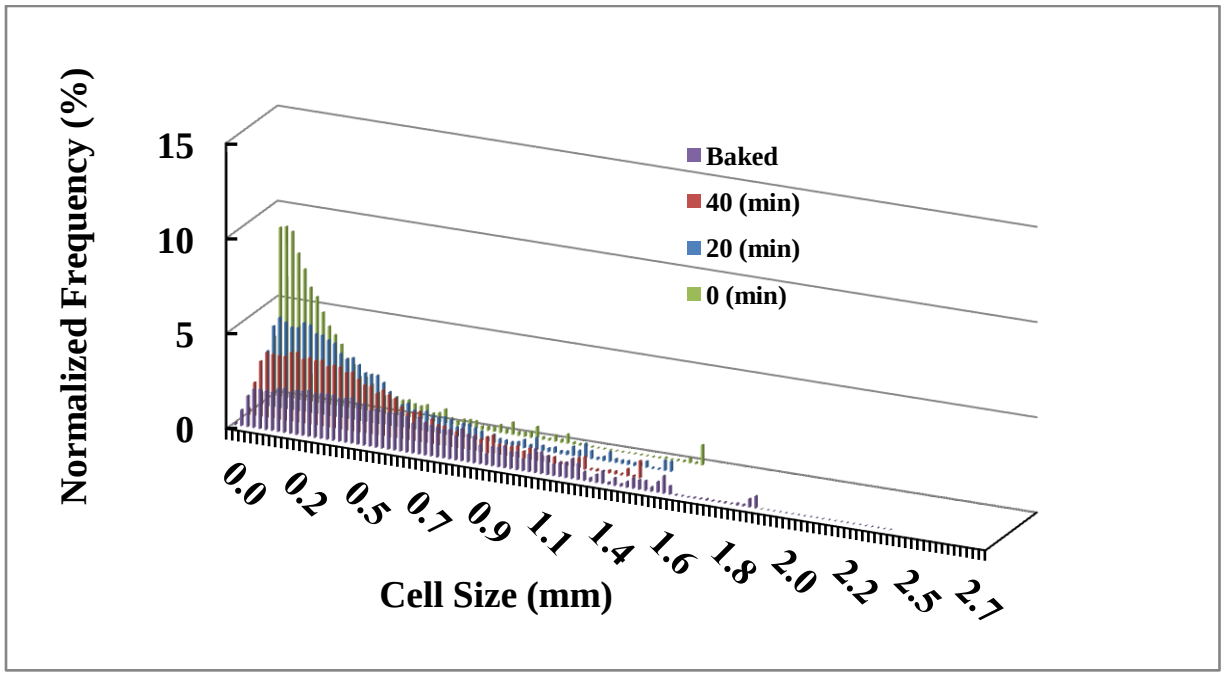

(c)

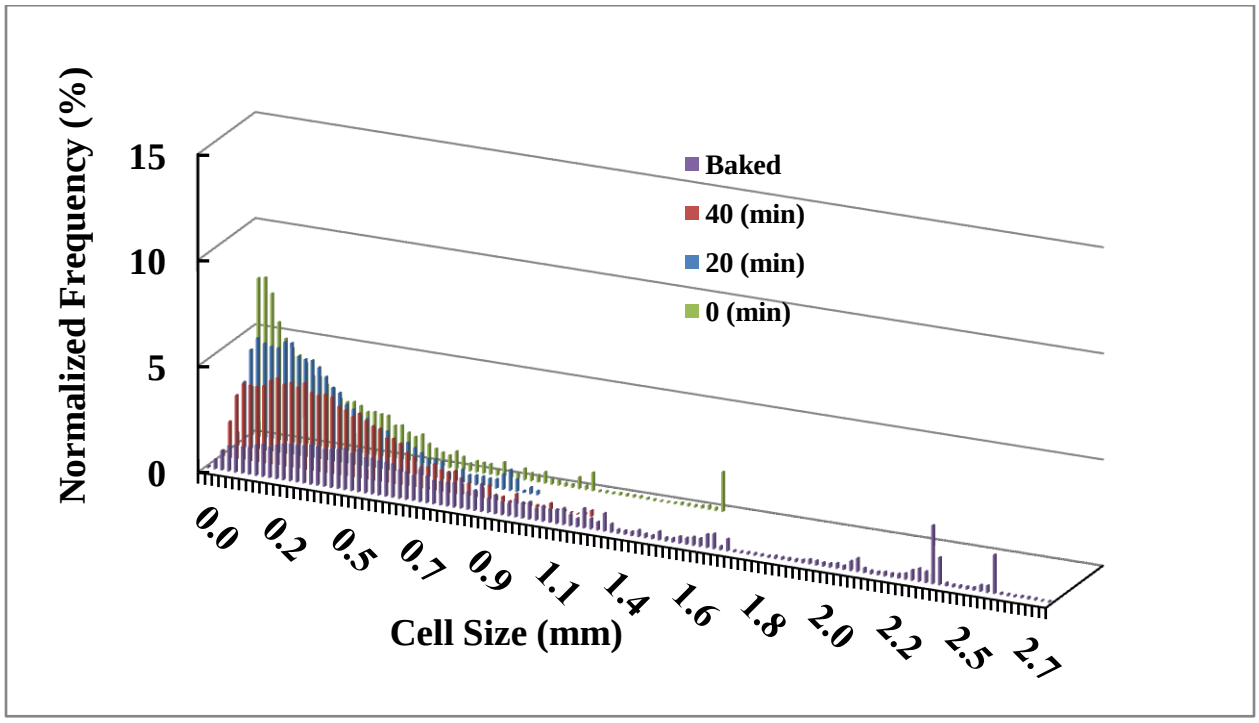
Normalized Frequency (%)
15
10
5
0
Baked
40 (min)
20 (min)
0 (min)
0.0
0.2
0.5
0.7
0.9
1.1
1.4
1.6
1.8
2.0
2.2
2.5
2.7
Cell Size (mm)

(d)

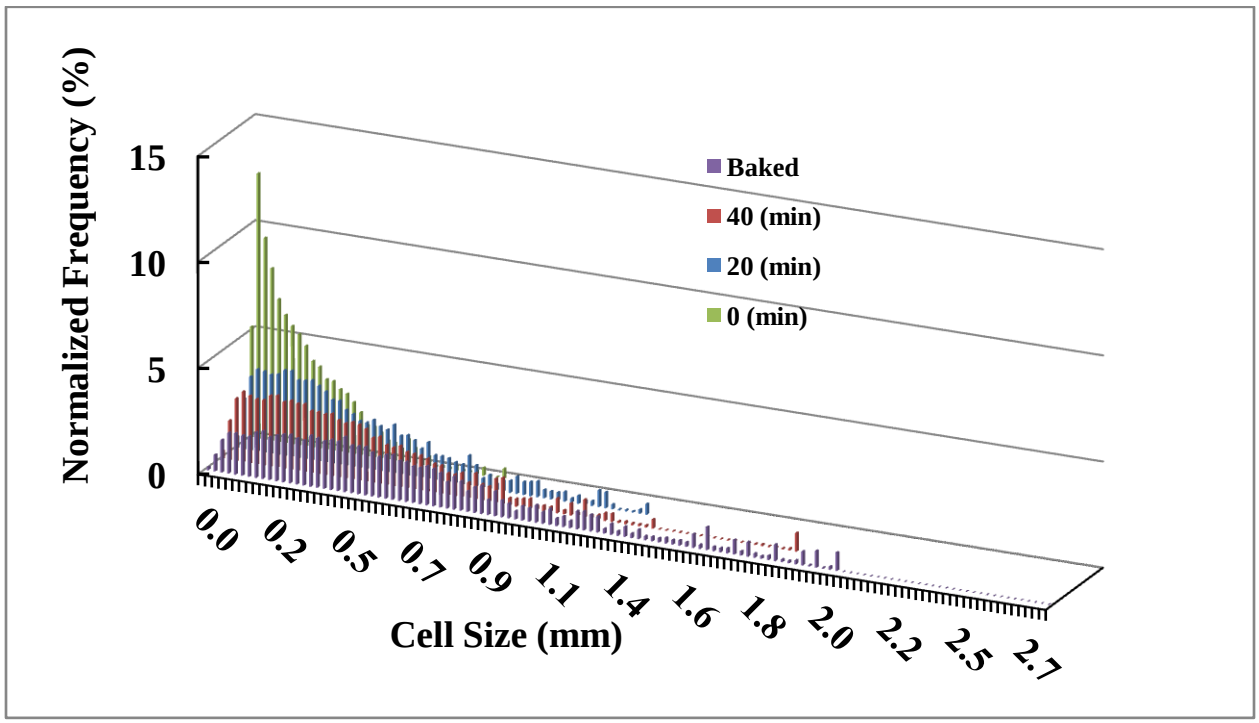
Normalized Frequency (%)
15
10
5
0
Baked
40 (min)
20 (min)
0 (min)
0.0
0.2
0.5
0.7
0.9
1.1
1.4
1.6
1.8
2.0
2.2
2.5
2.7
Cell Size (mm)

(d)

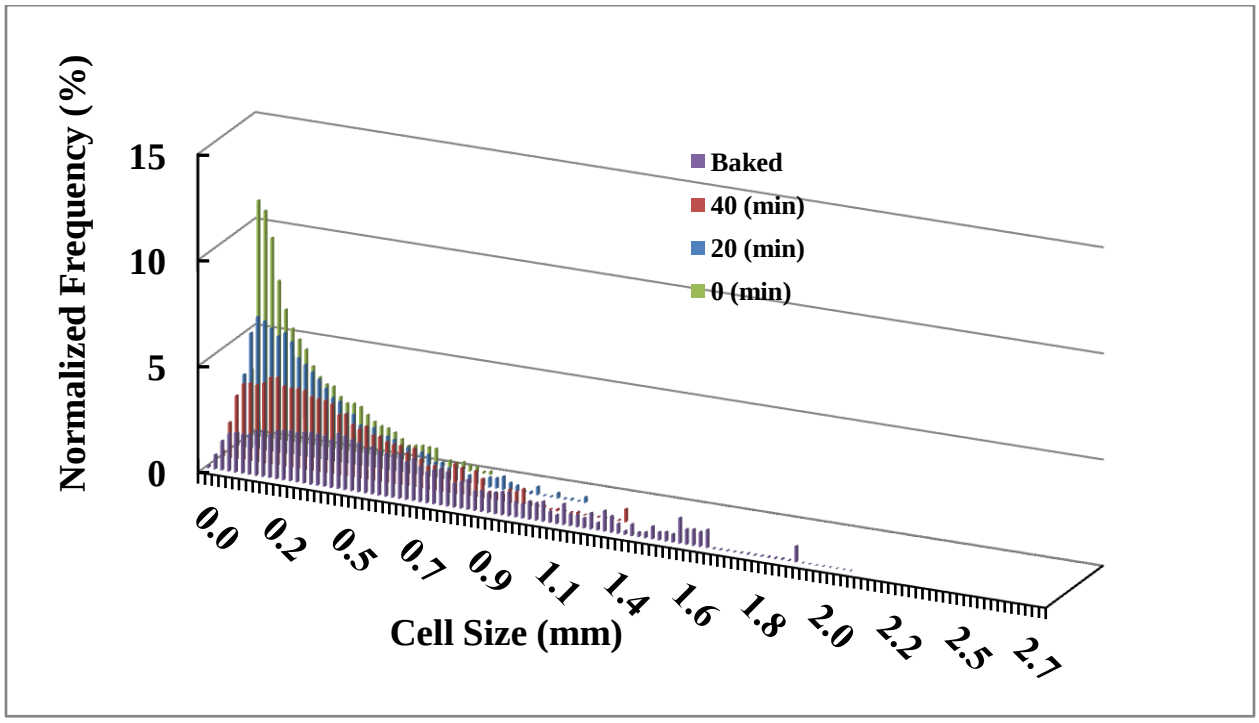
Normalized Frequency (%)
15
10
5
0
Baked
40 (min)
20 (min)
0 (min)
0.0
0.2
0.5
0.7
0.9
1.1
1.4
1.6
1.8
2.0
2.2
2.5
2.7
Cell Size (mm)

(e)

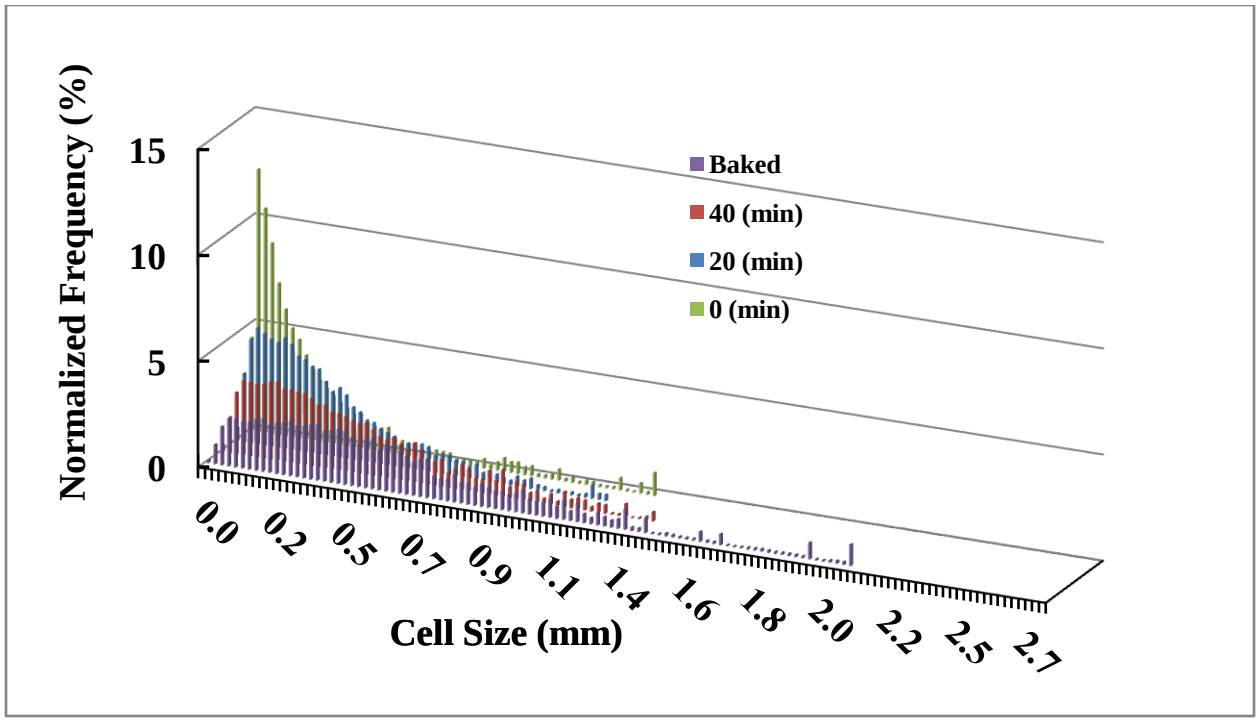
Normalized Frequency (%)
15
10
5
0
Baked
40 (min)
20 (min)
0 (min)
0.0
0.2
0.5
0.7
0.9
1.1
1.4
1.6
1.8
2.0
2.2
2.5
2.7
Cell Size (mm)

(f)

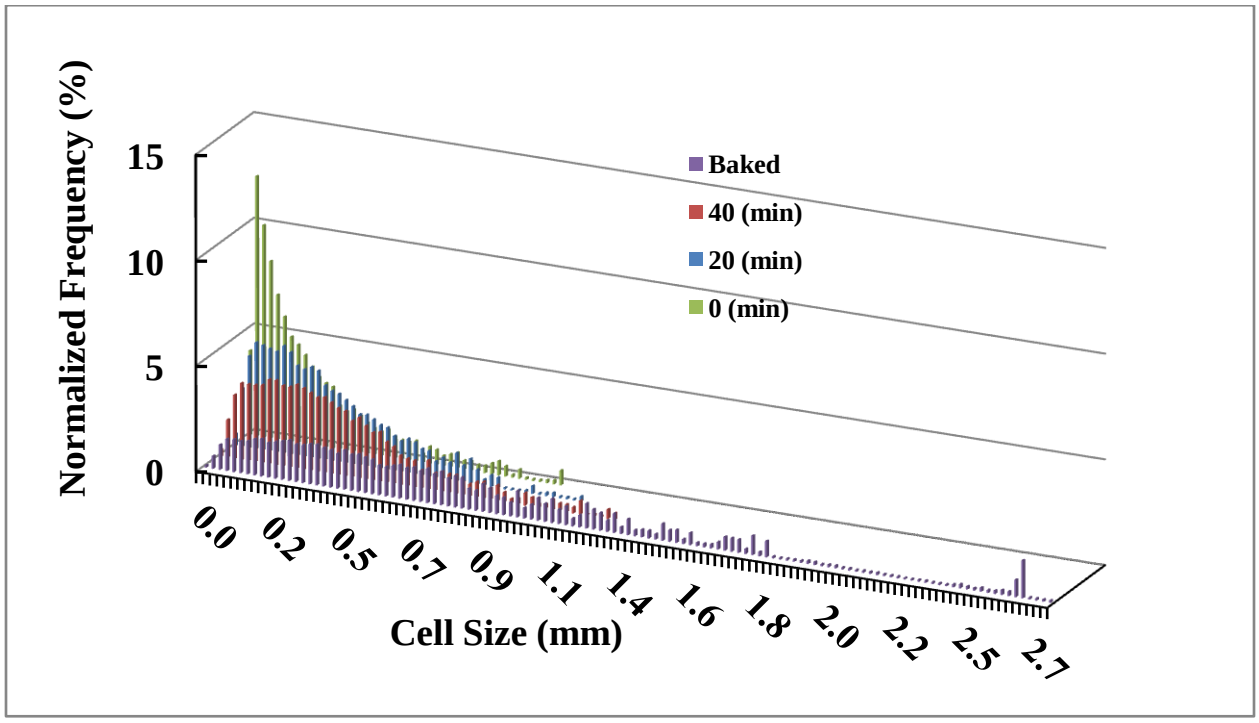
Normalized Frequency (%)
15
10
5
0
Baked
40 (min)
20 (min)
0 (min)
0.0
0.2
0.5
0.7
0.9
1.1
1.4
1.6
1.8
2.0
2.2
2.5
2.7
Cell Size (mm)

(g)

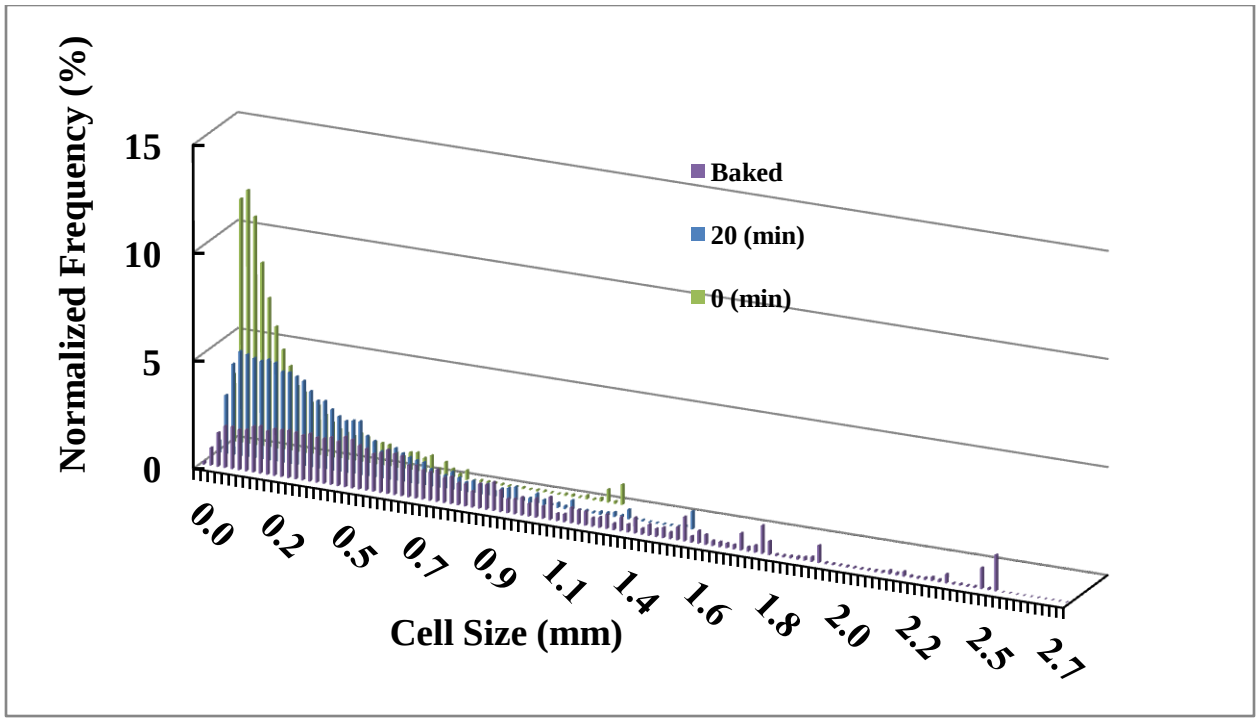
Normalized Frequency (%)
15
10
5
0
Baked
20 (min)
0 (min)
0.0
0.2
0.5
0.7
0.9
1.1
1.4
1.6
1.8
2.0
2.2
2.5
2.7
Cell Size (mm)

Figure A.2 Gas cell size distributions with respect to flour type (a) 0 min, top sample, (b) 0 min, middle sample, (c) 20 min, top sample, (d) 20 min, middle sample, (e) 40 min, top sample, (f) 40 min, middle sample, (g) baked, top sample, (h) baked, middle sample. (Data presented is the average of 3 replicate measurements)

(a)

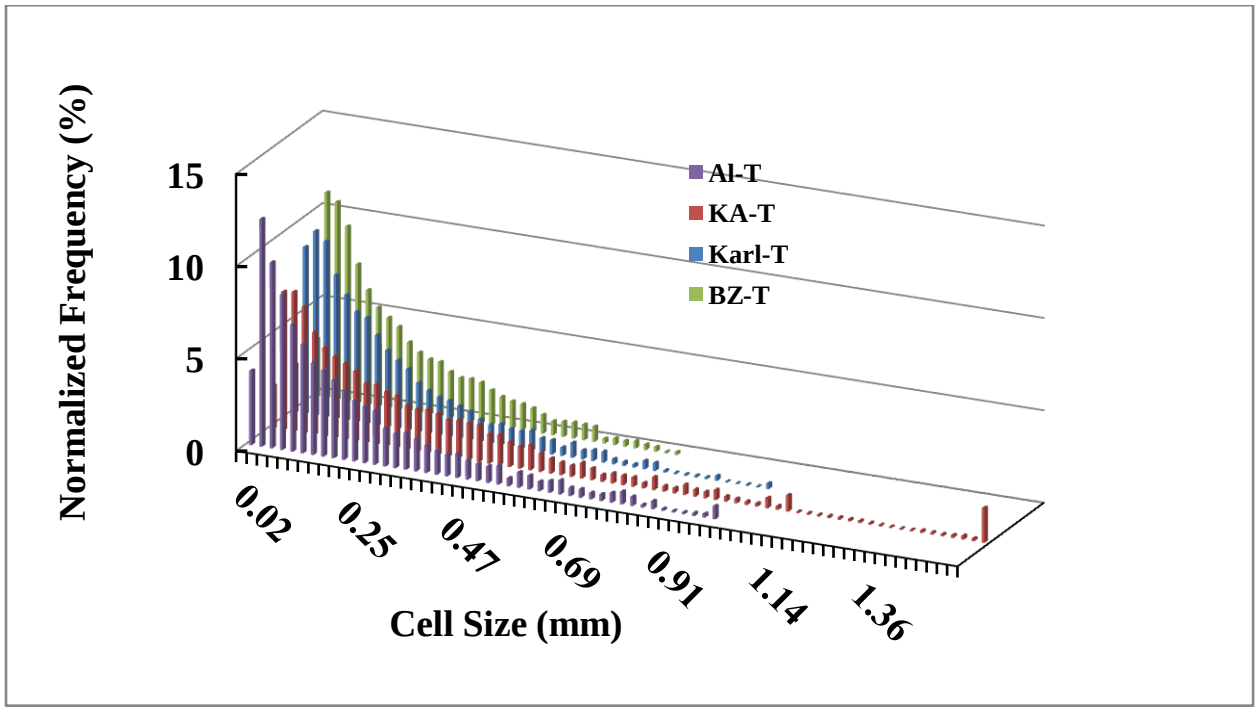

(b)

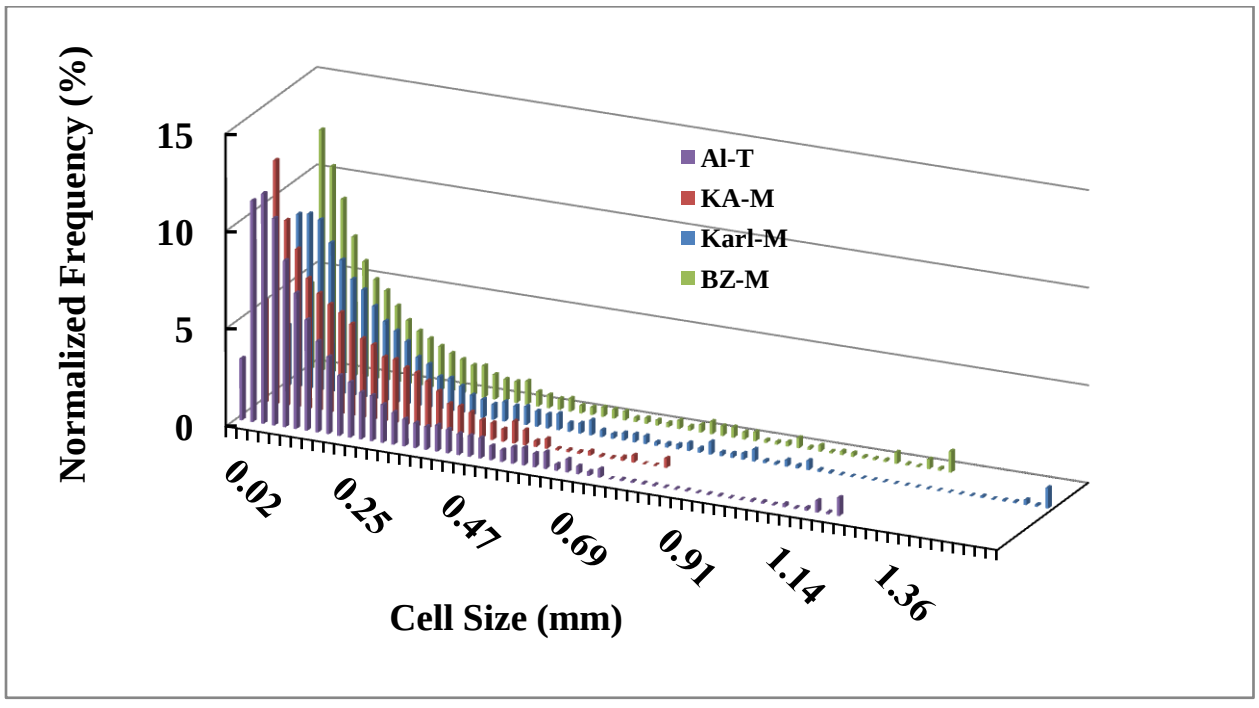

(c)

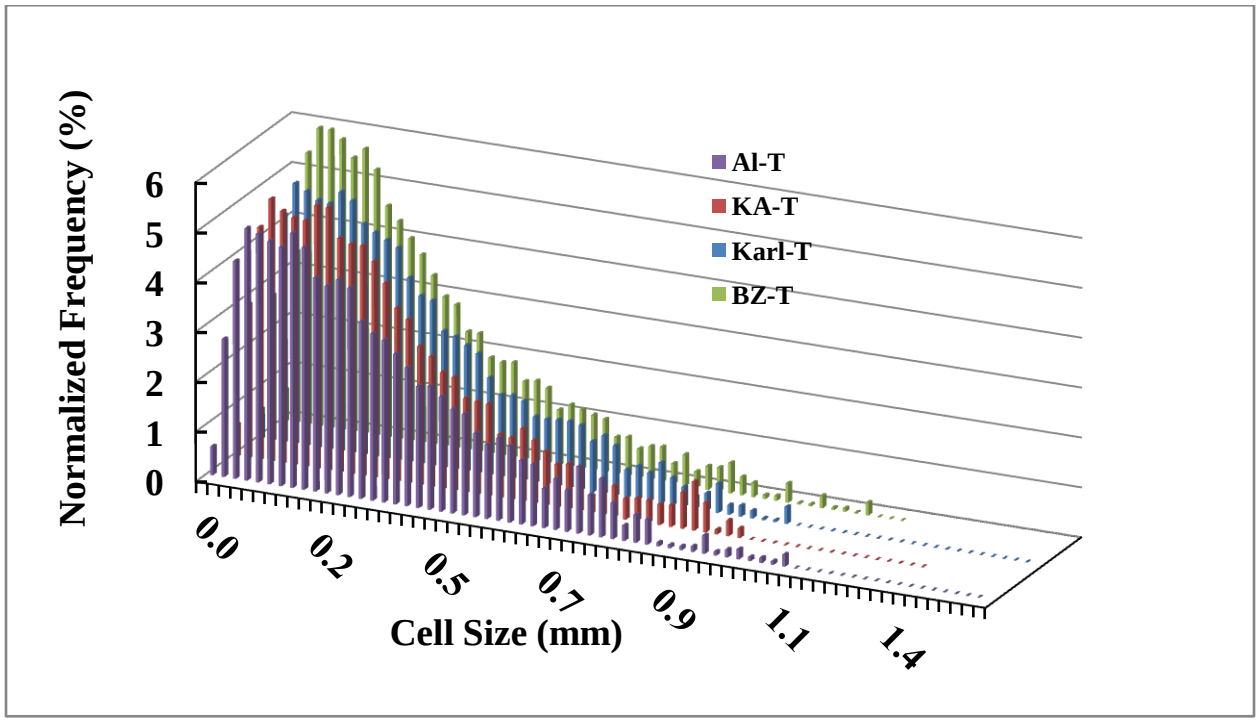
Normalized Frequency (%)
6
5
4
3
2
1
0
Al-T
KA-T
Karl-T
BZ-T
0.0
0.2
0.5
0.7
0.9
1.1
1.4
Cell Size (mm)

(d)

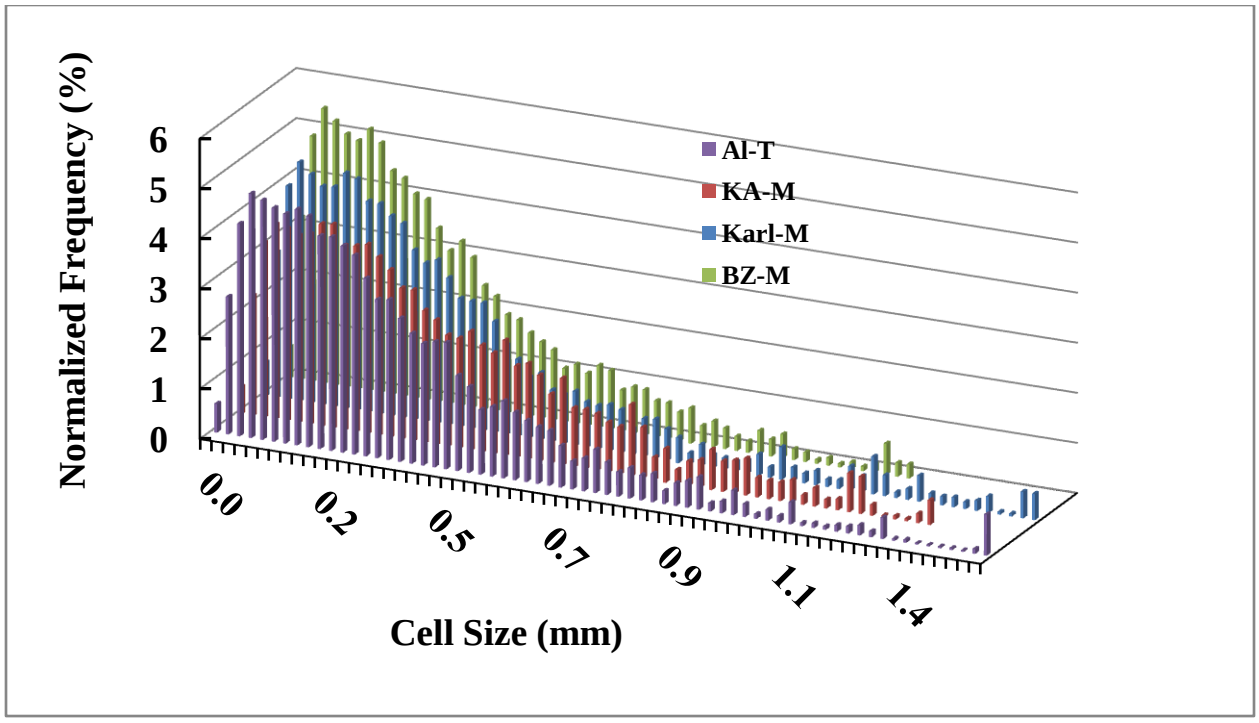
Normalized Frequency (%)
6
5
4
3
2
1
0
Al-T
KA-M
Karl-M
BZ-M
0.0
0.2
0.5
0.7
0.9
1.1
1.4
Cell Size (mm)

(e)

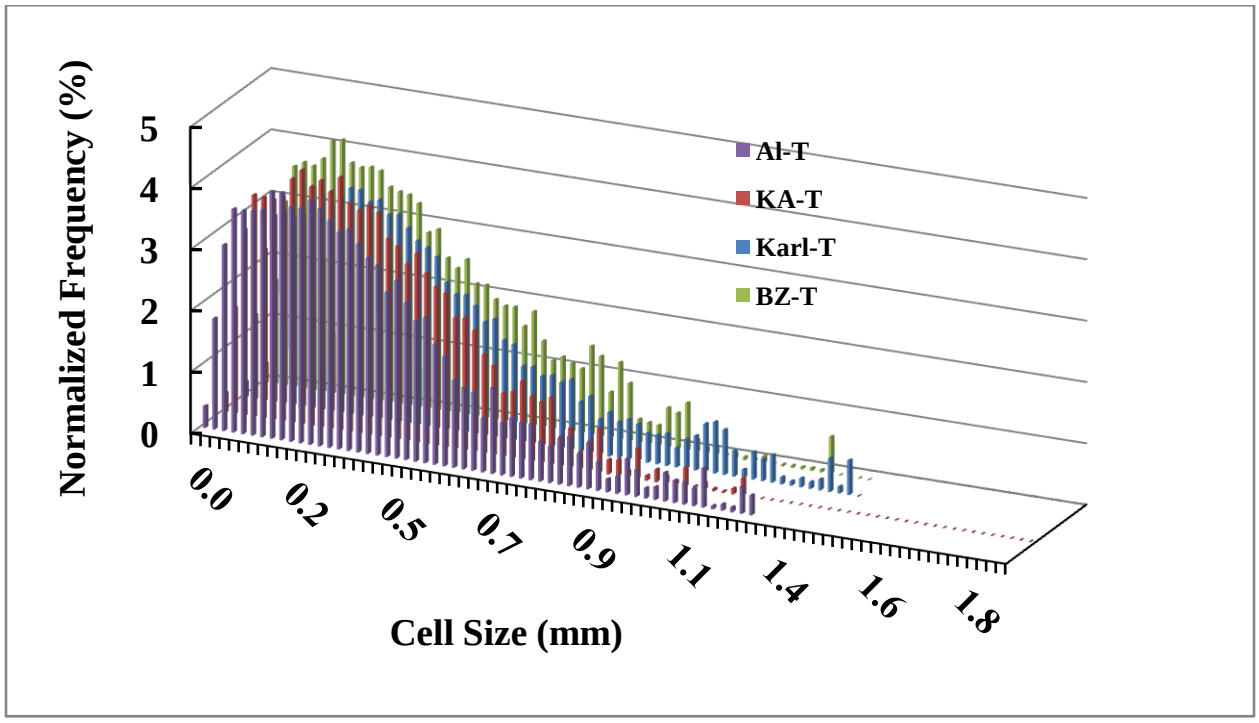
Normalized Frequency (%)
5
4
3
2
1
0
Al-T
KA-T
Karl-T
BZ-T
0.0
0.2
0.5
0.7
0.9
1.1
1.4
1.6
1.8
Cell Size (mm)

(f)

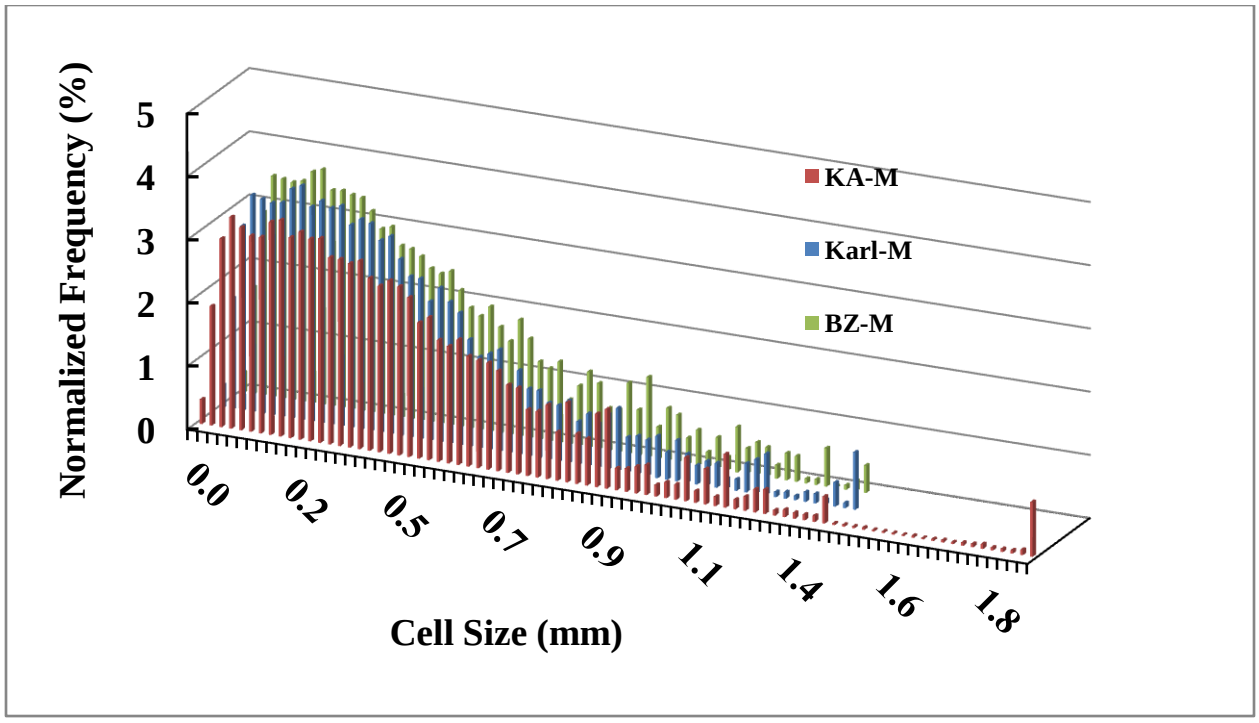
Normalized Frequency (%)
5
4
3
2
1
0
KA-M
Karl-M
BZ-M
0.0
0.2
0.5
0.7
0.9
1.1
1.4
1.6
1.8
Cell Size (mm)

(g)

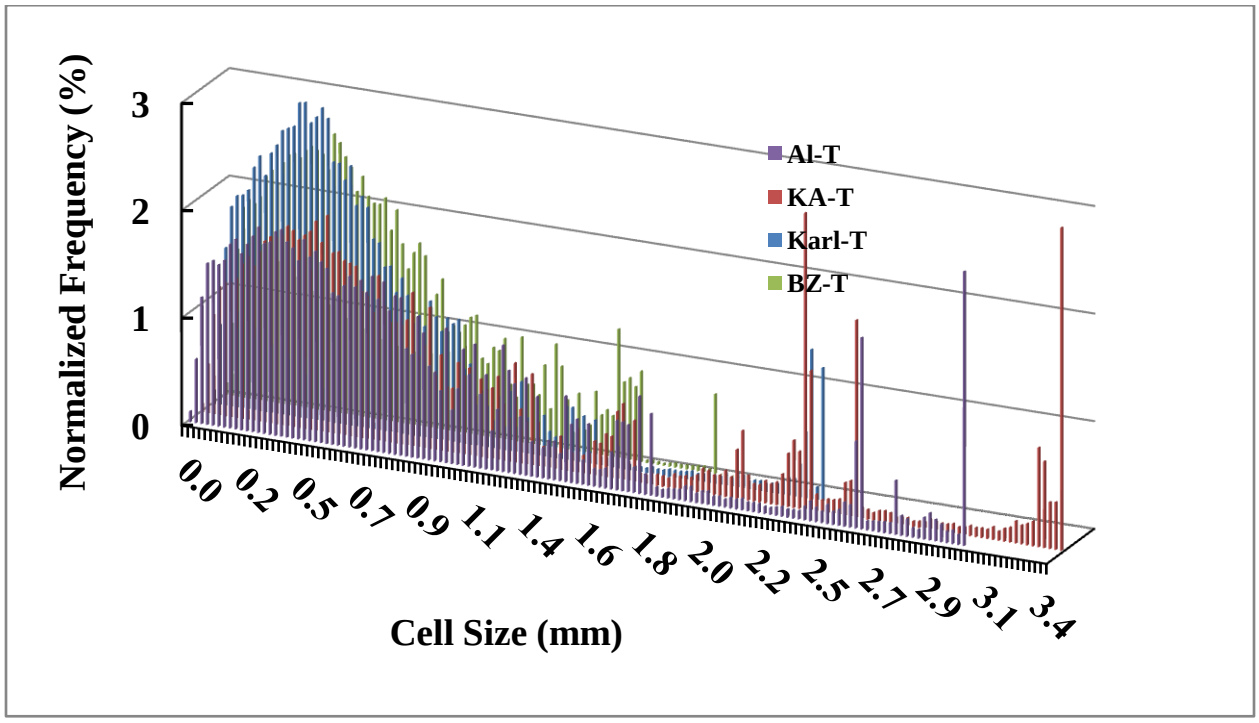
Normalized Frequency (%)
3
2
1
0
Al-T
KA-T
Karl-T
BZ-T
0.0 0.2 0.5 0.7 0.9 1.1 1.4 1.6 1.8 2.0 2.2 2.5 2.7 2.9 3.1 3.4
Cell Size (mm)

(h)

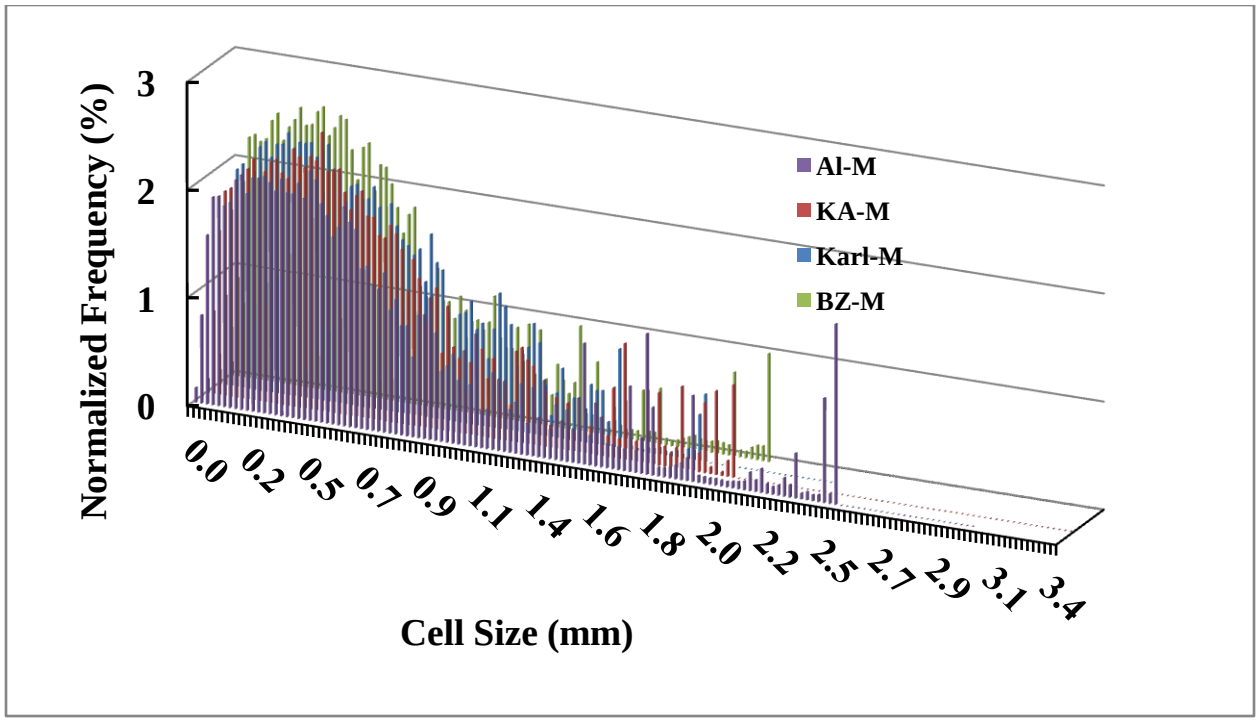
Normalized Frequency (%)
3
2
1
0
Al-M
KA-M
Karl-M
BZ-M
0.0 0.2 0.5 0.7 0.9 1.1 1.4 1.6 1.8 2.0 2.2 2.5 2.7 2.9 3.1 3.4
Cell Size (mm)

Appendix B - Cell Wall Thickness Distribution Data

Figure B.1 Cell wall thickness distributions with respect processing stage (a) Karl, top sample, (b) Karl, middle sample, (c) KA, top sample, (d) KA, middle sample, (e) BZ, top sample, (f) BZ, middle sample, (g) Alpowa, top sample, (h) Alpowa sample. (Data presented is the average of 3 replicate measurements)

(a)

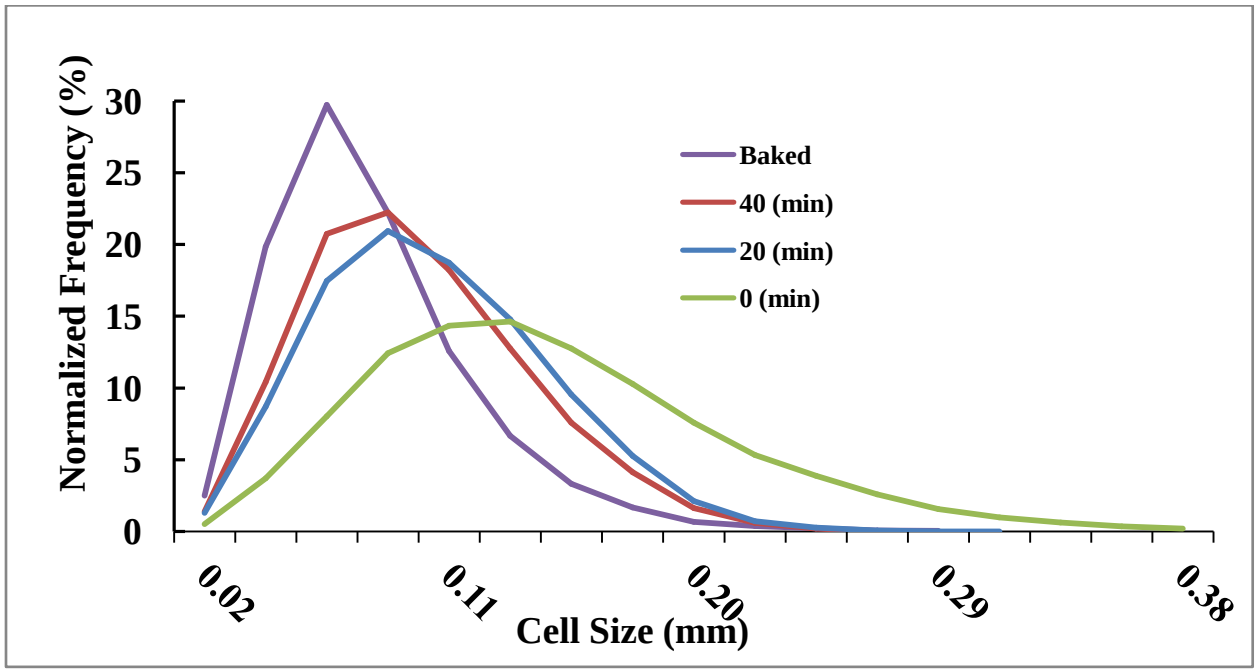

(b)

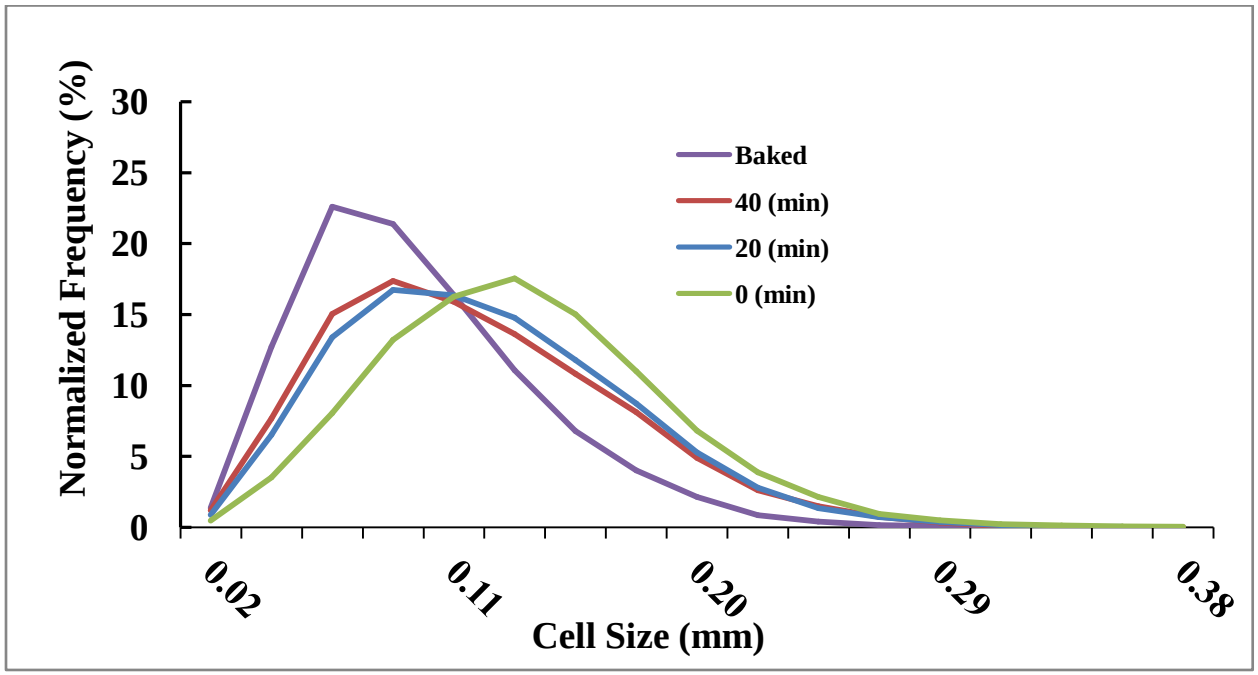

(c)

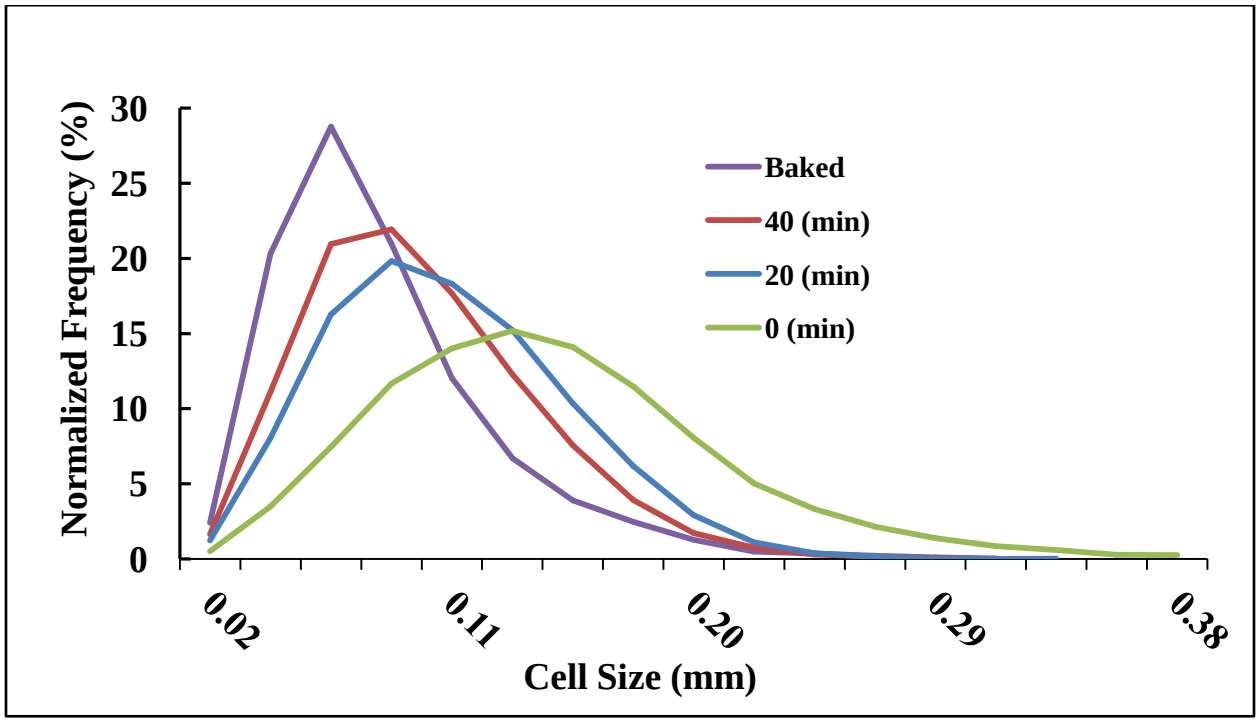
Normalized Frequency (%)
30
25
20
15
10
5
0
0.02
0.11
0.20
0.29
0.38
Cell Size (mm)
Baked
40 (min)
20 (min)
0 (min)

(d)

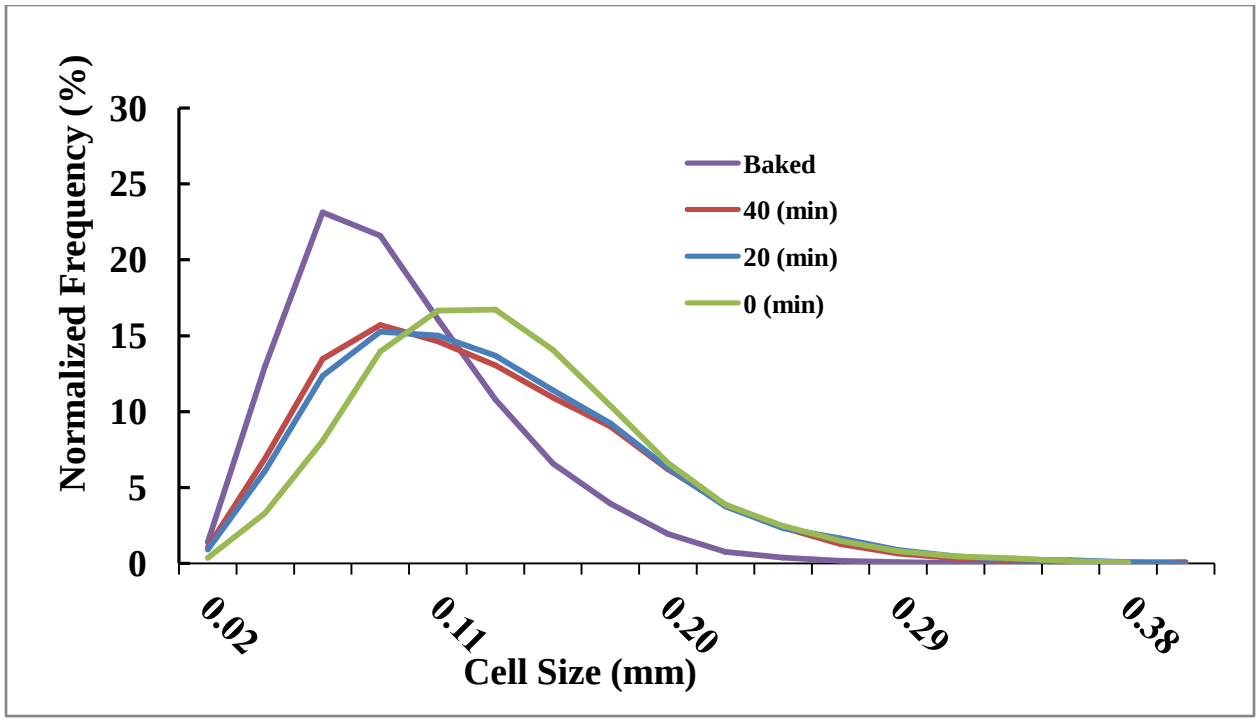
Normalized Frequency (%)
30
25
20
15
10
5
0
0.02
0.11
0.20
0.29
0.38
Cell Size (mm)
Baked
40 (min)
20 (min)
0 (min)

(e)

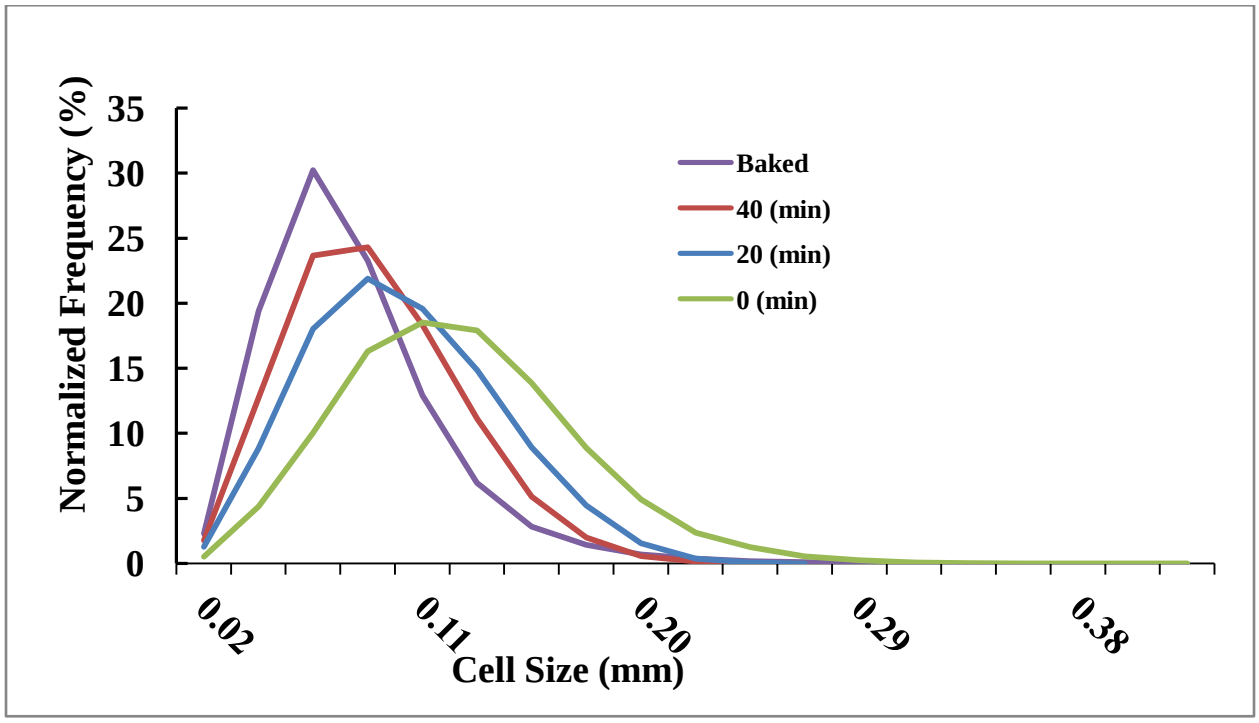
Normalized Frequency (%)
35
30
25
20
15
10
5
0
Baked
40 (min)
20 (min)
0 (min)
0.02
0.11
0.20
0.29
0.38
Cell Size (mm)

(f)

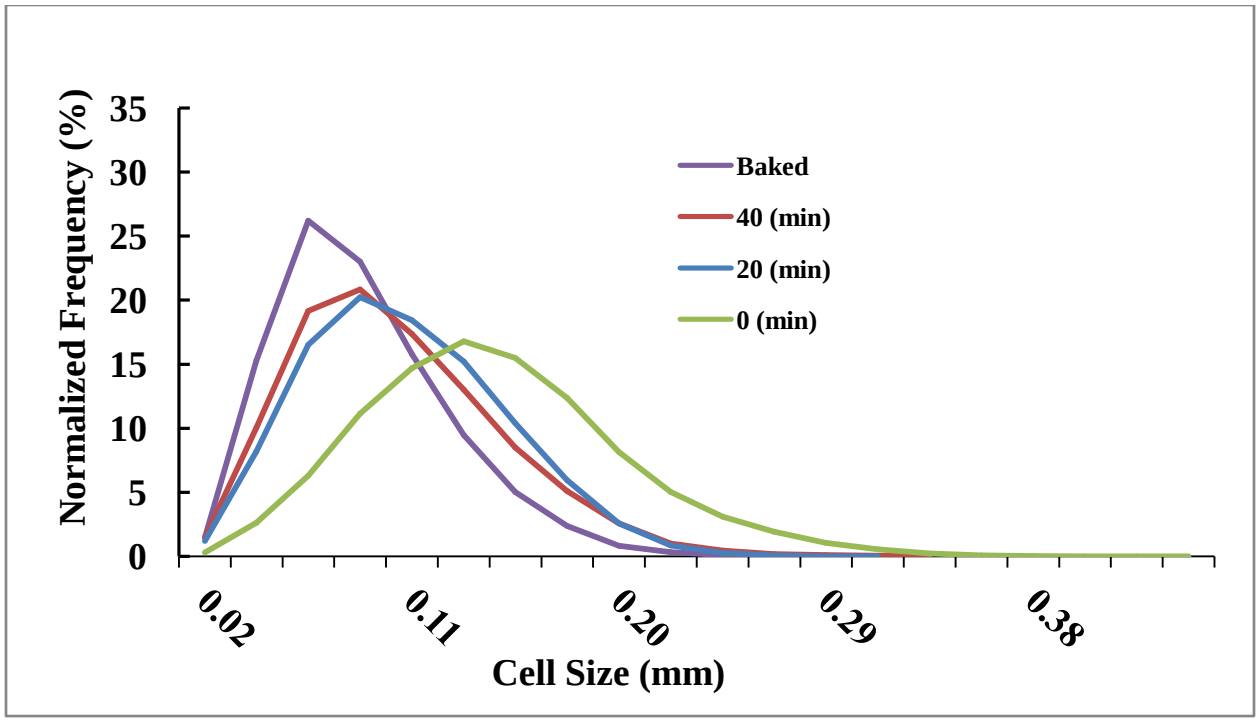
Normalized Frequency (%)
35
30
25
20
15
10
5
0
Baked
40 (min)
20 (min)
0 (min)
0.02
0.11
0.20
0.29
0.38
Cell Size (mm)

(g)

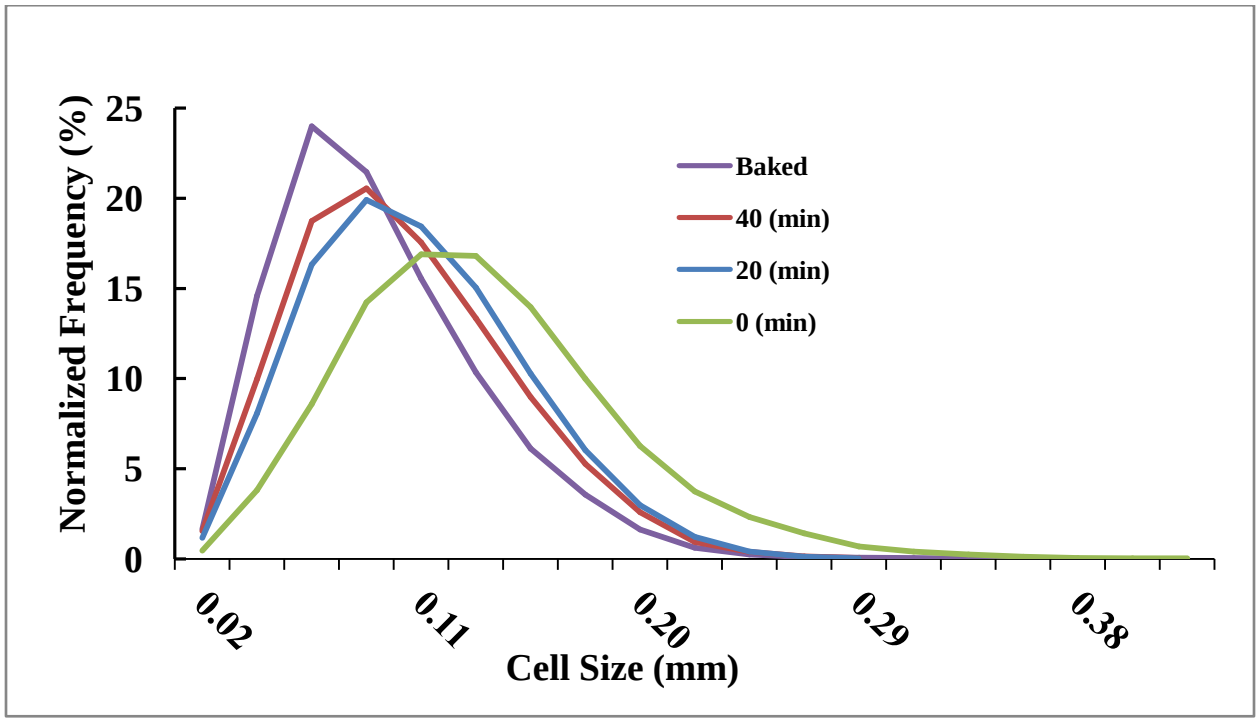
Normalized Frequency (%)
25
20
15
10
5
0
Baked
40 (min)
20 (min)
0 (min)
0.02
0.11
0.20
0.29
0.38
Cell Size (mm)

(h)

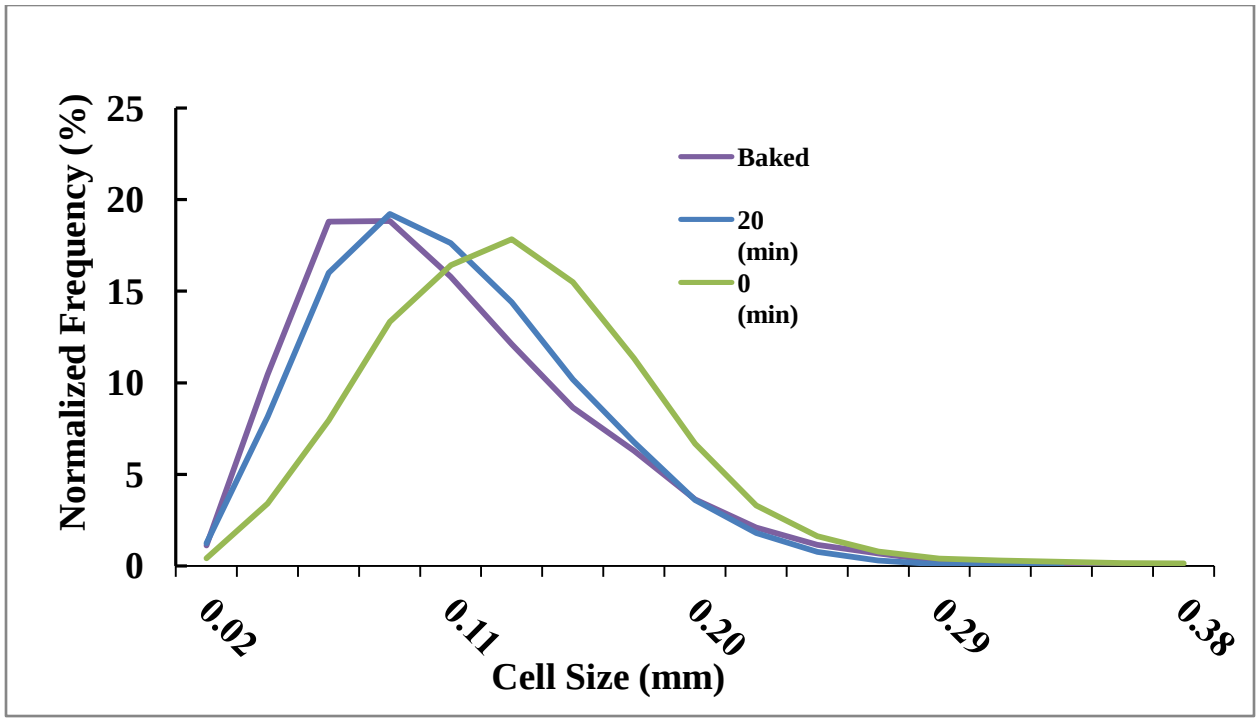
Normalized Frequency (%)
25
20
15
10
5
0
Baked
20 (min)
0 (min)
0.02
0.11
0.20
0.29
0.38
Cell Size (mm)

Figure B.2 Cell wall thickness distributions with respect to flour type (a) 0 min, top sample, (b) 0 min, middle sample, (c) 20 min, top sample, (d) 20 min, middle sample, (e) 40 min, top sample, (f) 40 min, middle sample, (g) baked, top sample, (h) baked, middle sample. (Data presented is the average of 3 replicate measurements)

(a)

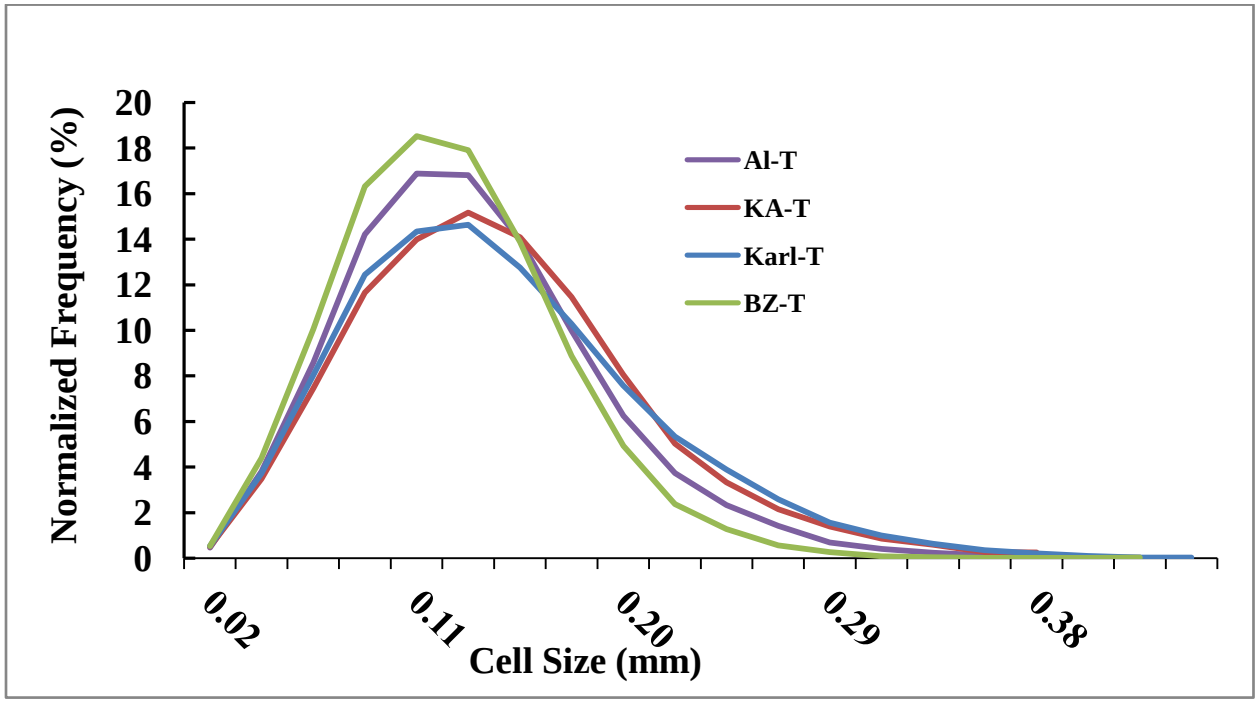

(b)

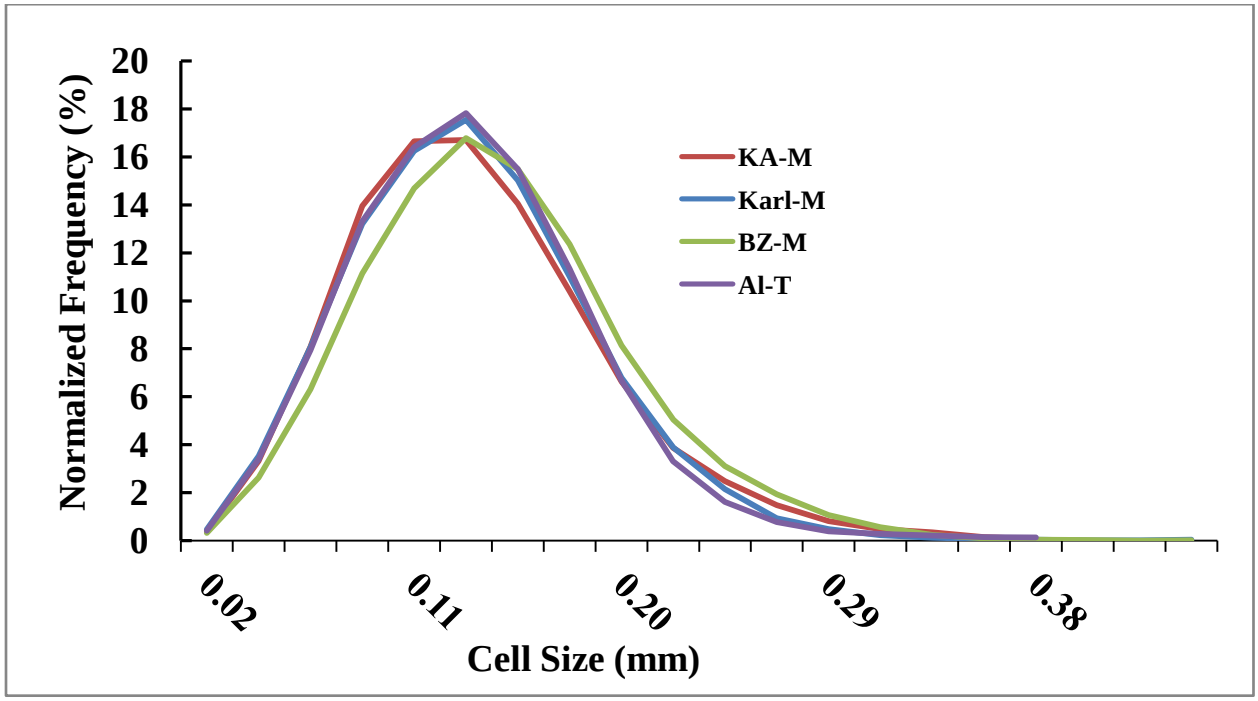

(c)

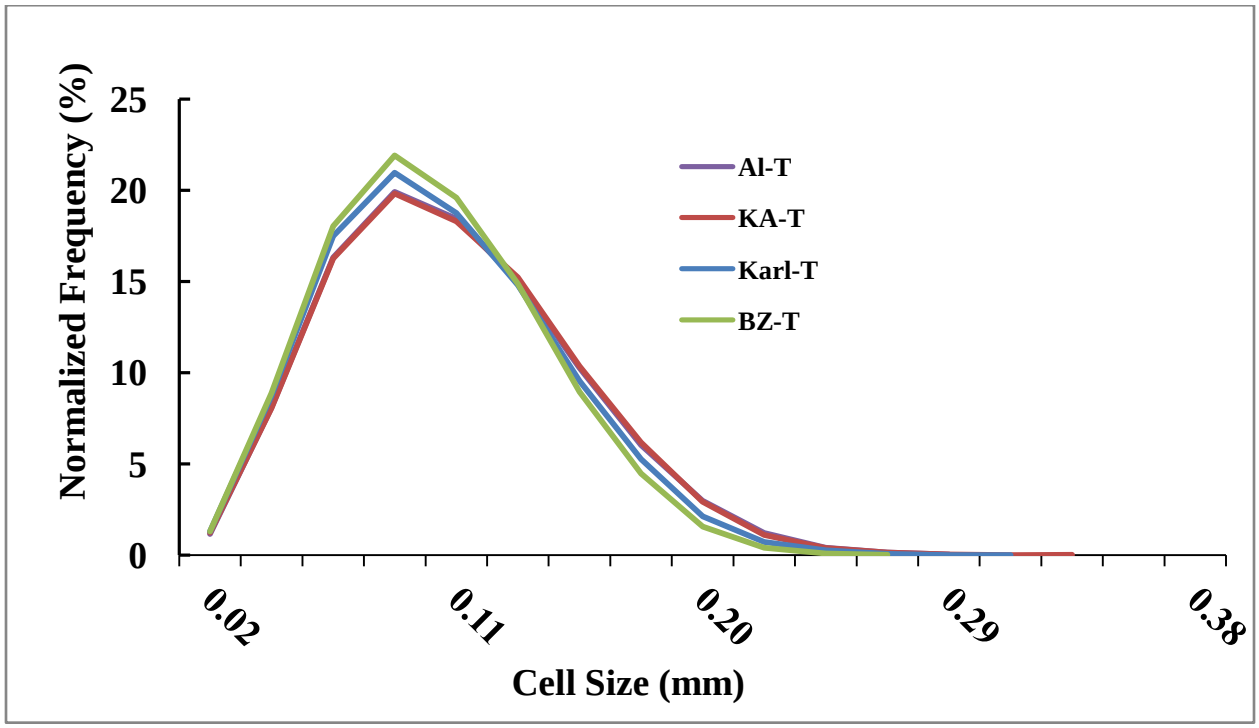
Normalized Frequency (%)
25
20
15
10
5
0
0.02
0.11
0.20
0.29
0.38
Cell Size (mm)
Al-T
KA-T
Karl-T
BZ-T

(d)

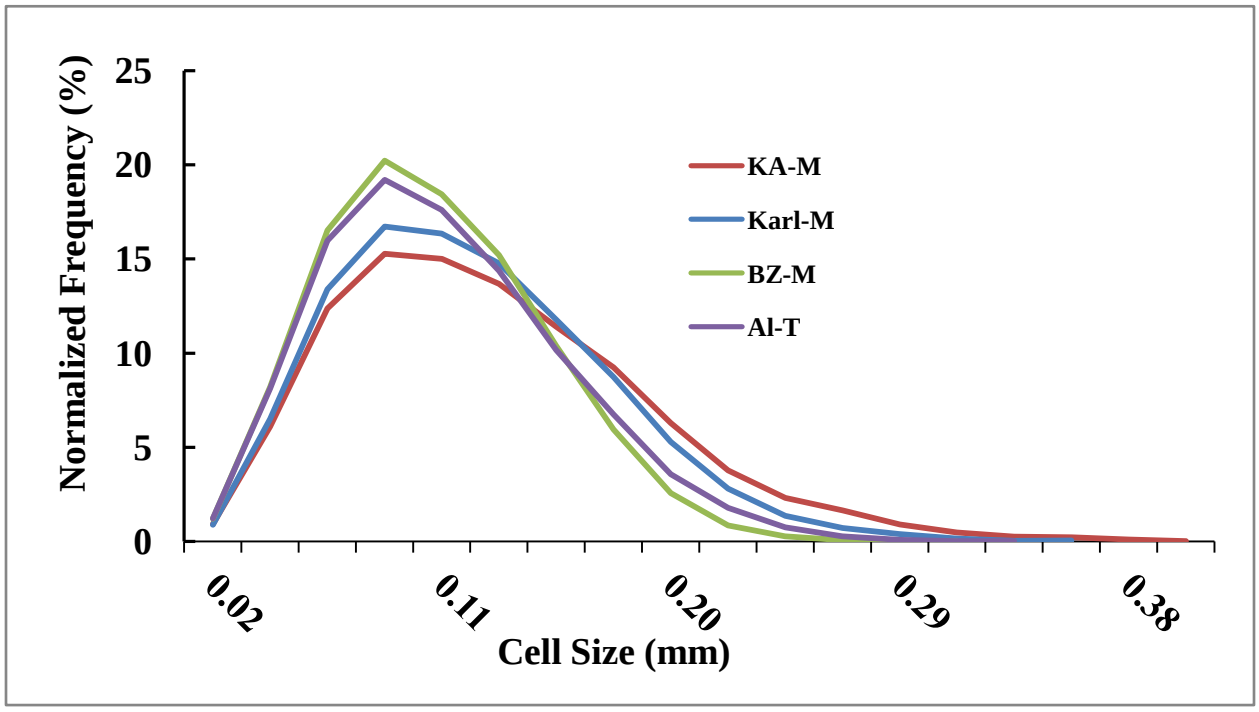
Normalized Frequency (%)
25
20
15
10
5
0
0.02
0.11
0.20
0.29
0.38
Cell Size (mm)
KA-M
Karl-M
BZ-M
Al-T

(e)

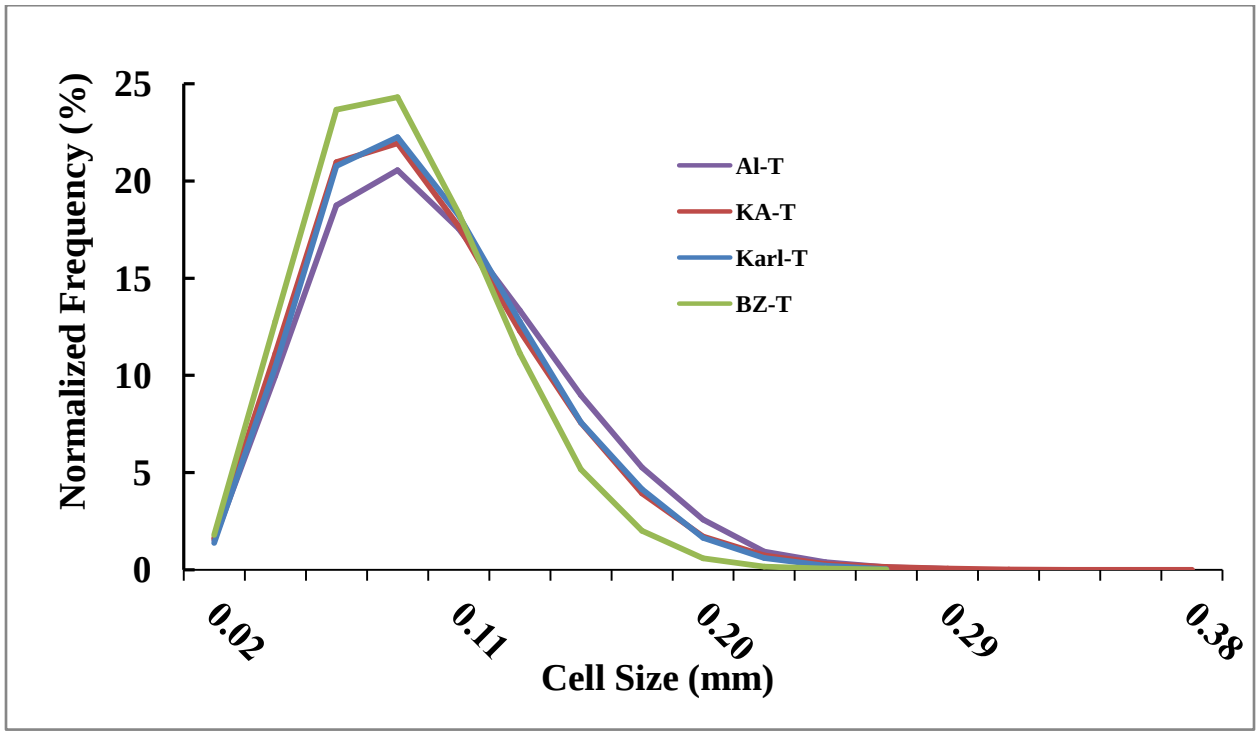
Normalized Frequency (%)
25
20
15
10
5
0
0.02
0.11
0.20
0.29
0.38
Cell Size (mm)
Al-T
KA-T
Karl-T
BZ-T

(f)

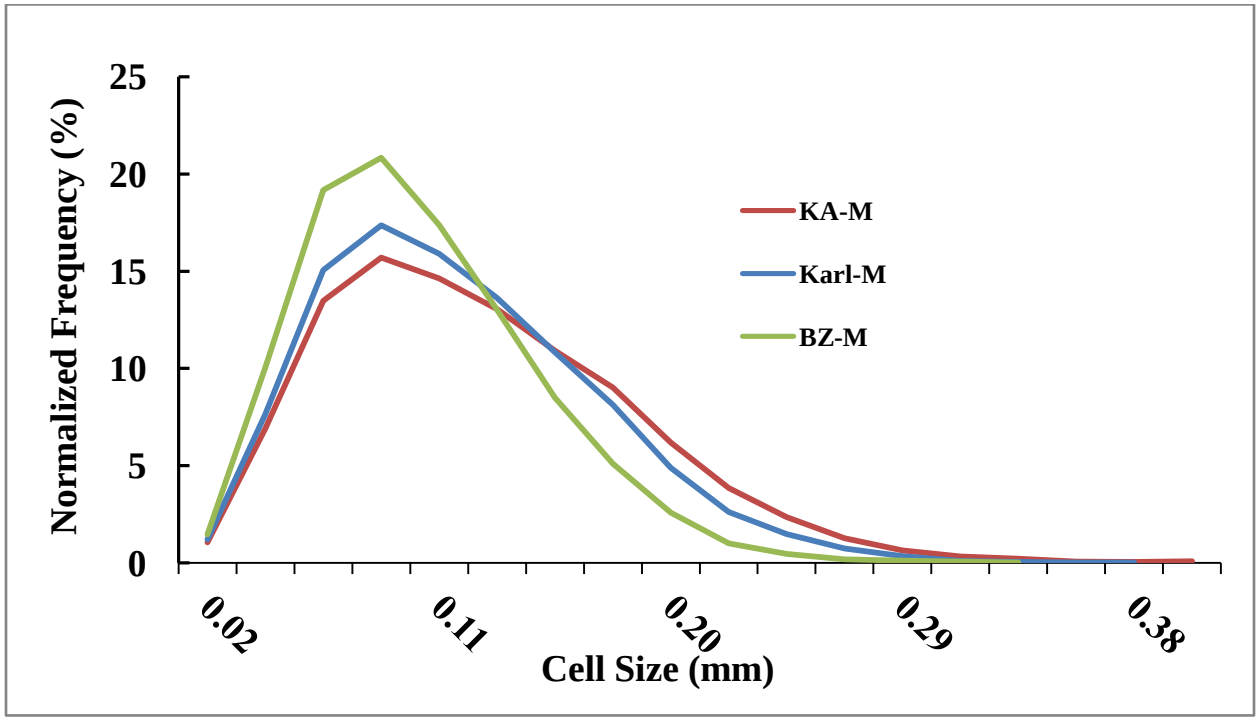
Normalized Frequency (%)
25
20
15
10
5
0
0.02
0.11
0.20
0.29
0.38
Cell Size (mm)
KA-M
Karl-M
BZ-M

(g)

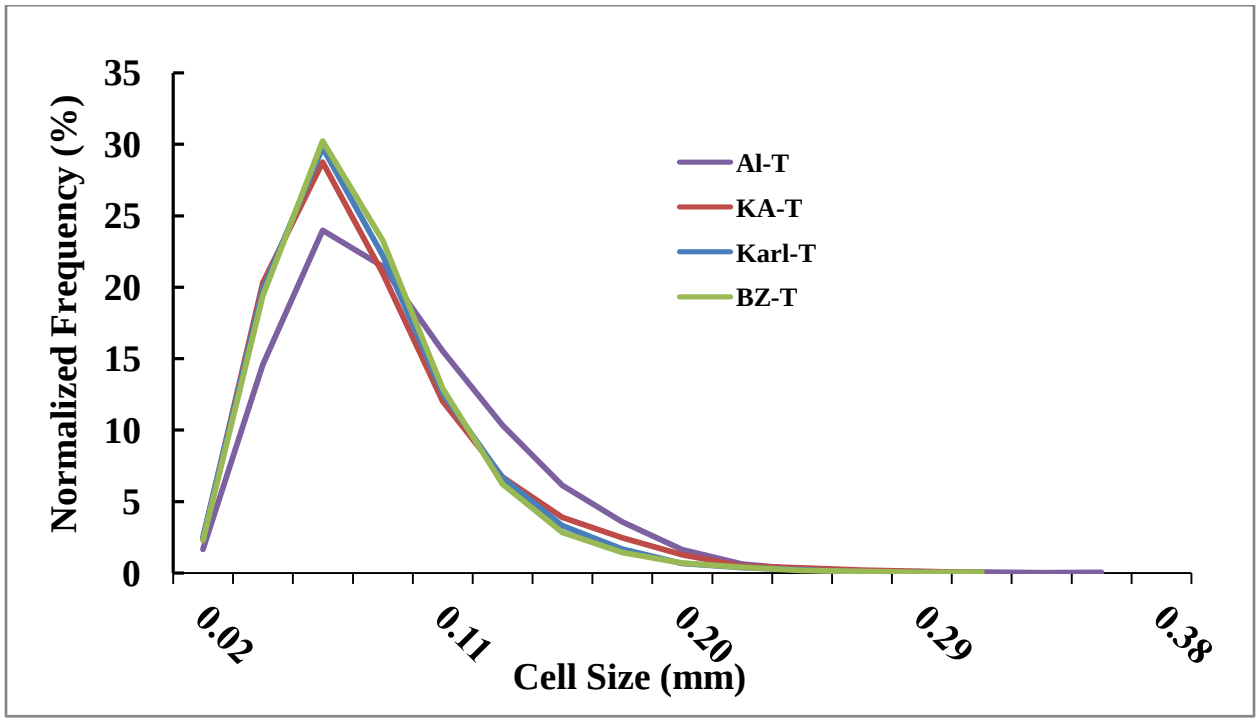
Normalized Frequency (%)
35
30
25
20
15
10
5
0
0.02
0.11
0.20
0.29
0.38
Cell Size (mm)
Al-T
KA-T
Karl-T
BZ-T

(h)

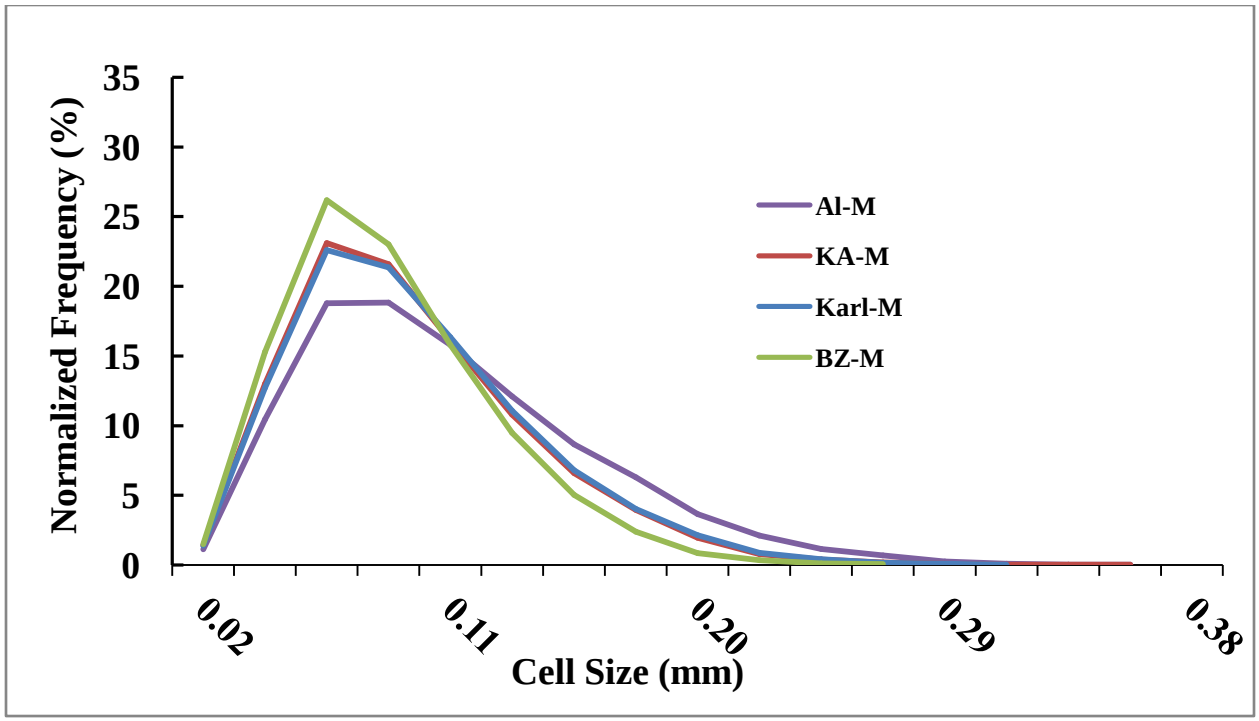
Normalized Frequency (%)
35
30
25
20
15
10
5
0
0.02
0.11
0.20
0.29
0.38
Cell Size (mm)
Al-M
KA-M
Karl-M
BZ-M